MECHANICAL BEHAVIOR AND STRUCTURE OF PASSIVE FILMS ON AUSTENITIC STAINLESS STEELS

By

ABDULAZIZ AL-AMR

A dissertation submitted in partial fulfillment of
the requirements for the degree of

Doctor of Philosophy

WASHINGTON STATE UNIVERSITY
School of Mechanical and Materials Engineering
Materials Science Program

May 2005

To the Faculty of Washington State University:

The members of the Committee appointed to examine the dissertation of ABDULAZIZ AL-AMR find it satisfactory and recommend that it be accepted.

_____
Chair

_____

_____

_____

ACKNOWLEDGMENT

I would like to express my appreciation to all those who gave me the possibility to complete this dissertation. I am deeply indebted to my advisor. Dr. David. F. Bahr whose help, stimulating suggestions and encouragement helped me in my research and writing of this dissertation.

My sincere thanks are due to Dr. Grant Norton, head of the department, for his detailed and constructive comments and for his important support throughout the TEM work. I especially would like to thank Dr. David Field for the help extended to me when I approached him and the valuable discussions that I had with him during the course of this research. Special thanks are due to Dr. Ursula Mazur for her interest in my work and for her guidance during my education.

I want to thank all my colleagues, Reza Yasser, Kevin Morasch, Kevin Nibur, and Gus Vasquez for all their help, support, interest and valuable hints.

Last but not least, I would like to give my special thanks to my wife Amal whose patient love enabled me to complete this work. Finally, I would like to thank all those people who made me feel not so foreign in this nice but quite different country.

Abdulaziz Al-amr

May 2005

MECHANICAL BEHAVIOR AND STRUCTURE OF PASSIVE FILMS ON

AUSTENITIC STAINLESS STEELS

Abstract

By Abdulaziz Al-amr
Washington State University
May 2005

Chair: David F. Bahr

The Taguchi analysis method was used in conjunction with ex-situ and in-situ nanoindentation tests to study the effects of alloy chemistry, solution pH, and halide ion concentrations on the mechanical fracture of electrochemically grown passive films formed at passive and metastable pitting potentials. Three austenitic stainless steels, SS, 304, 316, and 904L were anodically polarized in hydrochloric acid solutions for this study.

The ex-situ study indicated that the alloy chemistry is the dominant factor of the mechanical fracture of the film formed at a stable passive potential; the average load to fracture the films using a 450 nm radius diamond tip was 52 μN. The films formed on 904L were the strongest, while the films on 316SS were the weakest. The fracture load of the films formed at a metastable pitting potential, on the other hand, was equally influenced by the chloride ion concentration and the alloy chemistry. The load at fracture of films formed in the metastable pitting region was 64% of the fracture load of passive films formed at a stable potential

The fracture load of the passive films was depended on the degree of crystallinity of the passive film. The passive film on 316 SS with lower density of crystalline islands than that of 304 SS had the lowest fracture load. In contrast, when the film was epitaxial, the fracture load was the largest. The dichromate treatment results indicate that the increase in degree of crystallinity of the passive films is associated with the increase in the chromium content of the substrate.

In-situ measurements during anodic polarization led to similar behavior and results. The measured strength of films measured in ambient conditions after removal from the electrolyte was greater than when the films were measured in situ. However, the trends in film strength as a function of environment are the same between in situ and ex situ testing, suggesting the two tests are both feasible methods of analyzing environmental effects of film strength.

TABLE OF CONTENTS

Chapter 1 1
Introduction 1
1.1 Passive film growth models 4
1.2 Passive film breakdown 8
1.3 Influence of Alloying Elements on Passive Film Composition 11
1.3.1 Iron 11
1.3.2 Chromium 12
1.3.3 Molybdenum 13
1.3.4 Nickel 14
1.4 Environmental influence on the film composition 15
1.4.1 Potential 15
1.4.2 Passivation time 16
1.4.3 Aggressive Halide Ions 17
1.4.4 pH 17
1.4.5 Temperature 19
1.5 Mechanical Properties Background 20
1.6 Research Focus 26
Chapter 2 28
Testing Methodology and apparatus used 28
2.1 Taguchi Method 28
2.1.1 Taguchi's Approach to Parameter Design 29
2.1.2 Guidelines for the Taguchi method 30
2.1.2.1 Determine the target 30
2.1.2.2 Identify the noise and control factors and their levels 31
2.1.2.3 Design the matrix experiment and define the data procedure 31
2.1.2.4 Conduct the matrix experiment 33
2.1.2.5 Analyze the data and determine optimum levels for control factor 33
2.1.2.6 Predict the performance at these levels 37
2.2 Potentiostat for electrochemical film growth 39
2.3 X-ray Photoelectron Spectroscopy 39
2.4 Transmission Electron Microscopy 42
2.4 Nanoindentation Technique 45
Chapter 3 47
Electrochemical Behavior 47
Experimental Procedure 47
Results 49
Chapter 4 52
Effects of alloy and solution chemistry on the fracture of passive films on austenitic stainless steel 52
Experimental Procedure 52
Result and Discussion 55
Conclusion 65
Chapter 5 67
Effects of alloy and solution chemistry on the fracture of anodic films formed at metastable pitting potentials 67

Experimental Procedure 68
Results and Discussion 69
Conclusion 76
Chapter 6 78
Correlating structure and mechanical behavior of passive films on austenitic stainless steels 78
Experimental Procedure 79
Result 80
Discussion 89
Conclusion 92
Chapter 7 93
Comparison between the in-situ and ex-situ results of the passive film strength formed on austenitic stainless steels 93
Experimental procedure 93
Results 95
Discussion 104
Conclusion 105
Chapter 8 107
Summary 107
Appendix 109
Appendix 1-1 110
Electrochemical behavior of the films formed at a stable passive potential. 110
Appendix 1-2 117
Fracture load of the films formed at a stable passive potential 117
Appendix 1-3. 121
Fracture load of the films formed at a metastable pitting potential. 121
Appendix 1-4 125
Ex-situ Results 125
1- Applied tensile stress fracturing the passive films formed at a stable passive potential 125
2- Applied tensile stress fracturing the passive films formed at a metastable pitting potential 129
In-situ results 133
1- Applied tensile stress fracturing the passive films formed at a stable passive potential 133
2-Applied tensile stress fracturing the passive films formed at a metastable pitting potential 137
References: 141

LIST OF TABLES

Table 2-1 L 9 (3^4) Orthogonal Array 30
Table 3-1 Typical Chemical Composition, Wt %, of Alloys, balance iron 48
Table 3-2 the solution conditions used to study the polarization behavior and the average of the passive current in mA 50
Table 4-1 Factors of The Design Matrix 53
Table 4-2 The Design, Conditions, and the averages of fracture load of Passive films Formed in stable potential passive region 56
Table 5-1 The design, conditions, and average fracture load of passive films formed in the metastable potential passive region 69
Table 6-1 The ratios of iron and chromium to other metallic elements 82
Table 7-1 The design, conditions, and average fracture load of passive films formed in the stable passive potential region 97
Table 7-2 The design, conditions, and average fracture load of passive films formed in the metastable pitting potential region 98

LIST OF FIGURES

Figure 1-1- electrochemical behavior of a 304 SS polarized in aqueous HCl solution 3
Figure 1-2 Schematic representation of the place-exchange mechanism; M, metal ion; O, oxygen ion……...5
Figure 1-3 schematic of passivity breakdown based on PDM, from [16] 10
Figure 1-4 a simplified version of the Pourbaix diagram for the iron-water system at ambient temperature, from [56] 18
Figure 1-5 schematic for Current measurement during one film rupture event, from [65] 21
Figure1-6 the load discontinuity event in the nanoindentation curve 23
Figure 2-1 Flowchart of the Taguchi method 31
Figure 2-2 the Crossed array format 32
Figure 2-3 Schematic plot of main effects, Cases B and D show significant effects on the response 36
Figure 2-4 Schematic for half-normal probability plot 37
Figure 2-5An example for a real XPS spectrum obtained from a Pd metal sample using Mg Kα radiation, from [101]. 41
Figure 2-6 Signals generated when the electron beam penetrates a thin sample 42
Figure 2-7 An exmaple of a diffraction pattern 44
Figure 2-8 Typical load-displacement curve obtained by nanoindentation 45
Figure 3-1 Standard Greene Cell 48
Figure 3-2 Polarization curves for 304 SS in different chloride solutions 49
Figure 3-3 Factor effect plot for the passive current of the systems. 50
Figure 4-1Electrochemical Behavior of 304SS in Solution of pH 1 and 0.01M NaCl..... 54
Figure 4-2 Load-Depth Curve for an indentation of Cr2O3 film on a 304 SS 55
Figure 4-3 The averages and standard deviations of the fracture loads obtained from at least six indentations for the passive films formed at different growth conditions represented by table 4-2 57
Figure 4-4 Main effects plot for the influence of the factors on the overall average of fracture load, the dashed line. SS stands for the stainless steel and SC stands for the salt concentration 58
Figure 4-5 Half-normal probability plot of the control factors affecting the passive film formed at a stable passive potential 59
Figure 4-6 The effect of noise factors on the averages and standard deviations of the fracture load obtained from at least 54 indentations for each column, the net shape represents the standard deviation 60
Figure 4-7 XPS- depth profile of passive films formed on (a) 304 SS, (b) 316 SS, and (c) 904L 61
Figure 4-8 The averages of the fracture loads of the films versus the iron concentration in the films 62
Figure 4-9 The load-displacement curve of the passive film formed on 904L SS in chloride solution 65
Figure 5-1 Electrochemical behavior of 304SS in solution of pH 1 and 0.01M NaCl. The arrow indicates to the potential at which the film is grown. 68
Figure 5-2 The effect of the controlled factors (salt concentration, pH, and stainless alloy composition) on the load at which the passive films fractured 70

Figure 5-3 half-normal probability plot of the control factor affecting the passive film formed at a metastable pitting potential 71
Figure 5-4 The effect of noise factors on the fracture load 72
Figure 5-5 XPS- depth profile of passive films 73
Figure 5-6 The fracture load of passive films as a function of total iron concentration in the films formed at a metastable pitting potential 74
Figure 6-1A typical polarization curve of 316 SS in chloride solution, 0.01M NaCl and pH of 1 adjusted by adding HCl 81
Figure 6-2load displacement curve measured for 316 SS alloy passivated at -0.13V for two hours in chloride solution, pH 1 and 0.01 M NaCl, without and after dichromate treatment 81
Figure 6-3 Sputter depth profiles for the passive films formed on: a) 304, b) 316, c) 904L, and d) 316 with dichromate treatment 83
Figure 6-4 diffraction pattern for 904L SS before the growth of the oxide film beam direction [011] 84
Figure 6-5 (a) a bright field image and (b) [011] diffraction pattern of the passive film formed on 904L SS 85
Figure 6-6 (a) a bright field image and (b) [011] diffraction pattern of thin film formed on 304 SS. 86
Figure 6-7 A bright field image of the passive film formed on 316 SS 87
Figure 6-8 The effect of pre-dichromate treatment on the passive film grown on 316 SS; (a) a bright field image and (b) [011] diffraction pattern of the passive film formed on 316SS after dichromate treatment. 88
Figure 7-1Structure of electrochemical cell for in situ nanoindentation 94
Figure 7-2 typical polarization curve for 304 SS in chloride solution, the arrows indicate to the potentials used to grow the films 96
Figure 7-3 Ex-situ and in-situ nanoindentation curves of the passive film formed on 904L in chloride solution 96
Figure 7-4The effect of the controlled factors (salt concentration, pH, and stainless alloy composition) on the tensile stress applied to the passive films formed at a stable passive potential 100
Figure 7-5 The effect of the controlled factors (salt concentration, pH, and stainless alloy composition) on the tensile stress applied to the passive films formed at metastable pitting potential 101
Figure 7-6 Ex-situ results of the tensile stress required to fracture the passive film 102
Figure 7-7 In-situ results of the tensile stress required to fracture the passive film 102
Figure 7-8 The overall averages of the applied tensile stress required to fracture the passive films formed at stable passive and metastable pitting potentials and indented in ambient air and in situ 103
Figure 7-9 The general contribution of each control factor in the strength of the passive films formed at stable passive and metastable pitting potentials, respectively, and ex-situ indented (A and B) and the strength of the passive film formed at stable passive 104

This dissertation is dedicated to my mother and father

Chapter 1

Introduction

Most of metals exist in natural states in different forms, such as oxides, sulfides or nitrides. In order to utilize them in industrial and engineering applications some energy has to be added to convert them to pure metals or useful alloys. This process raises the internal energy of the converted materials. As a result of that, these materials are often thermodynamically unstable in oxidizing environments and, therefore, tend to lower their energy through the reactions with the environment. The result of the reaction of the metals with their environments is known as corrosion. Corrosion can take different forms, such as uniform corrosion in aqueous environments, localized corrosion such as pitting, or stress corrosion cracking.

The performance of most structural and engineering metals or alloys, such as nickel, iron, titanium, and stainless steel alloys, is often controlled by an effect called passivity [1, 2]. In the 1840s, the phenomenon of passivity was discovered by Faraday based on his famous iron-in-nitric acid experiments. In these experiments, if a small piece of iron was immersed in concentrated nitric acid, no reaction was observed and the piece of iron was found to be immune. If water was added to dilute the nitric acid, no change took place, and the iron specimen remained inert. However, when he scratched the sample in situ, an aggressive reaction took place. These simple experiments show various important points. In the first case, the iron sample was in the passive state and the corrosion rate was very low. In the second case, the sample was protected by the unstable passive state which was damaged by scratching the sample. As a result of this process, the sample changed its state from the passive to the active state [1]. Passivity takes place

when the dissolution rate decreases by increasing the potential to more positive values. The result is low corrosion rate at potentials more positive than open circuit potential due to the formation of oxide passive films on the surfaces of metals or alloys.

The behavior of a passive metal in a corrosive environment can be described by the polarization curve. The polarization curve is a plot for the current density in log scale vs. potential. The polarization is said to be either anodic, when the specimen potential is changed in positive (noble) direction or cathodic when it is changed in the negative direction. The potential at which the rate of oxidation is equal to the rate of the reduction is called equilibrium potential. Figure 1-1 represents a typical polarization curve of a passive metal. The curve is divided into three states; an active state, a passive state, and a transpassive state. The active state is the state where the metal starts to oxidize by increasing the potential. The oxidation is seen as an increase in current density. A further increase in the potential promotes corrosion, until the current density begins to decrease and passivation begins. In this state the metal surface is covered by an oxide film which acts as a barrier between the metal and its corrosive environments. In this potential region, passivation state, an increase in the potential leads the metal cations to oxidize to a higher oxidation valence than in the primary passive region, creating a stable passive film. Raising the oxidation states of metal cations leads not only to higher valence metal cations but also a break down in the passive film and initiating unstable pits. The transpassive state begins when the current density rapidly increases and the unstable pit changes to stable pits.

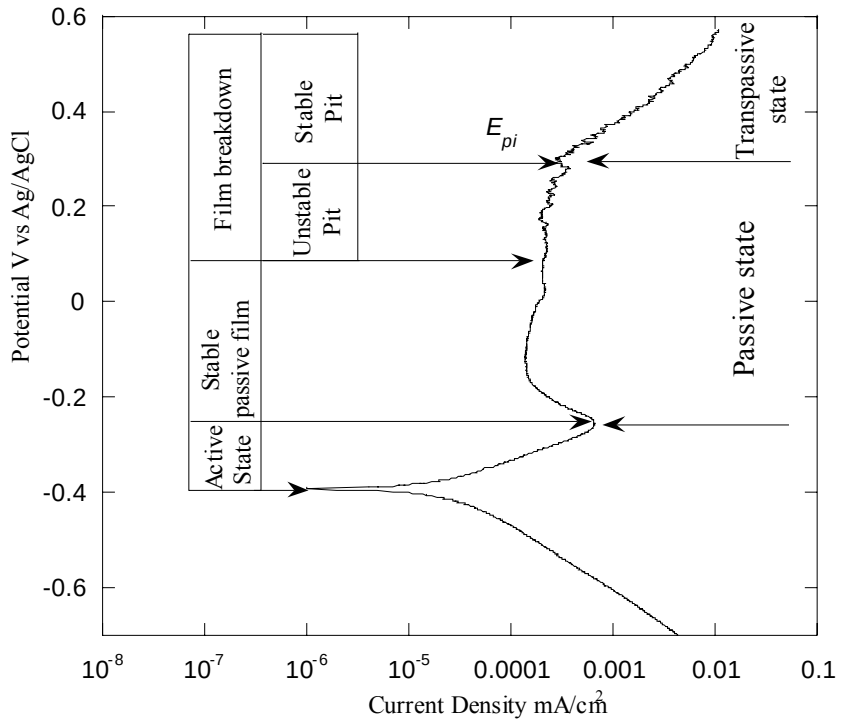

Figure 1-1- electrochemical behavior of a 304 SS polarized in aqueous HCl solution

The nature and the composition of these passive films have been the subjects for several investigations. The passive films are formed from the metal itself and the components of the environments represented by oxygen and water [3]. Olefjord and Wegrelius pointed out by using Electron Spectroscopy for Chemical Analysis, ESCA, that the passive films formed in aqueous solution at room temperature are generally composed of two layers, an inner oxide and outer hydroxide layer [4]. The passive films formed on stainless steel alloys consist of inner layers composed mostly of chromium oxides and outer layer composed mainly of iron oxides and hydroxides [5,6]. The thickness of passive films formed on stainless steel alloy is generally between 10 and 50 Angstroms [7,8]. Olsson and Landolt [3] , and Brookes el al. [9] pointed out that the structure and the composition of the passive films formed on stainless steel alloys are not

only capable of adapting to the changes in the composition of the substrate alloy and the environments in which they are grown, but also depend on both time and potential.

1.1 Passive film growth models

Various theories have been proposed to describe the formation of the passive film. Most of the proposed theories assumed a monolayer of oxygen atoms will be adsorbed very rapidly, in about 10^{-2} sec. Uhlig [10] proposed two basic mechanisms for the phenomena of passivity: the diffusion barrier mechanism, and the adsorption mechanism. Several researchers proved the existence of the diffusion barrier oxide film either by using an ellipsometer or isolating an oxide film formed on Fe passivated in chromium solution by immersing the iron for several days in 10%KI saturated with iodine [11]. This barrier separates the metal from its environment and slows down the rate of reaction. Uhlig [10] pointed out two theories to explain the passivity for the transition metals and their alloys due to the adsorption mechanism as an adsorbed oxygen film chemically bonds with unfilled *d* electron level of the metal. Adsorbed oxygen decreases the exchange current density and thus increases the anodic polarization. Approaching a more noble potential and forming multilayer adsorbed oxygen is the result of increasing the anodic polarization. The marked negative charge of adsorbed oxygen attracts the positive charge of the metal ions forming the film. Another theory is the place-exchange theory. The place-exchange mechanism involves the following steps [10-13]:

(1) an oxygen atom is adsorbed

(2) simultaneous rotation of metal-oxygen ions

(3) a second oxygen atom is adsorbed followed by simultaneous rotation of the two M-O pairs

(4) thickness of the film increases due to the repeat of this process

Figure 1-2 is a schematic representation of the place-exchange mechanism.

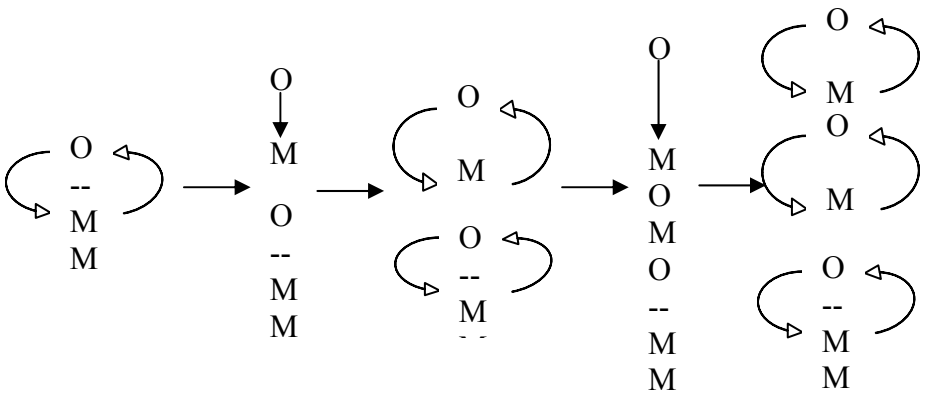

Figure 1-2 Schematic representation of the place-exchange mechanism; M, metal ion; O, oxygen ion.

Cabrera and Mott [14] proposed a model to explain the formation and growth the passive films. Their model is based on the fact that all oxides are to some extent polar, and the charges on oxygen and the metal ions must be strongly attracted to the substrate metal. Therefore, a monolayer of the oxide is formed on the metal surface due to the existence of strong cohesive forces between the metal and oxide. An atomic adsorbed oxygen layer on the surface of the oxide formed is due to the exposing the oxide to the oxygen. They assumed that electrons can pass through the oxide from the metal to the oxygen either by thermionic emission or a tunnel effect, and the electronic motion is faster than the metallic ion motion. As the result of this process some oxygen atoms will be converted into ions. Building up the negative and positive charges, through oxygen and metallic ions, in the two sides of the film creates a strong electric field across the thin

oxide layer. If the energy required to remove an electron from the metal into the conduction band of the oxide is too large for thermionic emission and the film is too thick for a tunnel effect, the film stops growing. They summarize the basic film growth rate by

$$\boldsymbol{i} = \boldsymbol{A}\exp(\boldsymbol{BE} / \boldsymbol{D}) \qquad (1\text{-}1)$$

where i is the growth rate, E the electrode potential, D the film thickness, and A and B are constants depending on the concentration of interstitial ions in the oxide and both the activation energy and temperature, respectively [14].

Chao *et al* [15] developed a model for the growth of the passive films under anodic polarization based on the movement of point defects assuming the following:

1- The passive film forms on the surface of the metal if the external potential exceeds the passivation potential, the Flade potential.

2- It is assumed the passive film is a defective oxide film which contains a high concentration of point defects. The Kroger-Vink notation is used to describe point defect species. X_Y means a Y lattice site is occupied by X species. For example, V_M, and $V_M^{X'}$ describe a vacancy occupying a metal site (a metal vacancy) and a metal vacancy carrying X negative charge in the oxide, respectively.

At the metal/film interface two reactions take place

$$\boldsymbol{m} \leftrightarrow \boldsymbol{M}_{\boldsymbol{M}} + \frac{\boldsymbol{x}}{2}\boldsymbol{V}_{\boldsymbol{O}}^{\bullet\bullet} + \boldsymbol{xe}' \qquad (1\text{-}2)$$

and

$$\boldsymbol{m} + \boldsymbol{V}_{\boldsymbol{M}}^{\boldsymbol{x}'} \leftrightarrow \boldsymbol{M}_{\boldsymbol{M}} + \boldsymbol{xe}' \qquad (1\text{-}3)$$

where the metal atom in the metal is represented by m, and the metal cation in the film is represented by M_M. At the film/solution interface two other reactions take place

$$V_O^{\bullet\bullet} + H_2O \leftrightarrow 2H^+(aq) + O_O \qquad (1\text{-}4)$$

and

$$M_M \leftrightarrow V_M X' + M^{x+}(aq) \qquad (1\text{-}5)$$

Where M^{x+} represents the hydrated metal cation in the electrolyte solution. It is obvious from equations (1-2) and (1-4) that the oxide ion vacancies are produced at the metal/film interface and consumed at metal/solution interface. This fact is indicative to the diffusion of oxide ion vacancies from the metal/film to the film/solution interfaces. Similar arguments using equation (1-3) and (1-5) show metal cations diffuse from the metal/film to the film/solution interfaces. The film growth, thus, can be shown by combining reactions (1-2) and (1-4), and (1-3) and (1-5)

$$\frac{2}{x}m + H_2O \leftrightarrow \frac{2}{x}M_M + O_O + 2H^+(aq) + 2e' \qquad (1\text{-}6)$$

$$m \leftrightarrow M_M(aq) + xe' \qquad (1\text{-}7)$$

equation (1-6) reveals that the film growth is a result of the diffusion of oxygen anions while equation (1-7) discloses that the diffusion of metal cations leads to metal dissolution only.

All the models mentioned above did not predict the steady-state in the film thickness or current and ignored the dissolution of the oxide film. Macdonald [16] modified the Point Defect Model (PDM) to predict and explain the steady-state under potentiostatic transient conditions. As the film becomes thicker, the driving force injecting cations from the metal to the film and generating oxygen vacancies reduces due

to a decrease in the voltage drop a cross the metal/film interface. The film thickness and the current, thus, reach the steady-state.

1.2 Passive film breakdown

Passive films greatly decrease the dissolution rate of metals, but the metal surfaces are not permanently protected from corrosion since the passive films are subjected to different forms of localized corrosion such as pitting corrosion and stress corrosion cracking. In order for these phenomena to take place, an initial breakdown of the passive films is required. As a result of film rupture the surface of the underlying metal is exposed to the corrosive environments. Several facts about the film breakdown have been proved, and these facts can be summarized as follow [16,20]:

1- There is a critical potential, V_c, above which the film breakdown takes place

2- The critical potential for a given metal depends on the presence of aggressive ions such as (Cl^-, Br^-, and I^-)

3- The presence of halide ions and the applied potential influence the incubation time needed to observe the pits.

Several theories and models have been proposed to describe the breakdown of the passive films. Uhlig and Bohni [17] proposed the breakdown of the passive films using competitive ion adsorption theory. It was pointed out that both Cl^- and oxygen anions can be adsorbed on the metal surface. The metal passivates when the oxygen anions are adsorbed. On other hand, adsorption of chloride ions does not result in a passive surface. Therefore, above a critical potential, where chloride ion adsorption is favored over oxygen anion adsorption, breakdown of the passivity takes place.

Hoar and Jacob [18] postulated the complex ion formation theory to explain the passive film breakdown. They assumed that a highl energy complex is formed due to the adsorption of a small amount of chloride ions around a cation in the film surface. Once formed, this complex will readily dissolve in the solution resulting in local thinning of the film. The localized thinned site creates a stronger anodic field at this site. Another cation, will, therefore, be transferred to the surface and react with another chloride ion to form more complex ions. This process promotes the breakdown of the passive films.

Sato [19] proposed the first mechanical mechanism for the breakdown of passivity. He thermodynamically derived the following expression for the pressure, P, acting vertically to the film using the atmospheric pressure, P_o, the interfacial tension due to a very thin film, and the electrostriction pressure produced by the electric field

$$\boldsymbol{P - P_o} = \frac{\varepsilon(\varepsilon - 1)\boldsymbol{E}^2}{8\pi} - \frac{\gamma}{\boldsymbol{L}} \qquad (1\text{-}8)$$

Where ε is the dielectric constant, E the electric field, γ the surface tension, and L is film thickness. The first term in the right side of equation (1-8) represents the electrostriction effect and the second the interfacial effect. Sato showed that there is a critical compressive stress, which is represented in the left side in equation (1-8), above which the breakdown of the metal oxides occurs. When the value of the right side is larger than the left side in equation (1-8), the breakdown of the film takes place.

L. Lin *et al* [20] used the point defect model (PDM) to describe the passivity breakdown and pit initiation. The concept of passivity breakdown based on the PDM can be illustrated by the next two point defect reactions and Figure1-3:

$$\boldsymbol{m} + \boldsymbol{V}_{\boldsymbol{M}}^{\chi'} \rightarrow \boldsymbol{M}_{\boldsymbol{M}} + \boldsymbol{V}_{\boldsymbol{m}} + \chi\boldsymbol{e}' \qquad (1\text{-}9)$$

$$m \rightarrow M_M + \left(\frac{\chi}{2}\right)V_O^{\cdot\cdot} + \chi e' \qquad (1\text{-}10)$$

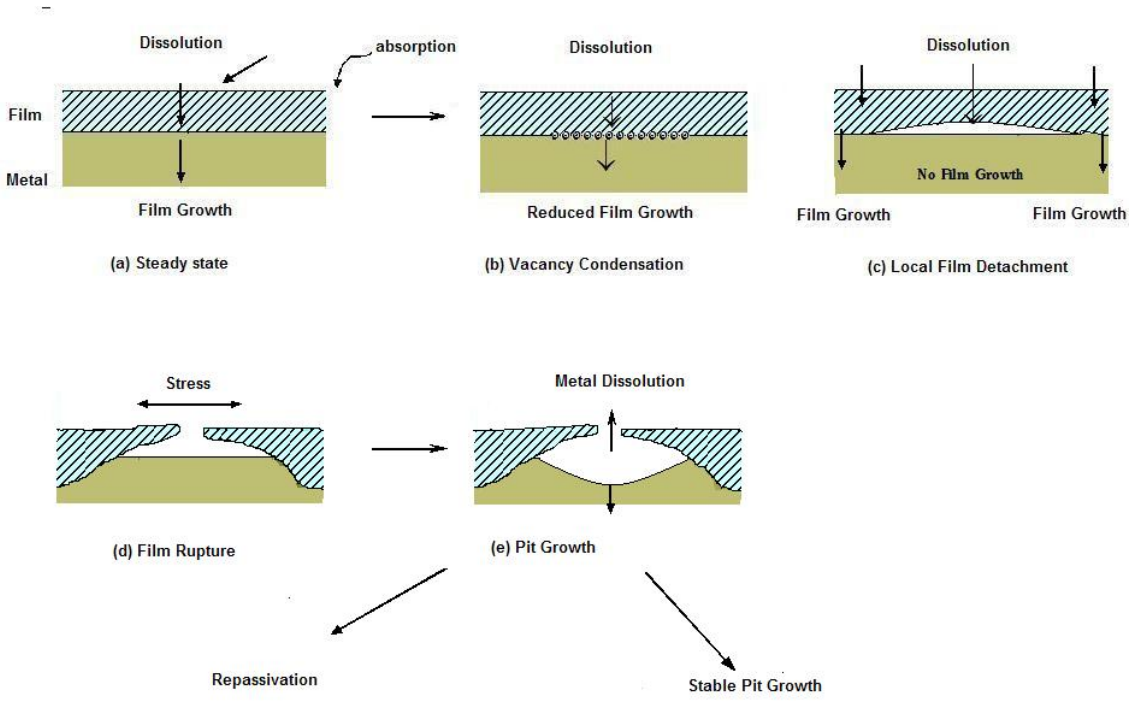

Figure 1-3 schematic of passivity breakdown based on PDM, from [16]

When reaction (1-9) is not able to annihilate the flux of cation vacancies across the oxide film, the cation vacancies condense at the metal/film interface. This process results in both the separation of the film from the metal and prevention of subsequent growth of the film, reaction (1-10), above the vacancy condensation. The film keeps growing at those regions where it is attached to the substrate. At the same time, dissolution of the film at the film/electrolyte interface results in the thinning of the cap over the vacancy-condensation area. Further thinning of the film leads to both a hole and penetration of the electrolyte into the vacancy-condensation area and, consequently, the initiation of a

micropit. As long as the micropit is below a critical size the metal has the ability to repassivate. Achieving the critical size allows the micropit to develop into a stable pit. The critical size of the pit is determined by the critical values of current density, *i*, and the radius of hemispherical nucleus.

1.3 Influence of Alloying Elements on Passive Film Composition

Stainless steels are iron based-alloys containing at least 12% chromium to improve its corrosion resistance. Other elements, such nickel and molybdenum are added to improve the corrosion resistance of stainless steels. Due to the selective oxidation of some elements in the film, one or more components of a stainless steel alloy are enriched in the film as the result of corrosion. The influences of these elements on the passive film composition are summarized below:

1.3.1 Iron

Kirchhmeim *et al*. [21] studied the passive film composition of Fe-Cr, Fe-Al, and Fe-Mo alloys formed in acidic solutions at a passive potential. It was found that due to both the selective dissolution and the high mobility of iron compared to Cr and Al, the passive films were enriched in both Cr and Al. Similar results were obtained by analyzing the passivity of Fe-Cr alloy in 0.5M H_2SO_4 using X-ray Photoelectron Spectroscopy (XPS) and Ion Scattering Spectroscopy (ISS). In addition to that, an enrichment of iron, which changes valence above the Flade potential, was found in the outer layer of the passive film. [22]. Bastidas *et al*. (23) analyzed the passive film formed on 304SS in a 5%NaCl aqueous solution using X-ray absorption spectroscopy (XAS). According to XAS spectra they suggested that iron and nickel were not present in the oxide film.

1.3.2 Chromium

Chromium is an alloying element by which the passivity of Fe-base alloys can be achieved. The selective dissolution of iron leads to the formation of the passive films through the formation of bridges between the chromium and the oxygen ions when they are exposed at the alloy surface. In order to form a continuous passive film, the chromium concentration in an alloy should be at least 12% [24,25].The passive film on stainless steel consists basically of chromium in its trivalent state. Hamm et al. [26] pointed out that for a passive film formed on Fe-Cr alloys in acidic solutions; when the potential increases above the stability limit of chromium III, the passive film starts to change its composition and the fraction of trivalent iron in the film increases. Haupt *et al*.[22] has shown that increasing the Cr content of the alloy decreases the passive current density, corrosion rate, and increases the pitting potential. Wallinder *et al*. [27] used Electrochemical Impedance Spectroscopy,(EIS), and XPS to study the influence of different parameters such as nitric acid concentration, passivation time, and ageing in air on the passive film formed on a 316 SS. It was found that all these parameters improved both the stability of the passive film and corrosion resistance due to chromium enrichment in the passive film.

Ryan *et al*. [24] pointed out the relation between the structures of the passive film formed on Fe-Cr alloys in acidic solution and the chromium contents in the alloys. When the chromium content in the alloy is more than 17%, the resultant film is amorphous. Lowering the chromium content crystallizes the passive film. Brooks *et al*. [28] investigated the role of chromium in the passive films anodically formed on 304 SS in acid solutions at 0.25V (vs. saturated calomel electrode, SCE) and held there for a

particular period of time. They concluded that a hydrated amorphous chromium-rich film was initially formed containing a certain amount of CrO_3 through the reaction of chromium with H_2O. This film was then recrystallized during the first hour. Doh *et al*. [29] obtained similar results when the passive films formed on different stainless steel alloys in a borate buffer solution was investigated by XPS. They found that at the initial stage of passivation, less than 2 minutes, the chromium existed in the film as a mixture of Cr_2O_3, $Cr(OH)_3$, CrO_3, and CrO_4^{2-}. Increasing the passivation time to more than an hour resulted in the chromium in the passive film existing only as Cr_2O_3.

1.3.3 Molybdenum

Molybdenum, Mo, is an alloy element with a strong beneficial effect on the pitting resistance of stainless steel alloys. Even though pure molybdenum does not form a passive film, it plays a significant role in the stability and the composition of the passive film formed on stainless steel alloys [3,9,30]. The addition of molybdenum to a stainless steel alloy results in a passive film mixed of Cr, Fe, and Mo whose oxidation states depends on the potential of passive film. This addition improves pitting corrosion resistance of stainless steel alloys. The effect of the Mo on pitting resistance depends on the chromium concentration in the alloy. The chromium concentration in the passive films can be increased due to the addition of some minor elements such as molybdenum [9]. The effect of molybdenum is not found only in the decreasing of the dissolution rate due to the buildup of Mo and Cr in the outer layer of the passive film during the active dissolution, but also in the presence of either insoluble molybdenum chloride complexes which improve the pitting corrosion resistance of stainless steels or MoO_2 as major passivation species [3,9,31].

Several theories have been proposed to explain the exact mechanism by which Mo enhances the passivation of stainless steel but they can be classified in two main groups: effects during active dissolution, and effects on the passive film [5,30,32,33]. During the active dissolution the primary cations in the passive film are Cr^{+3} and Fe^{+3}. In addition to these cations, ferrous iron (Fe^{+2}) is also present and is accompanied by point defects which could be dissolution sites. These sites will be occupied and canceled by the presence of molybdenum. Therefore, the penetration of aggressive ions such as chloride ions will be decreased due to a lowering of the defect concentration [34,35]. An alternative mechanism is that molybdenum is oxidized to form MoO_4^{2-} in the solid state in the outer layer of the passive film. The presence of MoO_4^{2-} in outer layer of the passive film results in changing its intrinsically anionic selectivity into a cation one and induces the formation of a dipolar layer which resists the combination of anions such as OH^- and Cl^-, and promotes the migration of O^{2-}, and, as a result of that, the formation of Cr_2O_3 or CrO_3 [3,34-36]. Ogawa *et al* [37] and Montemor *et al* [33] observed that molybdenum had an effect on the chromium content in passive film formed on different alloys in 5% H_2SO_4; the presence of the molybdenum in the alloy led to an increase of the chromium content in the internal layer of the passive film. [33].

1.3.4 Nickel

Even though only a small amount of nickel present is as hydroxide in the passive film, nickel can influence the formation and possibly improve the corrosion resistance of austenitic alloys [3]. Iron and chromium are oxidized easier than nickel. Therefore, a Ni enrichment in its metallic state underneath the passive film, at the metal oxide interface, can be observed. The enrichment of nickel could lead to the formation of an unstable

nickel nitride. A first stage in passivation is a result of the reaction of unstable nickel nitrides with Mo and Cr to form a strong bonding intermetallic compound such as Ni_2Mo_3N [38]. Maurice *et al*. [39] studied the passive films formed on (110) Fe-22Cr and (100) Fe-18Cr-13Ni single crystal surfaces in 0.5M H_2SO_4 using XPS and Scanning Tunneling Microscopy (STM). They pointed out that the presence of Ni in the alloy, which is enriched in the metallic phase underneath the passive films, modified the crystallization rate and slowed down the formation of the chromium oxide in the inner layer of the passive film by reducing the rate at which metallic chromium became available.

1.4 Environmental influence on the film composition

The passive film on stainless steel is a dynamic system which is in constant exchange with its environment. Passive films adapt to changes in the environmental factors such as the time, the potential, anion concentration in the electrolyte, solution pH, and temperature.

1.4.1 Potential

The applied potential in the passive region either forms or breaks down the passive films. The breakdown of passive films on metal surfaces can lead to initiation sites for pitting as they become susceptible to localized attacks resulting in accelerated dissolution of the underlying metal. Anodic passive films break down at a certain potential range, as shown in Figure 1-1, leading to either unstable pitting sites, which are repassivated, or stable pitting sites if the potential is above the critical pit initiation potential, E_{pi} [40]. Haupt and Strehblow [22] investigated the effect of the applied potential on the passive films formed on a Fe-15Cr alloy in 0.5M H_2SO_4. They showed

that as the applied potential increased, the thickness of the film linearly increased in the passive region and decreased when the applied potential reached the transpassive region. A similar effect of the potential on the thickness of the film formed on different substrates have been obtained in different electrolytes [4,41-43]. The composition and chemistry of the film are also influenced by the applied potential; in the passive region for Fe/Cr alloys, at a low potential below the Flade potential, Fe^{2+} was formed. However, increasing the potential above the Flade potential oxidized the Fe^{2+} to Fe^{3+}. Moreover, a further increase in the potential changed the oxidation state of the chromium from a trivalent to a hexavalent state [22, 44, 45].

1.4.2 Passivation time

Passivation time or ageing time, which is the time held in the passive region to grow the film, has significant effect on both the thickness and chemistry of the film. It was found that the thickness of the film formed on a Fe/Cr alloy in acid solution increased with the log of the passivation time [22, 27, 42,45]. Increasing the passivation time resulted in a higher chromium content due to the change of chromium hydroxide to chromium oxide in the passive film formed [25,27, 42]. Doh *et al* [29] pointed out that the amount of molybdenum in the passive film increased by the replacement of Cr oxide by Mo oxide with increasing the passivation time. The passive film was found to be a gel-like structure because of the large amount of bound water included in the film; with increasing the passivation time, the film changed first to a less hydrated structure and finally to a perfect oxide [46].

One way to measure the stability of passive films is to measure the potential decay time, the time necessary to break down the passive films when the applied

potential in the passive range is switched to open circuit potential. Longer times at potential in the passive region result in longer times for potential decay [47].

1.4.3 Aggressive Halide Ions

The presence of aggressive halide ions, especially chloride ions, in the electrolyte increases the breakdown possibility of the passive film and leads to corrosion pitting [48-50]. The development of corrosion pits on stainless steel immersed in chloride solutions takes place in three different stages: nucleation, metastable growth, and stable growth. The destruction of passive films due to localized corrosion has been explained by three models: the adsorption of chloride ions leading to local film dissolution, the penetration of chloride ions in the film leading to weakening of the oxide bonds, and mechanical film break down at defects such as cracks and vacancies [3,51,52]. A high chloride concentration in the electrolyte decreases the breakdown and pitting potentials, noted in figure 1, down to less noble potentials [53, 54]. Ernst and Newman [55] studied pit growth in 304 SS at different chloride concentrations in NaCl solutions. They showed that the change of pit growth in depth rather than width was due to the lowering chloride concentrations. Costa *et al* [25] investigated the passive film formed on chromium in acidic solutions with and without chloride ions using XPS. No incorporation was found in the inner layer of the passive film when the chloride ions were added after the passivation of chromium for two hours in a sulphuric acid solution. For passive films formed in chloride electrolytes, on the other hand, chloride ions were incorporated both in the inner oxide layer and the outer hydroxide layer.

1.4.4 pH

pH and potential are the two factors that influence the thermodynamic stability of the metal or an alloy in given environments through what is called a Pourbaix diagram

[56]. Figure 1.4 represents a simplified version of the Pourbaix diagram for the iron-water system at ambient temperature.

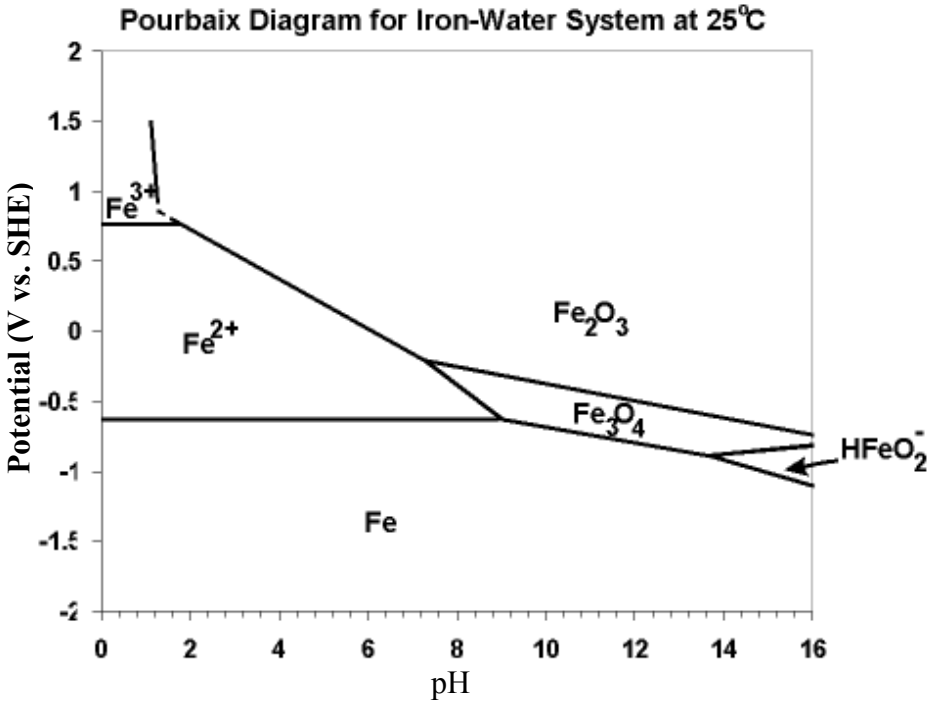

Figure 1-4 a simplified version of the Pourbaix diagram for the iron-water system at ambient temperature, from [56]

The effect of solution pH on the passivation of stainless steel was investigated by many researchers, including Schmutz and Landolt [45], Elsener and Rossi [57], Carroll and Walsh [58], and A.U. Malik *et al* [59]. Schmutz and Landolt [45] studied the behavior of Fe/Cr and Fe-Cr-Mo alloys under changing the applied potential in the passive region formed in basic and acidic solutions using the Electrochemical Quartz Crystal Microbalance, EQCM .EQCM utilizes the converse piezoelectric effect of a quartz crystal to determine the change of the resonance frequency which is opposite to the change of the crystal mass [60]. In the basic solution, they found that increasing the potential resulted in a mass increase due to the low dissolution rate and film growth. On

the other hand, a mass loss was observed with increasing the potential in the passive region of acidic solution. Consequently, a thicker passive film was obtained in basic solutions because of the low dissolution rate and a high content of iron oxides in the film [45].

Elsener and Rossi [57] investigated the influence of changing the solution pH in the acidic range on the thickness and composition of the passive film formed on stainless steel using XPS. At a constant potential, they showed that increasing the pH of the solution resulted in a thicker film. Increasing the pH of the solution enriched the film in iron oxide. At low pH, on the other hand, Cr^{3+} content was enriched in the film. Hara and Sugimoto [61] found similar result; the Cr^{3+} content decreased with increasing pH with a corresponding increase of the Fe^{3+} content. Carroll and Walsh [58] used the stability of the passive film, which is measured by monitoring the time for the current to reach a steady state, to investigate the influence of pH. Reducing the solution pH increased the current fluctuations which are indicative of an increase in the dissolution rate. Malik *et al* [59] studied the influence of pH on the pitting behavior of 316 SS. They showed that at a particular temperature and chloride ion concentration, decreasing the pH of the solution shifted the pitting potential to a more negative potential and increased the dissolution rate.

1.4.5 Temperature

Among the factors that influence the passivity breakdown is temperature. Pallotta *et al* [62] investigated the pitting behavior of 316 SS in different solutions containing chloride ions at different temperatures. At a particular sodium chloride concentration, increasing the solution temperature from 0 to 15°C shifted the breakdown potential at

which the current fluctuations were observed to a less noble potential. A further increase in the temperature to 25°C reduced the film ability to repassivate and resulted in a significant shifting in the breakdown potential toward more negative values. Ernst and Newman [55] studied the effect of the temperature on the passivity breakdown; they showed that the pit growth increased with increases in the temperature. Carroll and Howley [63] used current fluctuations in the pitting potential region to investigate the effect of the temperature. The current peaks and fluctuations were larger for the film formed at a higher temperature. Increasing the passivation time resulted in bigger and wider peaks. As a result of that, the passivity breakdown takes place and the pitting potential is shifted to a less noble potential. Jin and Atrens [64] studied the effect of the temperature, 25, 60, and 90 °C on a passive film formed on Fe-Cr and Fe-Cr-Mo alloys in 0.1M NaCl solution. They observed that the temperature had little influence on the structure and composition of the passive films because of the less aggressive environment conditions which did not break the passivity and initiate pitting corrosion; the slight influence at the high temperature was with more Fe and less Cr dissolving.

1.5 Mechanical Properties Background

When passive alloys are scratched by a ceramic pen, or any other hard point contact, in a corrosive solution, a fresh metal surface is exposed to the solution. As a result of that, the anodic current increases because of electrochemical dissolution. When the scratching is completed, the anodic current decreases quickly due to the repassivation of scratched surface. Figure1- 5 shows the current measurement and the change in the film thickness after one film rupture event. At (1), the surface of the specimen is under anodic polarization in the passive range, the sample is completely covered by the passive

film and the current is small, but >0. At (2), the passive film has been ruptured and a current peak appears. At (3), the passive film has partly regrown and the repassivation current is decreasing. Finally, at (4), the surface is completely repassivated and the current is small again [65,66]. The current-time relationship can be utilized to evaluate the repassivation capability of an alloy. However, the traditional scratch test and related repassivation tests can not measure the initiation of breakdown, only the rate at which the film regrows [67].

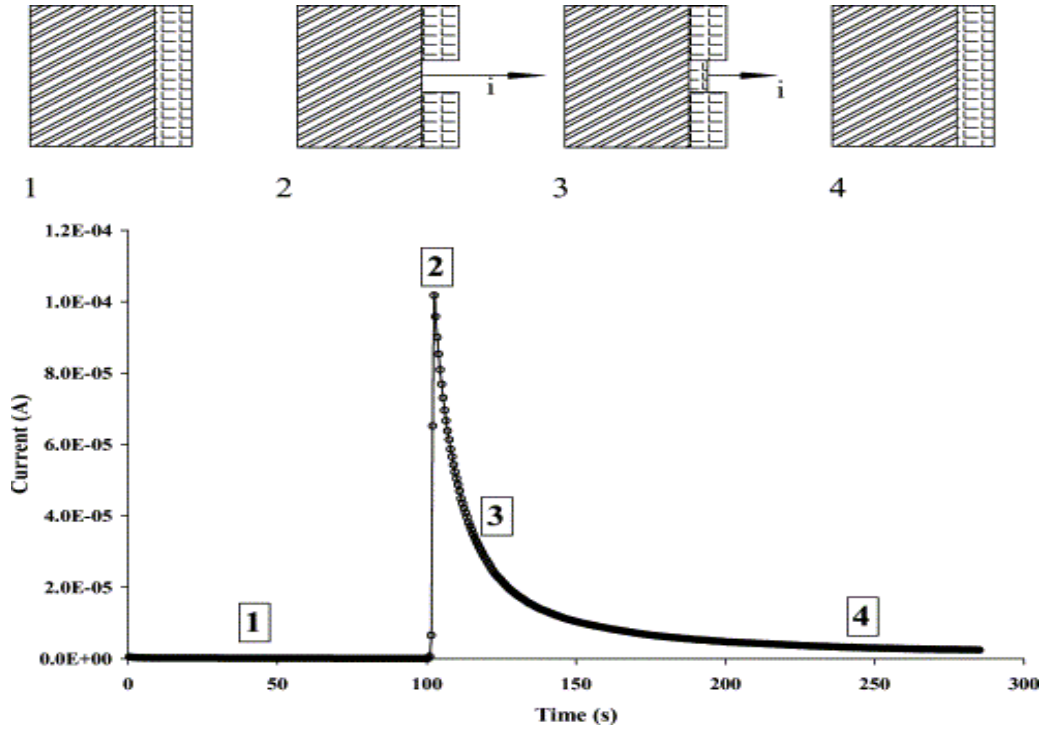

Figure 1-5 schematic for Current measurement during one film rupture event, from [65]

Wang, and Li [68] utilized the micro-scratching technique to evaluate the mechanical behavior of the passive film formed on 304SS as-received and after exposing to 3.5 %NaCl for 16 hours. During the micro-scratching test, the passive film is scratched under an applied load, which is increased linearly, at a constant rate; the contact electrical

resistance (CER) changes during the scratching with respect to the applied load. The load at film failure leads to a sharp drop in the CER. Wang and Li [68] observed that when the passive film on 304 SS as-received was exposed to 3.5%NaCl for 16 hours, the load at failure was decreased when compared to the load required to fracture the passive film on a nanocrystalline 304SS surface made by sandblasting and annealing.

Chiba and Seo [69] investigated the influence of the test condition on the frictional coefficient, which is the ratio of the lateral force to the normal force, for the passive iron surface passivated in borate solution by comparing the results of in-situ and ex-situ nanoscratching test; the fractional coefficient obtained with ex-situ nano-scratching was remarkably smaller than that obtained with in-situ nanoscratching; in-situ nanoscratching results shown that increasing the potential in the passive region resulted in a higher frictional coefficient. On the other hand, the frictional coefficient obtained with ex-situ test was independent of the applied potential. They interpreted these results to the repassivation of the rupture sites at the moving front of the indenter tip. The movement of the indenter was resisted by the pile up formed due to the repassivation process. The repassivation process was promoted by the potential difference between the substrate and the solution.

The most common technique used to measure the mechanical properties of thin films is nanoindentation technique [70,71]. More details about the nanoindentation technique are introduced in the next chapter. The load discontinuities, as shown in figure 1-6, in the loading direction of the indentation curve are indicative of either dislocation nucleation and multiplication or a through-thickness fracture of the film [70,72-75]. Bahr

et al [70] suggested that the critical load at which the load discontinuity takes place depends on the presence of surface roughness, possible inclusions, and dislocations.

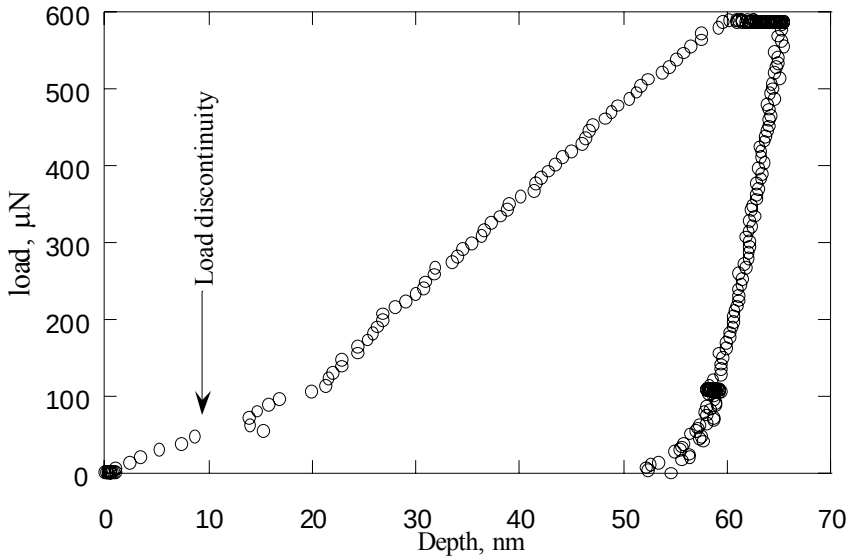

Figure1-6 the load discontinuity event in the nanoindentation curve

Oliver and Pharr [74] preformed nanoindentations into an electropolished single crystal of tungsten specimen; at low nanoindentation loads, the specimen exhibited purely elastic deformation upon unloading. A further increase in the load led to a rapid increase in the depth. An increase of the load above this load excursion resulted in that the material exhibited permanent plastic deformation. Similar behavior was observed by other researchers. Venkataraman *et al* [76] performed microindentation tests into an electropolished single crystal of Fe-3 wt. %Si. Prior to the load discontinuity, all the deformation was elastic upon unloading. A further increase in the load resulted in plastic deformation. The load discontinuity was not observed when the film was removed by a drop of 5% HCl solution on the surface of the specimen. Replacing the hydrochloric acid by distilled water led to the typical behavior, in which the load discontinuity was observed, of the experiment carried out without a liquid environment.

Mann and Pethica [77] have performed the first nanoindentation experiments where a tip and a sample are immersed in liquid. The experiments were conducted on GaAs in distilled water and single-crystal tungsten in aqueous HCl and distilled water. They demonstrated that the angle between the extension of the indenter and the liquid must be low to avoid the influence of capillary forces on nanoindentation results. Gerberich *et al* [78] investigated the yield phenomenon and the influence of the oxide film formed on a single crystal of an electropolished Fe-3 wt % Si specimen on its occurrence; they concluded that the yield point was controlled by a through-thickness fracture of the oxide film. Bahr *et al* [79] investigated the yield phenomena through the indentations of single crystals of tungsten and iron specimens; they pointed out that the absence of an existing dislocation field was the condition for the yield point process to take place. They verified this assumption by indenting mechanically polished and electropolished single crystals of tungsten specimens. For a mechanically polished single crystal of tungsten, the yield point process was not observed. On the other hand, yield point process occurred when electropolished single crystal of tungsten was indented. In another paper, Bahr and co-workers noted that the presence of an oxide film on nanoindentation during electrochemical control influences, but does not necessarily control, the yield point behavior [80].Y. Yao *et al* [81] examined the behavior of 10nm-thick oxide films formed on 316 SS in borate solution using nanoindentation technique along with scanning probe microscopy to conduct the nanowear test; a sudden jump in the displacement was observed when the passive film formed on 316 SS was indented. On the other hand, an indentation into the wear hollow where the film is removed did not exhibit the sudden jump in the displacement.

Wang and Li [68] used the ratio of the elastic deformation energy to the total deformation energy to study the effect of immersion of 304 SS in 3.5% NaCl for 16 hours on the passive film. They found that the immersion of the 304 SS decreased the ratio of the elastic deformation to the total deformation energies. Rodriguez-Marek *et al* [82] studied the influence of the applied potential and salt concentration on the mechanical response of the passive film formed on 304 SS. They found that an increase in the applied potential, below the Flade potential, in the passive region increased the load at fracture; they interpreted the change in the film strength to the film-thickness changes. Moreover, increasing the salt concentration in the electrolyte weakened the film strength. They related the reduction in the film strength to the film thinning caused by the halide ions. Pang *et al* [83] explored the influence of the applied potential on the mechanical properties of anodic oxide films on titanium. At a potential below the oxygen evolution potential, the load excursion increased with increasing the applied potential. Mudali and Katada [84] used Electrochemical Atomic Force Microscopy (ECAFM) to study passive films formed on nitrogen-bearing austenitic stainless steel. Using the fact that the steepness of the slope values of the force-displacement curve is related to the stiffness of the surface, they indicated that the stiffness of passive films decreased with an increase of applied potential. However, ECAFM can not truly quantify the strength of the films. The slope value of force-displacement curve of the passive film formed at the same potential decreased as the condition of the test was changed from ex-situ to in-situ.

One of the most popular chemical treatments to enhance the corrosion resistance of stainless steel by stabilizing passive films on alloys is a chromate or dichromate treatment [85]. M. Chiba and M. Seo [86,87] investigated the influence of dichromate

treatment on the mechanical properties of single crystal iron surfaces passivated in pH 8.4 borate solution by using an in-situ nanoindentation technique. They used the areas under the loading and unloading curves to define the elastic and plastic work, respectively, to study the effect of dichromate on the mechanical properties. The dichromate treatment increased the hardness and the ratio of elastic work to the total work of the passivated surfaces of single crystal iron. The load discontinuity in the load-depth curve of (110) surface of single crystal of iron disappeared due to the dichromate treatment. They interpreted this observation to the change of the structure of the passive film [87].

1.6 Research Focus

The focus of this research is to evaluate simultaneously the effect of multiple variables such as pH, salt concentration, time, temperature, potential, and alloy composition on the electrochemical and mechanical behavior of passive films on austenitic stainless steels by using the Taguchi method. This will determine if there is a direct link between the easily measured electrochemical behavior and the more complicated mechanical measurement. The mechanical behavior will be correlated to changes in the chemistry and the structure of the films. The effect of a dichromate treatment on the mechanical behavior and chemical composition of the passive film formed on 316 SS alloy at a stable passive potential will also be explored. The influence of the test conditions on the mechanical behavior of the passive film will be investigated by comparing the in situ and ex situ nanoindentation measurements. The tensile stress required to fracture the passive films will be roughly calculated.

An EG&G173 potentiostat and Greene cell will be utilized to determine electrochemical behavior, while measurement of electrochemically-controlled

mechanical properties of passive films for both in-situ and ex-situ will be carried out by a nanoindenter, a Hysitron Triboscope. XPS and Transmission Electron microscopy (TEM) are going to be used to investigate the composition and the structure of the passive films formed on austenitic stainless steel alloys.

Chapter 2

Testing Methodology and apparatus used

The experiment is a method of research which investigates the inference of cause and effect. The most common approach used to study the effects of parameters as they are set at different levels is the one-factor at a time experiment. This approach has the ability to test many parameters; each parameter has different levels; the strategy consists of selecting a starting level for each factor, then successively varying each factor over its range with the other factors held constant at the starting level. After completing all trials, a series of graphs are usually constructed showing the effect on the response of varying each factor with all other factors held constant [88]. For example, to study the effects of four factors at 3 different levels on a target, 81 (3^4) possible experimental evaluations are required. However, this method needs a very long time and high cost to approach the goal of the experiment. An alternative method by which the cost and the time of the experiments are reduced is Taguchi's approach [89].

2.1 Taguchi Method

The Taguchi method, also called robust design, was pioneered by Genichi Taguchi, a Japanese engineer, to improve quality control and the design of experiments. It is a statistical experimental design method. Taguchi's design process model consists of three stages: system design, parameter design, and tolerance design. System design is the stage in which the function or the object is determined. Parameter design is the step in which the factors that affect the desired target are selected; the factors are divided into controllable and noise factors. Noise factors are those cannot be controlled, or are too

expensive to control, and affect the performance of the target. An example of noise factors is the variation in operation environments, such as time of operation. Control factors are those parameters that can be easily adjusted and maintained such as choice of material or pH of the electrolyte. Tolerance design concentrates on improving the quality and productivity. An increase in cost is usually accompanied with tolerance design. Tolerance design is beyond the scope of this thesis.

2.1.1 Taguchi's Approach to Parameter Design

One objective of the Taguchi method is to select the best combination of control factors so that the target can be achieved with respect to the noise factors. Parameter design is the stage by which the best combination among the factors is achieved. The Taguchi method uses an orthogonal array provided from design of experiments to investigate a large number of parameters with a small number of experiments. Orthogonal arrays significantly decrease the experimental configuration needed to study the influence of many factors simultaneously. Moreover, the conclusion drawn from small scale experiments is valid over all the experimental configurations [90]. In order to be used easily, orthogonal arrays are simplified and tabulated by Taguchi [88]. A typical tabulation is shown in table 2-1. In this array, the columns are orthogonal which means that for any two columns, all combinations of parameter levels occur; and they all appear the same number of times. Here there are four parameters A, B, C, and D, each at three levels represented by -, 0, and +. This array is called an "L 9" design, with the 9 indicating the nine rows. The rows of the array represent the experiments or tests to be performed. [91]. An advantage of this method is that the 81 configurations or runs required to study the influence of the same factor on the same target mentioned above are

reduced to 9 run by using L9. The number of columns of an array illustrates the maximum number of parameter that can be studied using that array.

Table 2-1 L 9 (3^4) Orthogonal Array

	A	B	C	D
1	-	-	-	-
2	-	0	0	0
3	-	+	+	+
4	0	-	0	+
5	0	0	+	-
6	0	+	-	0
7	+	-	+	0
8	+	0	_	+
9	+	+	0	-

2.1.2 Guidelines for the Taguchi method

Taguchi outlines a specific approach to parameter design. Figure 2-1 illustrates a brief overview of the procedure followed by Taguchi [89,92].

2.1.2.1 Determine the target

The first level in the Taguchi method is to determine the target of the experiments. This target is the output or the response variable to be observed. Examples are weight, cost, corrosion, and film thickness and strength.

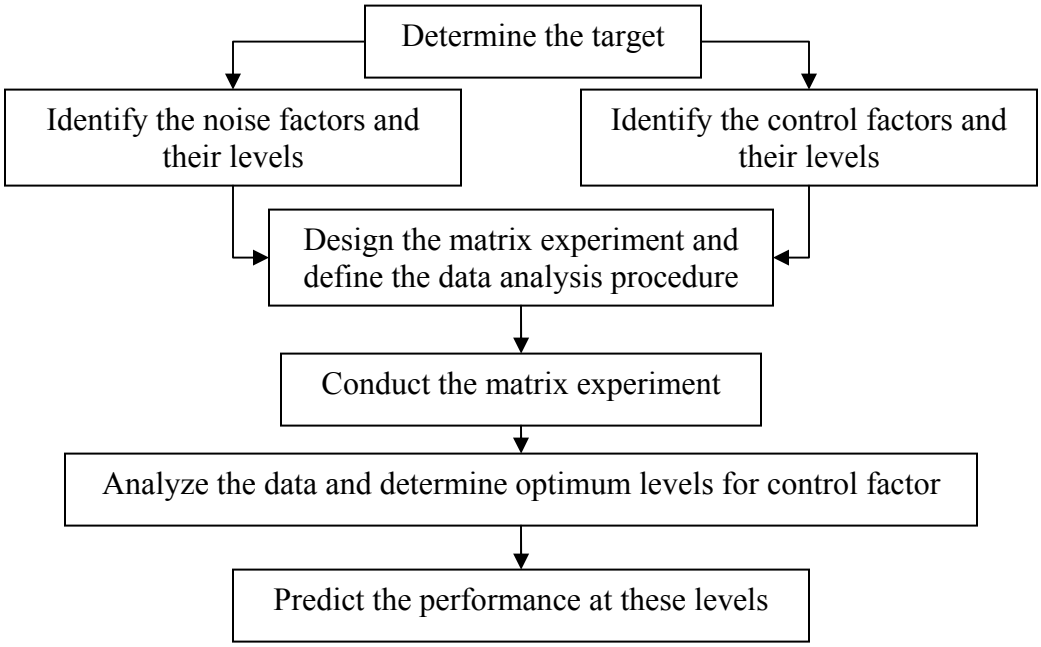

Figure 2-1 Flowchart of the Taguchi method

2.1.2.2 Identify the noise and control factors and their levels

The first step of the next level is to identify the noise factors which have a negative impact on the target of the experiments. Noise factors are the parameters which are out of control such as the environmental operation conditions. The second step in this level is to define and adjust the parameters thought to have significant effect on the target. Those parameters are the control factors, and are easy to set and maintain. The levels of noise and control factors must be chosen at this step in the process [93].

2.1.2.3 Design the matrix experiment and define the data procedure

The next step is to design the matrix experiment through selecting of the appropriate orthogonal arrays for both noise and control factors. Many standard orthogonal arrays are provided by Taguchi [88]. A procedure to analyze the influence of noise as well as control factors on the target needed to be defined after selecting the

appropriate matrix. The common procedure proposed by Taguchi to study the effect of the noise factors on the mean and variance of the target is based on using the orthogonal arrays as shown in figure 2-2 which illustrates what is known as the crossed array format. In figure 2-2, L 9 is used as control factor array, the inner array, combines with the 2^2 full factorial array, the outer array, to form the crossed array [94]. Using a crossed inner and outer array gives the chance to evaluate the mean and variance of the target's response resulted from the variation in the noise factors [88, 91,95]. Allowing each configuration of the inner array to be run at four different combinations of the noise array determines the mean and variance of each configuration of the control factors. The results of the experiment for each combination of control and noise array experiment are labeled by Y_{ij} in figure 2-2.

					E	-	-	+	+			
					F	-	+	-	+			
	A	B	C	D	Y_{ij}						Y_k	Std
1												
2												
3												
4												
5												
6												
7												
8												
9												

Figure 2-2 the Crossed array format

2.1.2.4 Conduct the matrix experiment

The next level in the Taguchi method is to conduct the crossed array experiments using the adjusted configurations and record the results. The standard deviation and the mean of each configuration is determined and recorded in a separated column.

2.1.2.5 Analyze the data and determine optimum levels for control factor

After the experiments have been carried out, the influence of the parameters on the target must be determined. Moreover, the recommended level, which improves the performance to achieve the desired target, for each factor is determined. Obtaining the significant factor and the recommended level depends on graphical and numerical methods.

The most common numerical method by which the influence of the factor is investigated is the P-value. The P-value is the largest level of significance which will lead to acceptance of the null hypothesis, which is that there is no difference among the factors being studied, with the given data. The P- value determines if the results are likely due to chance. Another numerical way is the sum of squares by which the contribution of each individual control factor on the target is determined. The way in which the sum of squares determines the contribution of each control factor is as follows, taking the average in figure2-2 as an example:

1- the overall average is given by

$$\bar{Y} = \sum_{K=1}^{9} Y_K \qquad (2\text{-}1)$$

Where Y_k is the average of each run.

2- the grand total sum of squares is determined by

$$GTSS = \sum_{K=1}^{9} (Y_K)^2 \qquad (2\text{-}2)$$

The grand total sum of squares can be divided into two parts:

a- the sum of squares due to the overall average

$$SS \text{ due to the overall average} = (\#\text{ of runs}) \times (\bar{Y}) \qquad (2\text{-}3)$$

b- The sum of squares due to the variation about the average, called the total sum of the squares

$$\text{Total SS} = \sum_{k=1}^{9} (Y_K - \bar{Y})^2 \qquad (2\text{-}4)$$

the grand total SS= total SS+ SS due to overall average.

3- The percentage contribution of each control factor on the overall average is found by using the following equation

$$\text{Percentage contribution} = (\boldsymbol{SS}_{\boldsymbol{factor}} / \text{total SS}) \times 100 \qquad (2\text{-}5)$$

For the L9,

- Three runs for factor A at level (-) (run1, 2, and 3)
- Three runs for factor A at level (0) (run, 4, 5, and 6)
- Three runs for factor A at level (+) (run 7, 8, and 9)

Therefore, for factor A, the sum of the squares, SS_A, due to variation about the overall average is

$$SS_A = (\#\text{ of exp. at A(-)})(\bar{Y}_{A(-)} - \bar{Y})^2 + (\#\text{ of exp. at A(0)})(\bar{Y}_{A(0)} - \bar{Y})^2 + (\#\text{ of exp. at A(+)})(\bar{Y}_{A(+)} - \bar{Y})^2 \qquad (2\text{-}6)$$

where $\bar{Y}_{Ai}$ is the average of the $3Y_k$ for each level (i = -, 0, or +).

The first graphical method by which the influence of the control factors on the response of the experiments is determined is called the main effect plot. The main effect plot is used to see if the overall mean varies with the levels of each individual control factor. The plot shows mean values for two or more levels of each factor. The means for a single factor are connected by a straight line. The main effect plot is formed by the vertical axis representing the mean for each level of the factor and horizontal axis illustrating the factors and their levels. The rules used to draw this plot are as follows:

1- Determining the overall average using equation (2-1)

2- Defining the deviation caused by a factor level from the overall mean. The effect of factor A at level (-) in figure 2 is taken as an example. Factor A is at level (-) for runs 1, 2, and 3. the average for these runs is given by

$$Y_{A(-)} = \frac{1}{3}(Y_1 + Y_2 + Y_3) \qquad (2\text{-}7)$$

Thus, the effect of factor A at level (-) is given by $(Y_{A(-)} - \bar{Y})$. The averages for level (0) and (+) of factor A, as well as those for the various levels of the other factors, can be obtained in a similar way. Figure 2-3 illustrates schematically a plot of the main effects. from the plot, factors B and D lead to a significant shift in the location of the response variable as we go from the "-" level to "+" level of the factor B and going from (+) level to (-) level of factor D.

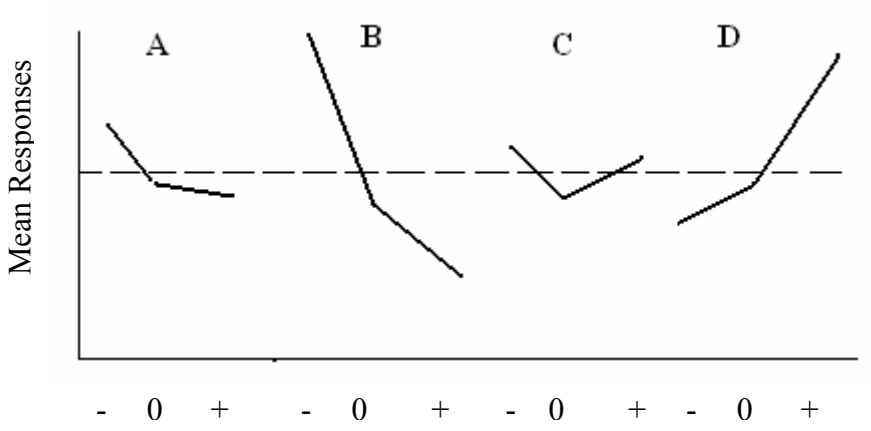

Figure 2-3 Schematic plot of main effects, Cases B and D show significant effects on the response.

The second graphical way to determine the significance of the factor is by using half-normal probability plot, which is a plot of points ($X_{(i)}$, $Y_{(i)}$), where $X_{(i)}$ the difference among the levels for each individual control factor. For factor 1 with two levels, $X_{(1)}$ is difference between the averages of the two levels. The values of $X_{(i)}$ are ordered from the smallest to the largest by $X_{(1)}$, $X_{(2)}$,……, $X_{(n)}$, where n the total number of the factors, on the X axis. The Y(i) values are determined by

$$\boldsymbol{P_i} = \frac{1}{2}\left(1 + \frac{\boldsymbol{i} - 0.375}{\boldsymbol{n} + 0.25}\right) \qquad (2\text{-}8)$$

The vertical axis is then formed by using the obtained P-values and using the table of the standard normal distribution [96,97]. Figure 2-4 illustrates a schematic of the half-normal probability plot. The procedure used to distinguish among the significance of the factors on the target is to draw a line from either the origin or near zero passing through most of the points as shown in figure 2-4; the points on or close to the line are not significant while the points which lie far away from the line have a significant effect on the target. The disadvantage of this plot is that the best level of a factor cannot be determined. The

numerical and graphical methods mentioned above are easily preformed by Minitab™ software , a commercially available statistical analysis software package.

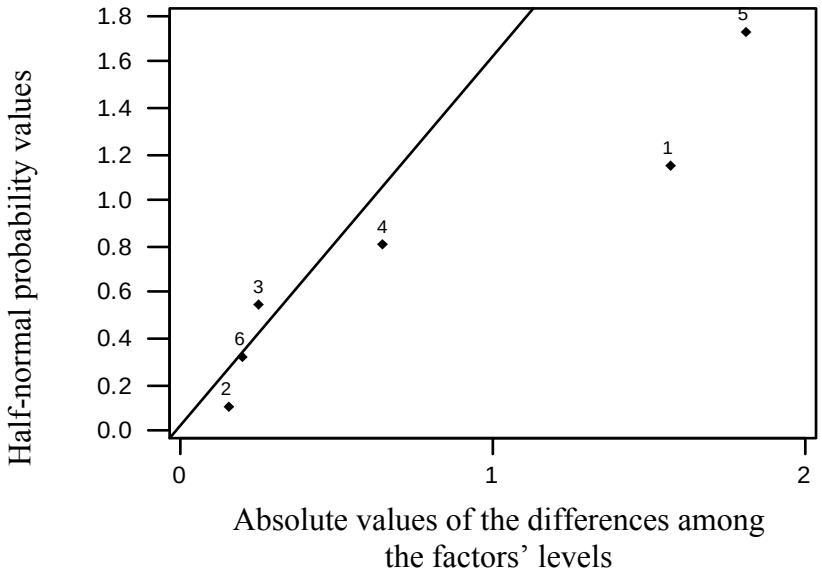

Figure 2-4 Schematic for half-normal probability plot

2.1.2.6 Predict the performance at these levels

The final level and the goal of the Taguchi method for parameter design is an experimental confirmation which is a run using the best settings of the control factors being investigated [91,98]. The significant factors as well as their levels are determined by the ways mentioned above such as the main effect and half-normal plots. These factors and their levels are combined to initiate the model, which is based on the regression model, used to predict the performance [90]. The general form of the predictive equation is as follow:

$$\mu = \beta_0 + \beta_1 x_1 + \beta_2 x_2 + ... + \beta_{12} x_1 x_2 + \varepsilon \qquad (2\text{-}9)$$

Where μ is the predicted average, β_0 is the observed average from the experiments, β_1, β_2 are the regression coefficients, x_1, x_2 are the control factors, and ε is the random error [88]. The regression coefficient of each individual control factor is estimated by using the least squares criterion. Factor A with two levels (-1) and (+1) is represented as an example to estimate β_A.

$$\beta_{\mathrm{A}} = \frac{\bar{\mathrm{A}}(+1) - \bar{\mathrm{A}}(-1)}{(+1)^2 + (-1)^2} \qquad (2\text{-}10)$$

where A bar is the average of the factor A at the specific level.

The variation of the predicted response, μ, due to the random error, ε, can be estimated as follow:

$$\mu \pm \boldsymbol{t}\sqrt{\mathrm{var}(\mu)} \qquad (2\text{-}11)$$

Where var(μ) involves the error variance σ^2 which must be estimated from the data with mean squared error, MSE, and t is the value from the t-tables with degrees of freedom that of MSE. More details about the variation of the new response due to the random error will be presented in the next chapters to predict the load at fracture of the passive films.

The method used to collect and analyze the data of the experiments through this thesis was described above. The reminder of this chapter gives an overview of the facilities used to grow, characterize the surface, investigate the structure, and to measure the load at fracture of the thin films. A brief description for the potentiostat, X-ray photoelectron spectroscopy, transmission electron microscopy, and nanoindentation techniques are introduced.

2.2 Potentiostat for electrochemical film growth

The corrosion rate as well as the growth of the passive film on stainless steel can be determined from the anodic polarization curves using a potentiostat [99,100]. The potentiostat is considered an amplifier to control the voltage between two electrodes, a working electrode and reference electrode, at a constant value. The potentiostat has two functions: to measure the applied potential between the working and reference electrodes and to compare it with the preset constant voltage, and convert the change in the potential to current and force a current flow between the counter and working electrodes.

In this study, the anodic passive films are grown using an EG&G Model 173 potentiostat coupled with an EG&G Model 175 universal programmer. Data are acquired at 3 Hz using a Hewlett-Packard 3497 A data acquisition system for analog to digital conversion, and stored onto a PC using an IEEE488 bus and software developed at Washington State University. To ensure the same test conditions, the scan rate for the polarization curves in this study is 2mV/sec for all the experiments. The commercially available Microsoft Excel software is used to develop a program which is able to visualize the measurements of a polarization behavior of the sample under the study in real time.

2.3 X-ray Photoelectron Spectroscopy

X-ray photoelectron spectroscopy (XPS) is a powerful technique used for the surface analysis of materials such as metals. In XPS a photon is absorbed by an atom in a molecule or solid, leading to ionization and the emission of a core (inner shell) electron, which in turn emits energy which can cause the release of an outer shell electron, a “photoelectron”. The kinetic energy distribution of the emitted photoelectrons can be

measured using an appropriate electron energy analyzer and a photoelectron spectrum can thus be recorded. One way to look at the process of photoionization is as follows:

$$A + h\nu \text{ --> } A^{+} + e- \qquad (2\text{-}12)$$

where A is an atom, hν is energy of a photon, and A^{+} is an ionized atom. This expression can then be expressed by using the kinetic energy, KE, of the photoelectron as follows:

$$KE = h\nu - (E(A^{+}) - E(A)) \qquad (2\text{-}13)$$

The final term in brackets, represents the difference in energy between the ionized and neutral atoms, is generally called the binding energy (BE) of the electron. Therefore, the kinetic energy of the photoelectron can be expressed by commonly quoted equation:

$$KE = h\nu - BE \qquad (2\text{-}14)$$

For each element, there is a characteristic binding energy associated with each core atomic orbital. For example, each element will give rise to a characteristic set of peaks in the photoelectron spectrum at kinetic energies determined by the photon energy and the respective binding energies. Therefore, the presence of peaks at particular energies indicates the presence of a specific element in the sample under investigation [101]. Figure 2-5 shows an example for a real XPS spectrum obtained from a Pd metal sample using Mg Kα radiation.

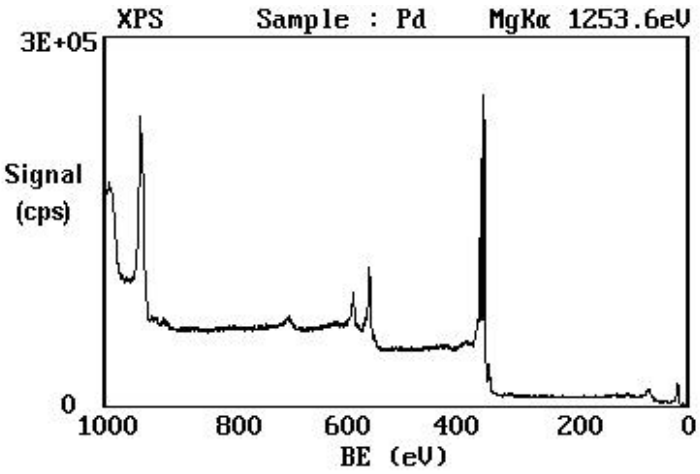

Figure 2-5An example for a real XPS spectrum obtained from a Pd metal sample using Mg Kα radiation, from [101].

XPS offers several features which make it ideal for characterizing thin oxide films: the relatively low kinetic energy of the photoelectrons makes XPS inherently surface sensitive (1-5 nm); the energy of the photoelectron is not only characteristic of the atom from which it was ejected, but also in many cases, is characteristic of the oxidation state of the atom [100,101]. The lateral resolution is about 60μm.

Measurements of the thickness of surface layer as well as the compositional depth profile are obtained by using ion sputtering such as Ar^+. Argon ions impact the surface of the sample at controlled power and rate. After a certain time of this process, the composition of the surface is analyzed before the next impact starts. A compositional depth profile, then, is obtained. The depth profiles are usually smooth curves especially in the curve of the oxygen due to redeposition during analyses. The XPS analyses of this study were performed with a Kratos Axis-165 X-Ray Photoelectron Spectrometer using a Mg K alpha-X-ray source.

2.4 Transmission Electron Microscopy

When a high energy electron beam strikes a sample, this beam is affected by reacting with the sample. Figure 2-6 illustrates most of the reactions of the incident electron beam with a sample. The reactions on the top of the sample are utilized when examining thick or bulk specimens by using scanning electron microscopy (SEM). On the other hand, the reactions on the bottom side, especially the direct beam and elastically scattered electrons, are used for imaging and diffraction modes of transmission electron microscopy (TEM).

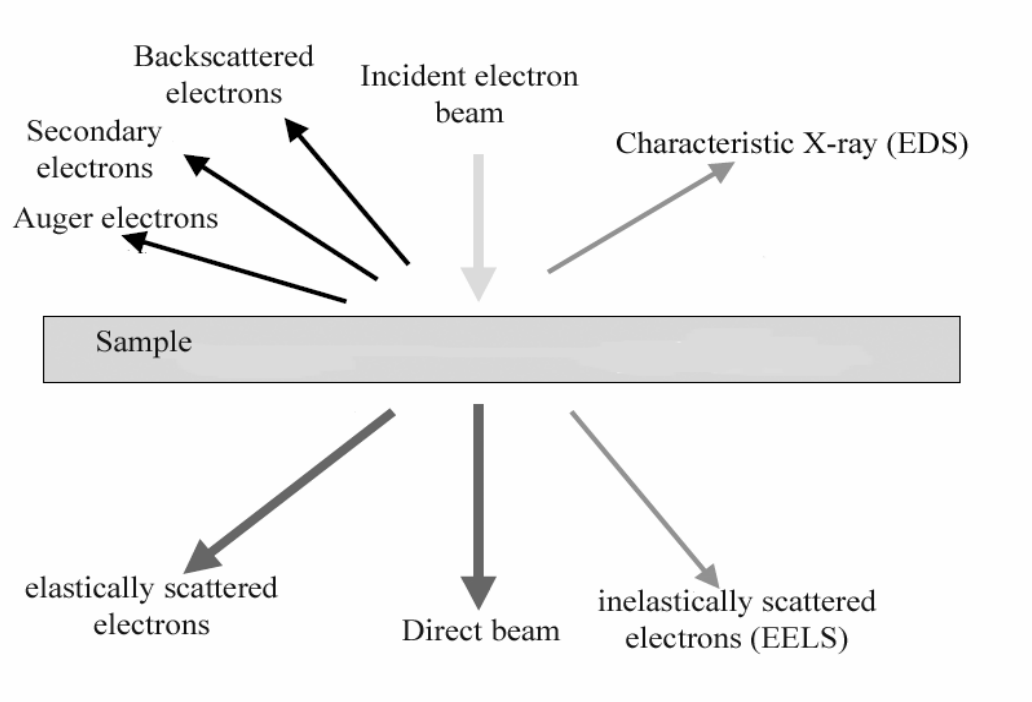

Figure 2-6 Signals generated when the electron beam penetrates a thin sample

The limited penetration of electrons requires that a sample must be very thin or sliced into thin section (50-100nm) to allow electrons to pass through. One of the greatest advantages of the TEM is the excellent resolution due to depending on the wavelength of

the electron, i.e., the smaller the wavelength the greater the resolution. The wavelength (λ) of 200Kv TEM is equal to 0.00251nm [102]. The high resolution, which is capable of investigating the structure of the thin films, is approximately determined as follow:

$$\delta = \frac{0.61\lambda}{\beta} \qquad (2\text{-}15)$$

where β is the semiangle of collection of the magnifying lens. Due to the limitation of the lenses, TEM does not approach the technique's theoretical resolution.

Diffraction mode and image mode are the two widely used methods of specimen observation obtained by TEM [101]. The microstructure, such as the grain size and lattice defects, is observed by image mode. On the other hand, the crystalline structure, such as the Bravais lattice and lattice parameters, is studied by diffraction mode [101]. The diffraction pattern is produced from diffraction of the electron beam off of planes in the sample. The pattern is a scaled representation of a section of the reciprocal lattice. Each spot represents a plane in the crystal that has diffracted. The diffraction patterns are typically taken when the sample is tilted so that the electron beam is passing down a particular crystallographic zone, with each diffracted spot in the pattern representing a plane which passes through that zone. The patterns produced will vary with different zones and for different crystal structures. Figure 2-7 is an example for an electron diffraction pattern.

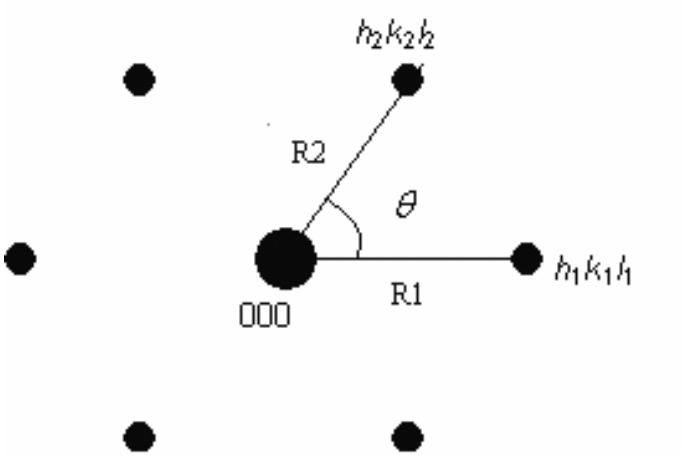

Figure 2-7 An exmaple of a diffraction pattern

Indexing the diffraction pattern utilizes the fact that the electron beam is not reflected from any array of atoms arranged in a plane, but from atoms arranged in planes that satisfy Bragg's law. Moreover, the inter-planar angles between these planes are constant. Therefore, each structure has allowed and forbidden reflections. The relation between the distance R, the distance between the spots, on a diffraction pattern and the interplanar spacing in a crystal is described by [103]:

$$Rd = \lambda L \qquad (2\text{-}16)$$

where L is the camera length. Indexing diffraction pattern is illustrated by using figure 2-7. The first method is by measuring R in a diffraction pattern. The interplanar spacing is then determined by using equation (2-16). If the crystal structure of the specimen is known, it is easy to index the diffraction pattern by comparing the d-spacing obtained from the diffraction pattern with those obtained from the allowed reflections. The second method is by using the angle between the line joining spots $h_1k_1l_1$ and $h_2k_2l_2$ to spot 000. This is equal to the angle between $(h_1k_1l_1)$ and $(h_2k_2l_2)$ planes [103]. In this study, a CM

200 Philips transmission electron microscopy operated at 200 kV is used to investigate the structure of the passive films grown in different conditions.

2.4 Nanoindentation Technique

One of the most advanced techniques available for determining the mechanical properties of very small volume materials is Depth Sensing indention, DSI. When carried out at very small (10 – 1000 nm) depths, the technique is referred to as nanoindentation. In the DSI technique, a known geometry indenter is forced into the surface of the examined material. This method produces a continuous record of the penetration depth of an indenter as the load is increased between the tip and sample, producing what is referred to as a loading-unloading curve [104]. The unloading portion of this curve is analyzed to obtain the mechanical properties such as the hardness and elastic modulus. Figure 2-8 illustrates

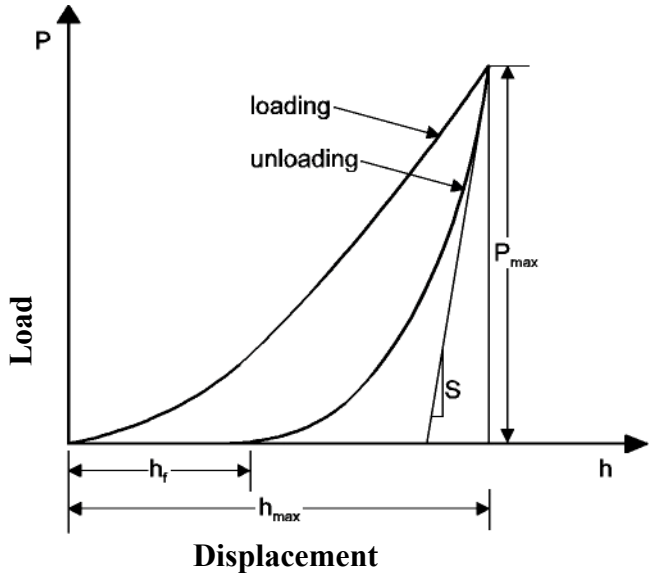

Figure 2-8 Typical load-displacement curve obtained by nanoindentation

a typical load-displacement curve obtained by indentation. In the loading direction, the indenter penetrates into the surface of the material resulting in increasing of the indentation depth as the load increased up to the maximum load. In the unloading direction, on the other hand, the nanoindentation depth decreased with decreasing the nanoindentation load. Due to the plastic deformation of the tested material, the indentation depth do not achieve zero when the nanoindentation load reaches zero [105]. In the unloading direction, the regular removal of the load results in the recovery of the elastic deformation by which the most two mechanical properties, elastic modulus and hardness, are measured.

Oliver and Pharr [74] measured the elastic modulus E and the hardness H of the materials using the following equations:

$$\boldsymbol{S} = \frac{2}{\sqrt{\pi}} \boldsymbol{E_r} \sqrt{\boldsymbol{A}} \tag{2-17}$$

$$\boldsymbol{E_r} = \frac{(1-\nu^2)}{\boldsymbol{E}} + \frac{(1-\nu_i^2)}{\boldsymbol{E_i}} \tag{2-18}$$

$$\boldsymbol{H} = \frac{\boldsymbol{P}_{\max}}{\boldsymbol{A}} \tag{2-19}$$

Where S is the slope of the initial portion of the unloading curve as shown in figure 5, E_r is the reduced modulus, A is the projected area, $E,\ \nu, E_i, and \nu_i$ are the elastic modulus and Poisson's ratio for both the specimen and the indenter, H is the hardness, and P_{max} is the maximum load as shown in figure 2-5. In the study described in this dissertation, nanoindentation measurements of fracture loads of passive films anodically formed were performed using a Hysitron Triboscope with a Park Auto probe CP Scanning Probe Microscope (SPM).

Chapter 3

Electrochemical Behavior

The potentiodynamic polarization technique is a method used to measure the polarization behavior of an alloy in an electrolyte. The polarization curve is a plot of the current to or from the working electrode, specimen, in a log scale versus the applied potential. The corrosion rate can be determined from the corresponding current to which the corrosion rate is directly proportional. Once the measured current is known, the corrosion rate in millimeters per year, mm/year, is determined based on Faraday's law.

$$\text{Corrosion rate} = 3.15 \times 10^5 \frac{i_{cor} M}{FZ\rho} \qquad (3\text{-}1)$$

Where i_{cor} is the current density in Amp/m^2, M is molecular weight in g/mole, F is the Faraday constant, 96485 C mole^{-1}, Z is the valance state of metal in oxidized form, and ρ is the density of corroding species.

The aims of this chapter were to study the influences of the alloy chemistry, solution pH, and salt concentration, adjusted by HCl and NaCl, respectively, on the polarization behavior and to determine the ranges of stable passive and metastable pitting potentials. The polarization curves were then used as a reference to grow the passive film at the desired potential.

Experimental Procedure

Three different types of austenitic stainless steel, 304, 316, and 904L, were studied using rod specimens 12 mm long and 6mm diameter. The chemical composition of the alloys is given in Table 3-1. Specimens were abraded through 600 grit SiC paper. The exposed area of the test was 28 mm^2.

Table 3-1 Typical Chemical Composition, Wt %, of Alloys, balance iron

Stainless steel	C	N	Cr	Ni	Mo	Others
304	0.04	0.06	18.3	8.7	-	-
316	0.04	0.06	17	11	2.7	-
904L	0.01	0.06	20	25	4.5	1.5Cu

Electrochemical measurements were made using an EG&G 173 and 175 Potentiostat/Galvanostat and controller. A graphite and silver/silver chloride were used as a counter and reference electrodes, respectively. All the experiments were conducted in a Greene cell which is shown in figure 3-1. The electrolyte volume for all experiments was 500 ml.

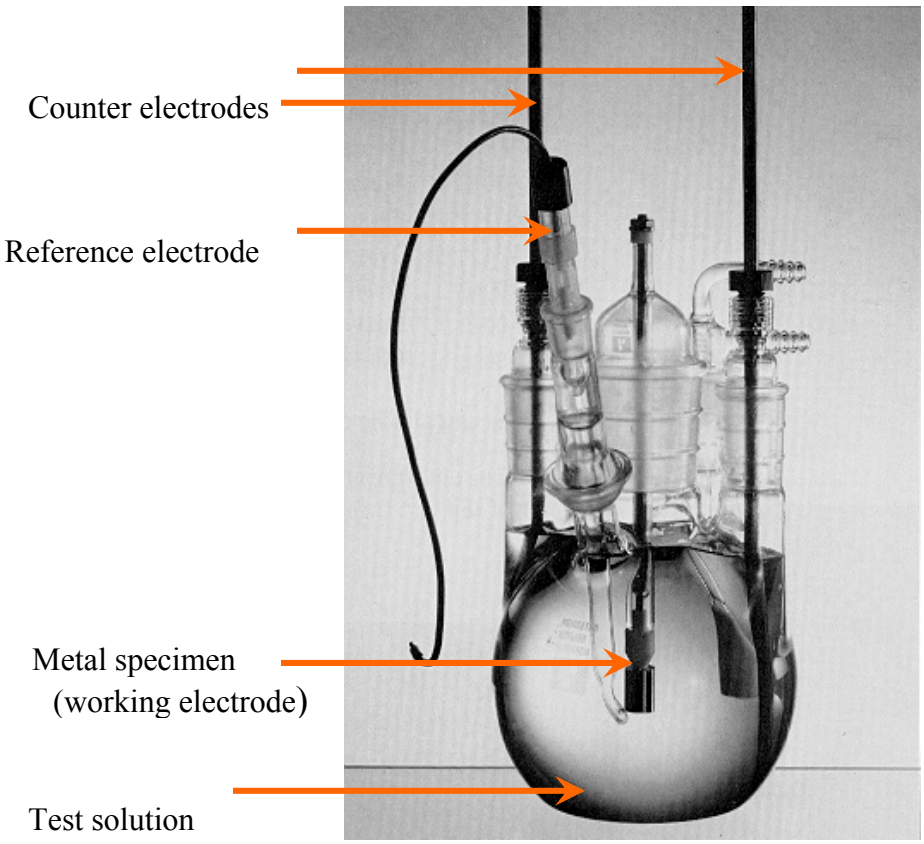

Figure 3-1 Standard Greene Cell

Nine different conditions were used to study the polarization behavior of the stainless steel alloys; for each condition, three experiments were conducted to determine the average of the passive current. The specimen was held cathodically for one hour prior to running potentiodynamic polarization curves to ensure steady state. After the experiments were conducted, the data were statistically analyzed using Minitab®, a commercial software program, as shown in appendix 1-1.

Results

Figure 1 shows the typical polarization curves of 304 SS alloy in different chloride solutions. Table 1-2 shows the solution conditions used to study the polarization behavior, the passive current, and the average of the passive current. SS stands for the stainless steel alloy, SC stands for the salt concentration in the electrolyte, and *i* (1-3) is the passive current for each experiment.

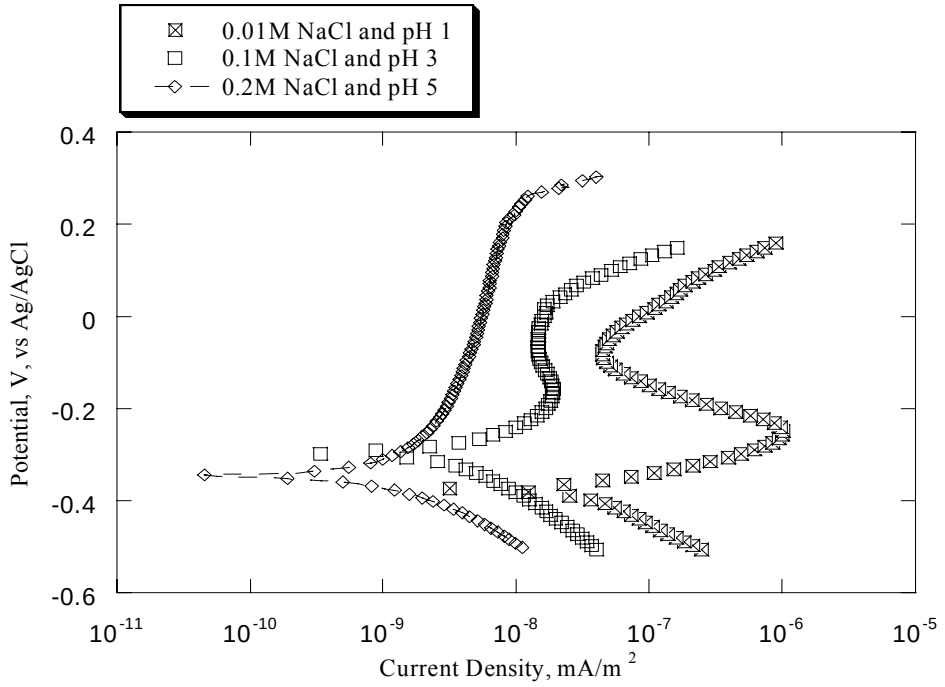

Figure 3-2 Polarization curves for 304 SS in different chloride solutions

Table 3-2 the solution conditions used to study the polarization behavior and the average of the passive current in mA

SS	pH	SC (M)	*i-1*	*i-2*	*i-3*	*Average*
304	1	0.01	0.0016	0.0019	0.0018	0.001767
304	3	0.1	0.0005	0.0011	0.0006	0.000733
304	5	0.2	0.00016	0.00015	0.0002	0.00017
316	1	0.2	0.0019	0.0016	0.0016	0.0017
316	3	0.01	0.0006	0.0006	0.00065	0.000617
316	5	0.1	0.0001	0.00008	0.00014	0.000107
904	1	0.1	0.001	0.00074	0.001	0.000913
904	3	0.2	0.0003	0.00047	0.00027	0.000347
904	5	0.01	0.0002	0.0001	0.00016	0.000153

The influence of the alloy chemistry, pH, and salt concentration overall average of the passive current is illustrated by figure 3-3 which is called the main effect plot.

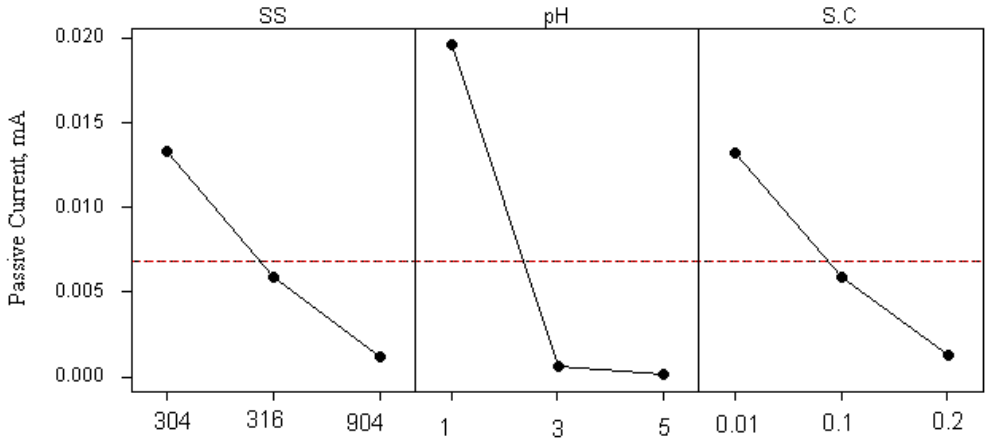

Figure 3-3 Factor effect plot for the passive current of the systems.

In figure 3-3, the dashed line illustrates the overall average of the passive current obtained from the three tests of each of the nine conditions. For the alloy chemistry, increasing both the chromium and molybdenum content in the alloy decreased the corrosion rate. Similar results were obtained when the chromium content in the alloy increased [22]. The pH of the solution was found to be the most important factor affecting the corrosion rate. Increasing the pH from 1 to 3 decreased the dissolution rate. A further increase in the pH from 3 to 5 had almost negligible effect. Decreasing the chloride ion concentration in the electrolyte led to a wider passive potential region. On the other hand, an increase of the chloride ion concentration shifted the pitting potential to more negative value. Similar influences were observed by Zue *et al* [106] and Uhlig [107]. The passive current decreased when the salt concentration was increased from 0.01M NaCl to 0.2 M NaCl; this effect might be due to the formation of the salt film on the surface of the sample which might affect the escape of the metal ion to the electrolyte.

Chapter 4

Effects of alloy and solution chemistry on the fracture of passive films on austenitic stainless steel

Tremendous numbers of studies have covered the electrochemical behavior of the passive film formed on stainless steel alloys. The invention of facilities which are capable of probing the small volumes such as thin films, on the other hand, opened the door to the researchers to investigate the mechanical behavior of the thin films during last decade. As mentioned in chapter 1, the passive film is influenced by several factors such as solution pH, alloy chemistry, and salt concentration in the electrolyte.

The goal of this chapter is to simultaneously evaluate the effect of multiple variables such as pH, salt concentration, time, temperature, and alloy composition on the stress needed to cause fracture of passive films formed on austenitic stainless steel alloys in the stable potential passive region using the Taguchi method.

Experimental Procedure

Three different types of austenitic stainless steel, 304, 316, and 904L, were studied using rod specimens 12 mm long and 6mm diameter. The chemical composition of the alloys is given in Table 3-1. Specimens were abraded through 1200 grit SiC paper, and then were electropolished in a solution of 95% acetic acid 5% perchloric acid at room temperature at current density of approximately 1mA/mm^2. The exposed area of the test was 28 mm^2.

The Taguchi method was chosen to investigate the effects of multiple variables on the strength of passive films. Using this method provides the ability to study the effect of multiple variables simultaneously, to study the influence of individual factors on the performance, and determine which factor has the most significant influence. There are

usually two matrices that represent the design of Taguchi method. The design matrix (inner array), whose values are controllable, consists of three factors, each one has three levels, and Table 4-1 represents this matrix. The second matrix consists of noise factors (outer array) whose values are associated with the operational environment. In this study it consists of two factors; temperatures of 15°C and 40°C and polarization times of 60 and 120 minutes. The design matrix consists of three columns and nine rows. In each row of the inner array there are four observations across the outer array. The combination of outer and inner arrays varies the conditions used to grow the passive film.

Table 4-1 Factors of The Design Matrix

Salt Concentration (M) NaCl	pH	Stainless steel
0.01	1	304
0.1	3	316
0.2	5	904

Passive films were grown using an EG&G 173 and 175 potentiostat and controller. The chloride test solutions, adjusted to the required pH and salt concentration (with HCl and NaCl) were aerated in a Green cell with Ag/AgCl and graphite as reference and counter electrodes, respectively [82]. Nanoindentation measurements of fracture loads of passive films anodically formed were performed using a Hysitron Triboscope with a Park Auto probe CP Scanning Probe Microscope (SPM). A maximum force of 500 μN was used for the nanoindentation tests. The indentation tests were made using a diamond cube corner tip and the loading rate was 50 μN s^{-1}. The XPS analyses

were performed with a Kratos Axis-165 X-Ray Photoelectron Spectrometer using a Mg Kα-X-ray source.

Figure 4-1 shows the typical electrochemical behavior of 304 SS in a solution of a pH of 1 and salt concentration of 0.01 M NaCl, respectively. To measure the fracture load of the passive film formed in the same solution, the potential was held cathodically approximately for 40 minutes then anodically polarized by scanning the potential at constant rate of 2mV/s to -0.15V, as shown in figure 4-1, and then held for two hours at 40°C to grow the passive film.

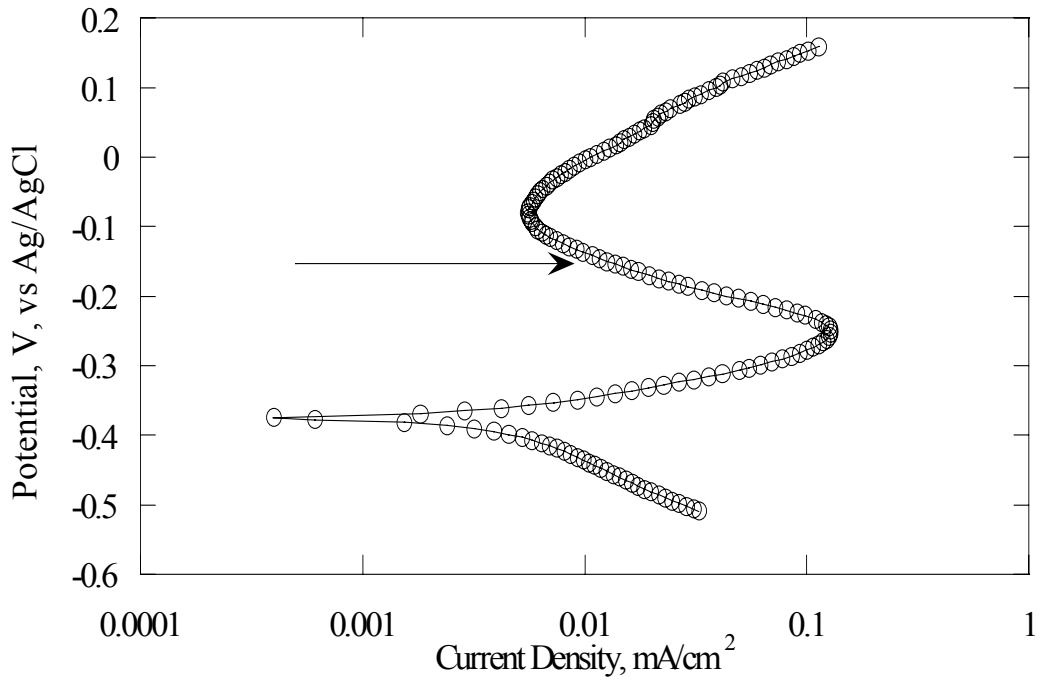

Figure 4-1Electrochemical Behavior of 304SS in Solution of pH 1 and 0.01M NaCl

The specimen was then removed from the solution, rinsed with deionized water, and glued on an iron disk to be indented. To ensure the similarity of the test conditions, the time between the polarization and indentation during which the specimen was

exposed to air was kept constant for all the growth conditions; the exposure time was 10 minutes. Indentations were performed in ambient air. The load at which the first loading discontinuity occurred, for instance 38 μN, for the indentation shown in Figure 2, was recorded from each indentation. After the nanoindentation measurements were carried out the specimen was cleaned sequentially in an ultrasound bath with acetone. For each growth condition the specimen was held cathodically for 40 minutes to remove the ambient passive film before growing the film.

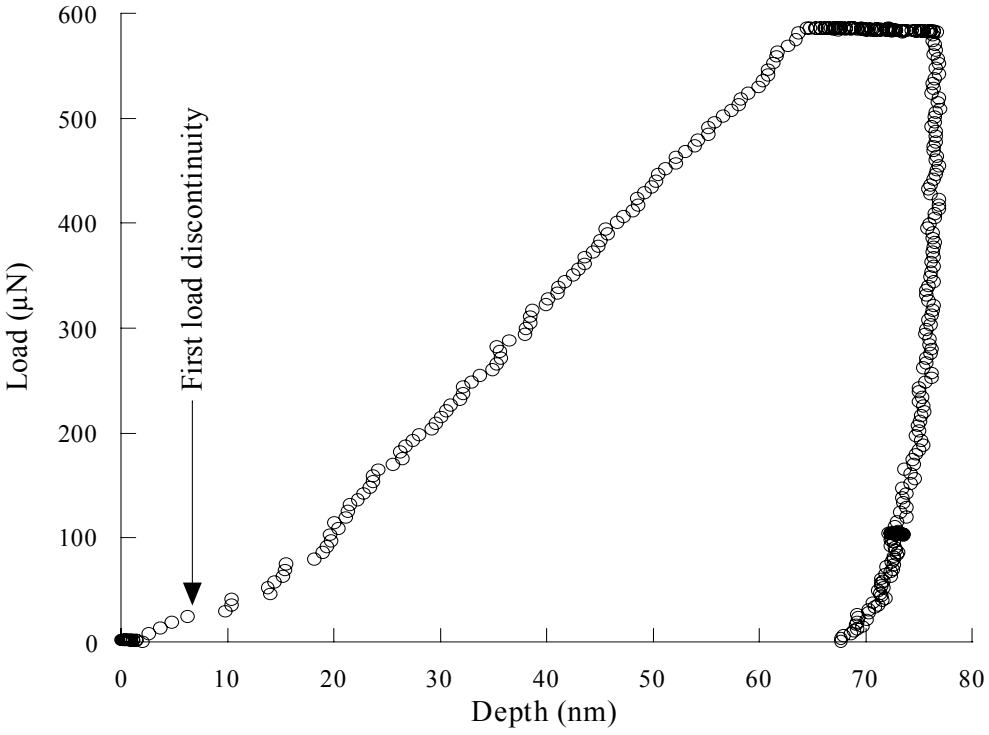

Figure 4-2 Load-Depth Curve for an indentation of Cr2O3 film on a 304 SS

Result and Discussion

To diminish the error in the load at fracture which might be produced by indenting a site which may have a subsurface defect such as an inclusion, multiple tests

were performed on each sample. The average of at least six indentations in two different grains of each alloy is shown in Table 4-2. Table 4-2 shows the design, conditions, and the averages of at least 400 indentations for the fracture loads of passive films formed in the stable passive potential range. The same procedure was used to determine the fracture loads of passive films formed under the different conditions. After the experiments were concluded the data were statistically analyzed using Minitab®, a commercial software program as shown in appendix 1-2.

Table 4-2 The design, conditions, and the averages of fracture load of passive films formed in stable potential passive region

Time (min)				**60**	**120**	**60**	**120**
Temperature (°C)				**40**	**40**	**15**	**15**
Run	**S.S**	**pH**	**Salt.Con (M)**	**Fracture Load, μN**			
1	304	1	0.01	42.11	68.15	74.89	69.00
2	304	3	0.1	49.78	50.06	43.20	41.89
3	304	5	0.2	46.66	57.91	53.27	60.48
4	316	1	0.2	46.39	40.086	37.52	42.75
5	316	3	0.01	41.489	48.03	38.01	41.58
6	316	5	0.1	26.49	40.52	35.32	47.21
7	904	1	0.1	55.18	60.83	56.65	60.93
8	904	3	0.2	65.67	68.45	50.480	58.93
9	904	5	0.01	51.489	62.59	58.24	67.84

Figure 4-3 shows the fracture load average of the passive film grown at each growth condition. The X-axis represents the growth conditions of the passive films while the Y-axis represents the load needed to break the passive film in micronewton. The bars show the standard deviation while the dots illustrate the fracture load average of the passive films for each growth condition.

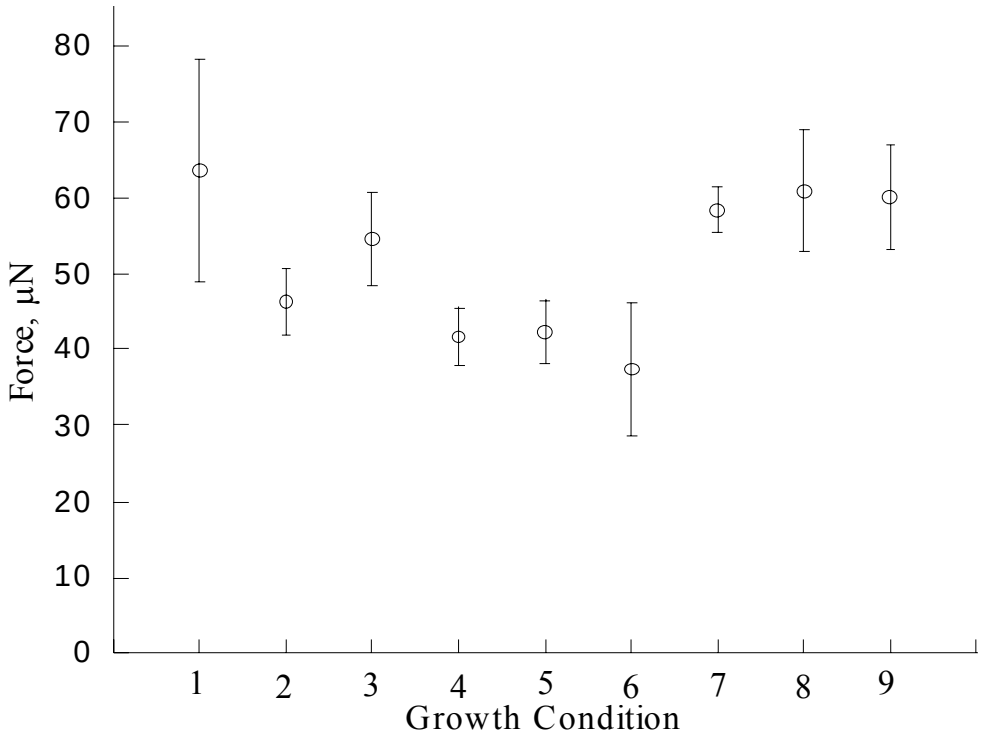

Figure 4-3 The averages and standard deviations of the fracture loads obtained from at least six indentations for the passive films formed at different growth conditions represented by table 4-2

Since each factor has three levels, its effect on the fracture load is either linear, L, or quadratic, Q. Analyzing the data using a 0.05 significance level shows the quadratic effect of alloy chemistry, as shown in Figure 4-4, has the most significant effect on the fracture load of passive films with a P- value equal to 0.027.

Figure 4-4 is called the main effect plot, which represents how the fracture load is affected. It is a plot of the load, μN, in the Y axis versus alloy chemistry (304SS, 316SS, 904L), pH (1, 2, and 3), and salt concentration (, 0.01, 0.1, and 0.2) in the X axis. The dashed line illustrates the overall average of the passive film fracture load. The passive film fracture load is affected by the substrate on which it is grown. The fracture load decreases by changing a 304 SS to a 316 SS substrate, and the maximum fracture load is observed when the films are grown on a 904SS substrate. Linking the fracture load of passive films with the chromium concentration of the alloy on which the passive films formed reveals that increasing the chromium concentration of the alloy increase the load needed to break the films. The fracture load decreases with increasing the pH of the solution from 1 to 3. Further increasing of the pH to 5 has almost a negligible effect. Increasing the salt concentration of the solution from 0.01 to 0.1 M NaCl weakens the passive film. Changing the salt concentration from 0.1 to 0.2 M NaCl increases the load required to break the films.

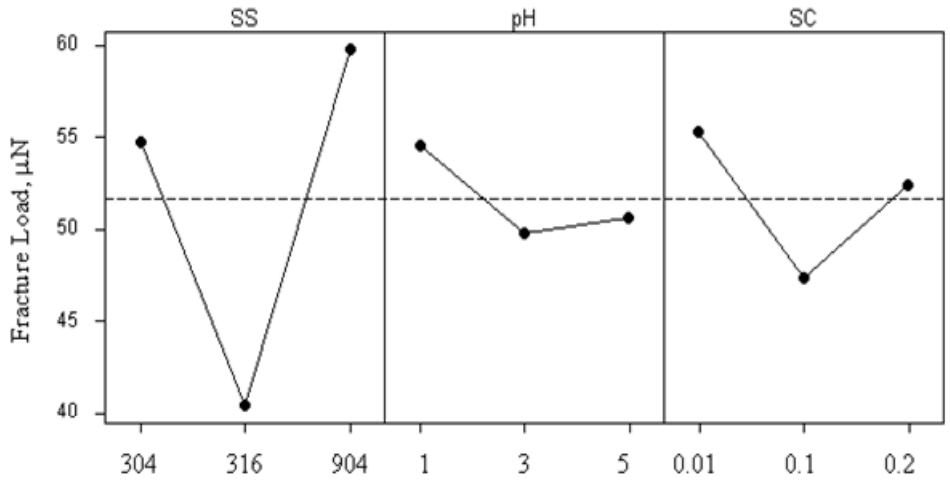

Figure 4-4 Main effects plot for the influence of the factors on the overall average of fracture load, the dashed line. SS stands for the stainless steel and SC stands for the salt concentration

Another way to distinguish among the influences of the factors on the overall average of the fracture load is by using the half-normal probability plot. This plot evaluates the normality of the distribution of the factors using the positive half of the normal curve. Figure 4-5 illustrates the half-normal probability plot of the control factors affecting the fracture load of the passive film formed at a stable passive potential.

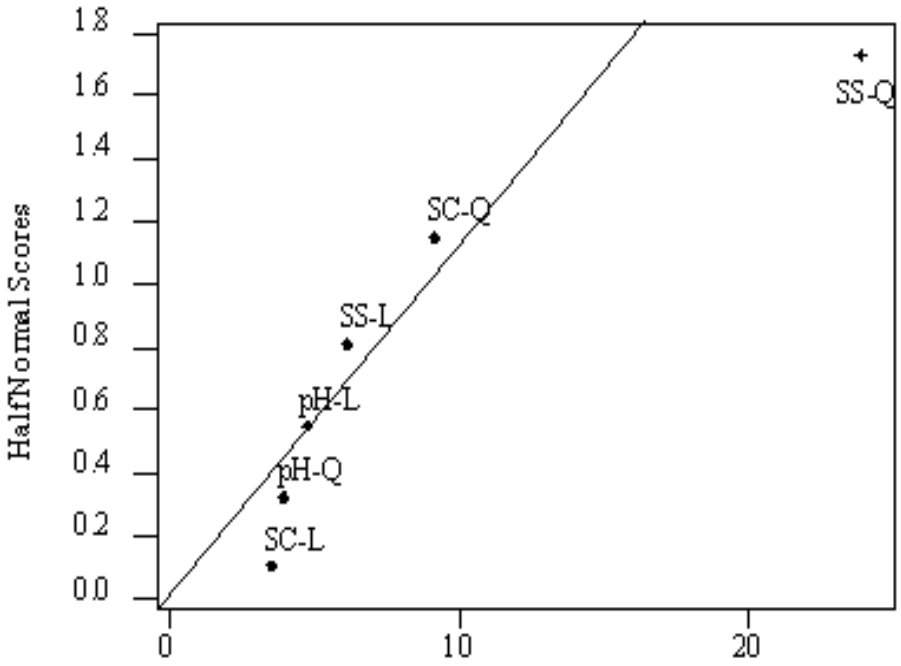

Figure 4-5 Half-normal probability plot of the control factors affecting the passive film formed at a stable passive potential

In the case of normality the points should fall onto a straight line. In figure 4-5, the linear and quadratic influences of each factors fall onto or close to the straight line with the exception of the stainless steel quadratic, SS-Q, effect. The point which represents the SS-Q, falls far away from the straight line, indicating the significant effect for this factor on the fracture load of the passive film formed at a stable passive potential.

The influence of noise factors whose values are associated with operational environment, temperature and time, is shown in Figure 4-6. The temperature effect on the fracture load is almost negligible. Prolonged anodic ageing time increases the load needed to break the passive films. Increasing the ageing time from 60 minutes to 120 minutes increases the average of the loads needed to break the passive film from 48.50 μN to 54.85 μN. The influence of ageing time on the fracture load of passive films formed in the stable region might be because of increasing of the film thickness, changing the structure of the film to a less hydrated one, and completing the growth of the oxide [29,46,108].

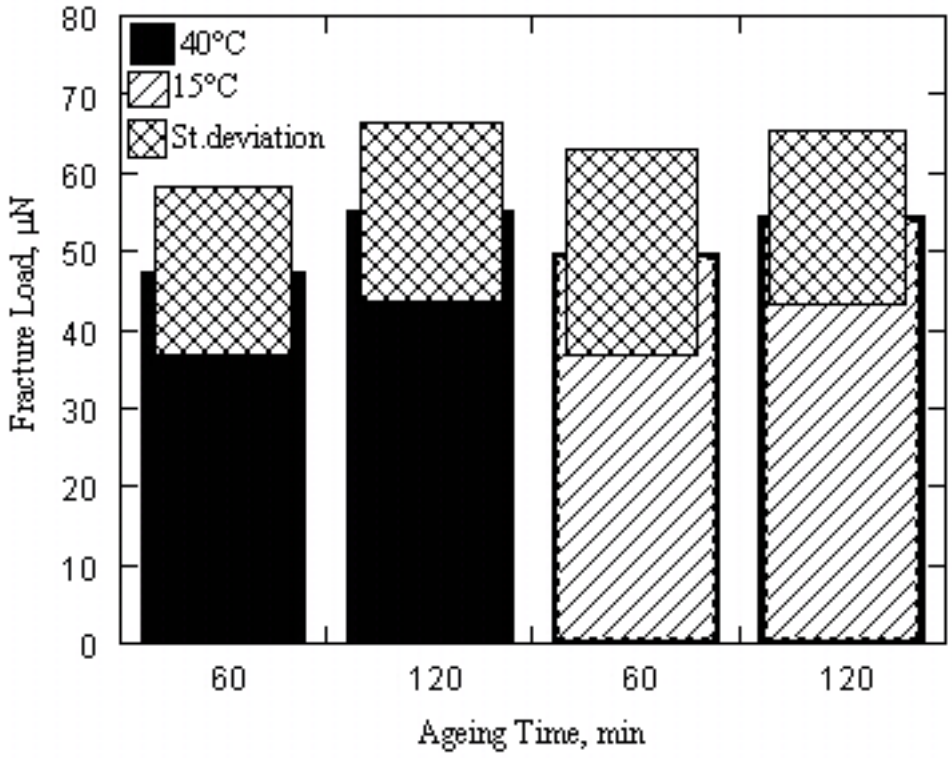

Figure 4-6 The effect of noise factors on the averages and standard deviations of the fracture load obtained from at least 54 indentations for each column, the net shape represents the standard deviation

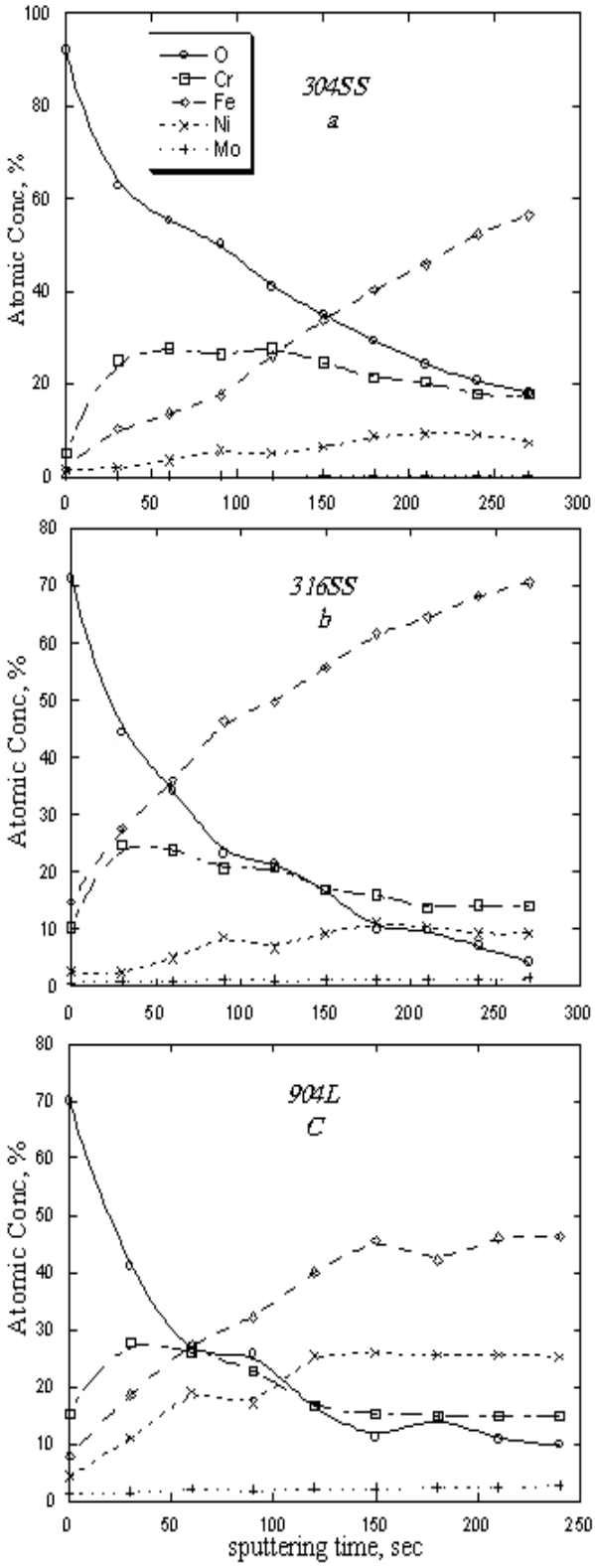

To study the influence of the different substrates on the strength of passive films, passive films were formed on three different substrates, 304SS, 316SS, and 904L, held for two hours in 0.01M NaCl and pH 1 at -0.1V. XPS was used to identify the chemical composition of the films under the same growth conditions. Sputter depth profiles are shown in Figure 4-7. A relative thickness of the films formed on different substrates can be determined by measuring the sputtering time needed for oxygen to reach 50% of the maximum oxygen concentration [83]. Thus, the thickest films were grown on the 304 SS. The film thickness decreased with the addition of Mo to the

Figure 4-7 XPS- depth profile of passive films formed on (a) 304 SS, (b) 316 SS, and (c) 904L

substrate. Similar results, a lower film thickness, were obtained by adding 6% of Mo to a similar stainless steel [57]. It is important to note that the film strength in these systems does not correlate directly with film thickness (as previously suggested by Rodriguez-Marek and co-workers [82].

The atomic concentration curves for Cr, Ni, Mo, and Fe were integrated to obtain the chemistry of the metallic atoms in the film. Although the chromium composition in 904 L is larger than the one in 304 SS, the atomic chromium concentration in the films formed on 904L is smaller than the one formed on 304 SS. This might be due to the replacement of chromium oxide by molybdenum oxide [29]. The atomic iron concentration was found to decrease, 65%, 51%, and 42%, in the films formed on 316 SS, 304 SS, and 904 L, respectively. Linking the fracture load of passive films to atomic concentration of the elements indicates an inverse relationship between the fracture load of passive films and the ratio of iron to the metallic atoms in the film, as shown in Figure 4-8

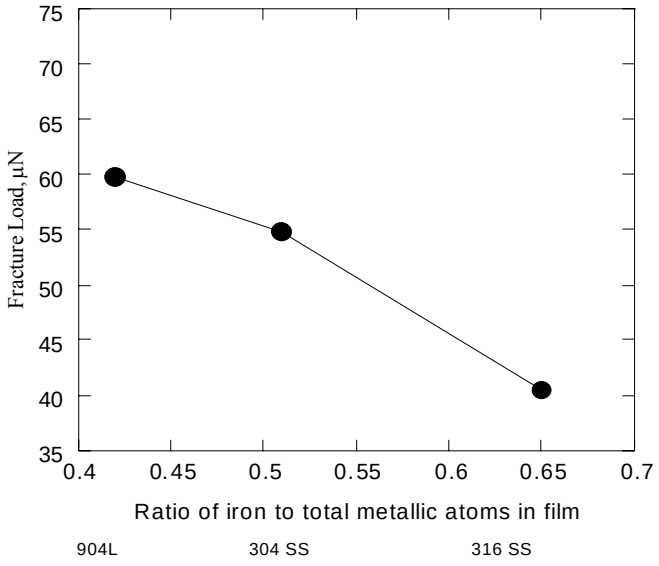

Figure 4-8 The averages of the fracture loads of the films versus the iron concentration in the films

Using these results, it is possible to develop an empirical model equation to describe the load at which film fracture would occur based in figure 4-4, optimum levels. For the case of the passive film formed on 904L SS in a chloride solution of pH 1 and salt concentration of 0.01 M NaCl the average load at fracture can be predicted using the following equation:

$$\mu = \beta_0 + \beta_{SS_L}\chi_{SS_L} + \beta_{SS_Q}\chi_{SS_Q} + \beta_{pH_L}\chi_{pH_L} + \beta_{pH_Q}\chi_{pH_Q} + \beta_{SC_L}\chi_{SC_L} + \beta_{SC_Q}\chi_{SC_Q} \quad (4\text{-}1)$$

Where β_0 is the overall average of the load at fracture, the dashed line in figure 4-4, β stands for the sing of the coefficients where

$$\beta_{SS_L} = +1, \beta_{SS_Q} = -1, \beta_{pH_L} = -1, \beta_{pH_Q} = -1, \beta_{SC_L} = -1, \beta_{SC_Q} = -1$$

and χ stands for the values for each coefficient in the regression equation. The average of the load at fracture can then be predicted by using figure 4-4 and the regression equation in the appendix 1-2 as follows:

$$\mu = 51.7 + 2.49 + 51.61 + 1.94 + 0.936 + 1.45 + 2.17$$

$$\mu = 66.24$$

$$\text{var}(\hat{\boldsymbol{Y}}) = \frac{7}{9}\sigma^2$$

The variation in the predicted average depends on the error variance, σ^2, the type of the orthogonal array, L9, and the terms included in the model equation. The error variance, which is equal to the error mean square, can be estimated as follows:

$$\boldsymbol{MSE} = \frac{\boldsymbol{SS_E}}{\boldsymbol{df_E}}$$

Where SS_E and df_E are the sum of squared due to error and degrees of freedom for error, respectively. Although the effects of pH and salt concentration factors on the load at

fracture were included in the prediction of the new average, their sum of squared as well as their degrees of freedom were used to estimate the error mean square, MSE. This method is called pooling. Using the sum of squares for the salt concentration and pH, each factor has two degrees of freedom, from appendix 1-2 the error mean square is then equal to:

$$\boldsymbol{MSE} = \frac{167.25}{6}$$
$$\boldsymbol{MSE} = 27.87$$

Using the MSE and 95% confidence interval for μ to estimate the influence of the error variance, σ^2, on the predicted average lead to:

$$66.24 \pm \boldsymbol{t}_{0.025,6} * \sqrt{(\boldsymbol{MSE})(\frac{7}{9})}$$

The predicted average is then:

$$\mu = 66.24 \pm 11.4$$

The next step is to verify the validity of the empirical model equation by growing a film on 904L SS in chloride solution of pH 1 and 0.01M NaCl. The same procedure described in this chapter was used to grow and indent the film. Figure 4-8 illustrates an example of the load-displacement curve of the passive film formed on 904L SS in 0.01M NaCl solution which was adjusted to pH 1. Eight indentations were made into two different grains. The average and the standard deviation of the fracture loads of the nanoindentations were 69 ±5 μN. The average of the fracture load experimentally observed falls in the range of the predicted average.

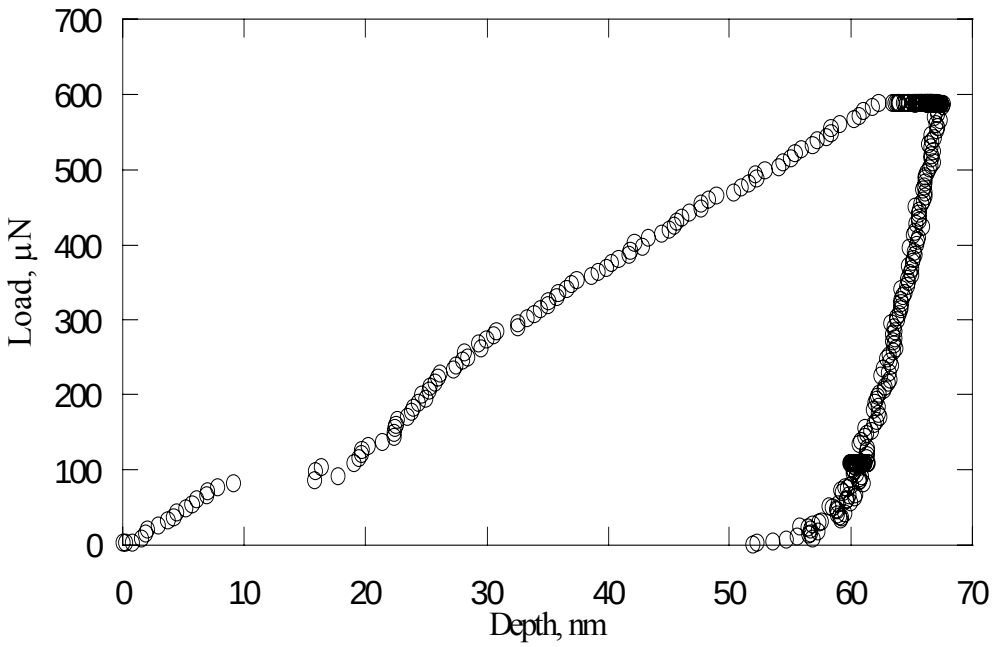

Figure 4-9 The load-displacement curve of the passive film formed on 904L SS in chloride solution

Conclusion

The Taguchi method was used to study the effect of the multiple variables on the fracture load of the passive films. Passive anodically controlled films have been grown on 304 SS, 316 SS, and 904 SS at acidic pH's with Cl^- concentrations of 0.01M, 0.1M, and 0.2M. Nanoindentation tests show that the steel chemistry plays the most important role in the fracture load of passive films formed in the stable potential region. Passive films formed on a 904L SS needed the largest load to be broken, while the 316 alloy has the mechanically weakest passive film. The fracture load increased with increasing the chromium concentration in the alloy. XPS results show the fracture load of passive films is dominated by the fraction of iron in the passive film, with fracture loads decreasing with increasing iron concentration. Prolonged anodic ageing time only slightly increases the fracture load of passive films held in the stable passive potential region. The average

of the load at fracture obtained experimentally verified the validation of the model equation developed to predict the average of the load fracture at optimum levels.

Chapter 5

Effects of alloy and solution chemistry on the fracture of anodic films formed at metastable pitting potentials

In the passive region, there is a critical potential at which the breakdown of the passive film takes place; this process eventually results in the initiation sites of localized corrosion such as pitting. As showing in figure 1-1, the breakdown sites are repassivated as long as the applied potential does not exceed the critical potential for pitting. The range in which the breakdown sites are repassivated is known as the metastable pitting potential range. This range is illustrated as electrochemical noise or current transients as shown in figure 1-1. The metastable pitting potential range is affected by the concentration of the halide ions in the solution especially chloride ions, the pH of the solution, and the alloy chemistry of the substrate on which the film is formed. An increase of the halide ion concentration in an electrolyte shifts the metastable pitting potential to more negative value. Moreover, the pitting potential increases toward more noble potential value with increasing the solution pH and alloying the metal with molybdenum.[1,32,106, 107].

In the previous chapter the influences of alloy chemistry, pH of the solution, the chloride concentration, temperature, and the aging time on the load at fracture of the passive film formed at a stable passive potential were investigated by using the Taguchi method. The goal of this chapter is to evaluate the effects of the same variables on the fracture load of the passive film formed on austenitic stainless steel alloys at a metastable pitting potential.

Experimental Procedure

The specimens and the procedure used to prepare the specimens in this chapter were similar to that mentioned in the previous chapter, chapter 4. The main difference between the two procedures was the potential at which the passive film was formed. Figure 2 shows the typical electrochemical behavior of 304 SS in a solution of a pH of 1 and salt concentration of 0.01 M NaCl, respectively. To measure the fracture load of the passive film formed in the same solution at 40°C, the potential was held cathodically for approximately 40 minutes. Then the sample was anodically polarized at constant rate of 2mV/s to 0.05V, as indicated by the arrow in figure 5-1, and then held for two hours to grow the passive film. The specimen was then removed from the solution, rinsed with deionized water, and glued on an iron disk to be indented. Indentations were performed in ambient air.

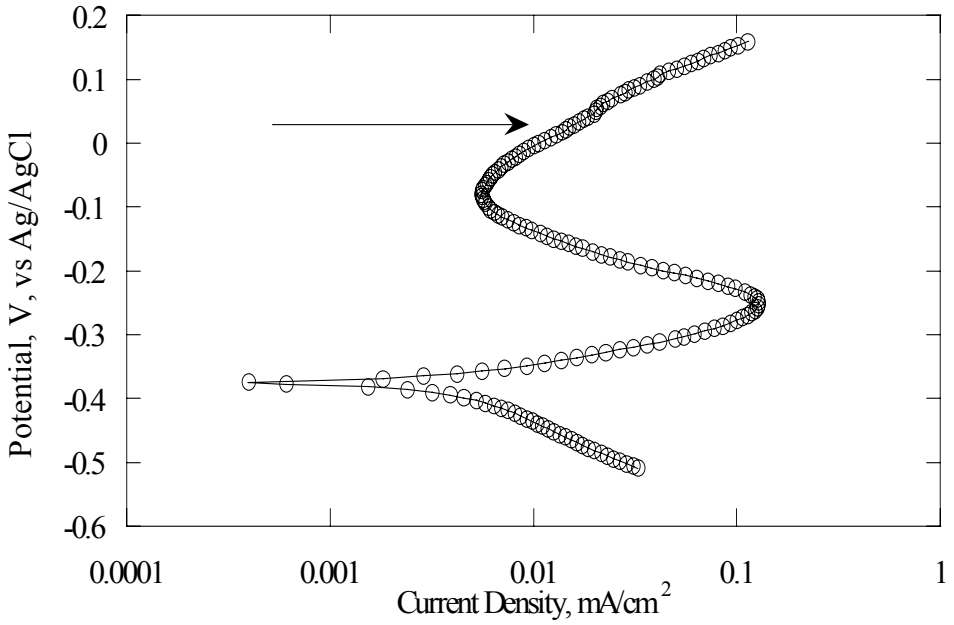

Figure 5-1 Electrochemical behavior of 304SS in solution of pH 1 and 0.01M NaCl. The arrow indicates to the potential at which the film is grown.

Results and Discussion

The load at which the first loading discontinuity occurred, shown by the arrow in Figure 3, in this case 30 μN, was recorded from each indentation. To diminish the error in the load at fracture which might be produced by indenting a pitted site or a site which may have a subsurface defect such as an inclusion, the average of at least six indentations in two different grains of each cell is shown in Table 5-1. The same procedures were used to grow the passive films and to determine their fracture loads under different conditions. Table 5-1 shows the design, conditions, and the averages of at least 400 indentations for the fracture loads of passive films formed in the metastable pitting potential range. After the experiments were concluded the data were statistically analyzed using Minitab®, as shown in appendix 1-3.

Table 5-1 The design, conditions, and average fracture load of passive films formed in the metastable potential passive region

Time (min)			60	120	60	120
Temperature (°C)			40	40	15	15
S.S	pH	S.C (M)	Fracture Load, μN			
304	1	0.01	32 ±11	30 ±5	24 ±5	39 ±10
304	3	0.1	26 ±6	25 ±2	28 ±7	35 ±5
304	5	0.2	26 ±6	29 ±8	28 ±6	38 ±5
316	1	0.2	32 ±5	27 ±5	31 ±8	22 ±8
316	3	0.01	35 ±5	27 ±8	43 ±4	40 ±6
316	5	0.1	45 ±6	38 ±7	40 ±7	28 ±7
904	1	0.1	43 ±6	37 ±6	43 ±6	37 ±6
904	3	0.2	27 ±5	23 ±5	34 ±6	32 ±10
904	5	0.01	45 ±5	37 ±7	36 ±5	38 ±13

Since each factor has three levels, the factor's effect on the fracture load is either linear, L, or quadratic, Q. The data were analyzed using the probability that the result can be explained by a random variation of less than 0.15. The results showed that the linear effects of both alloy chemistry and salt concentration, as shown in Figure 5-2, have the most significant effects on the fracture load of passive films with the actual P- values of these effects being 0.138 and 0.117, respectively.

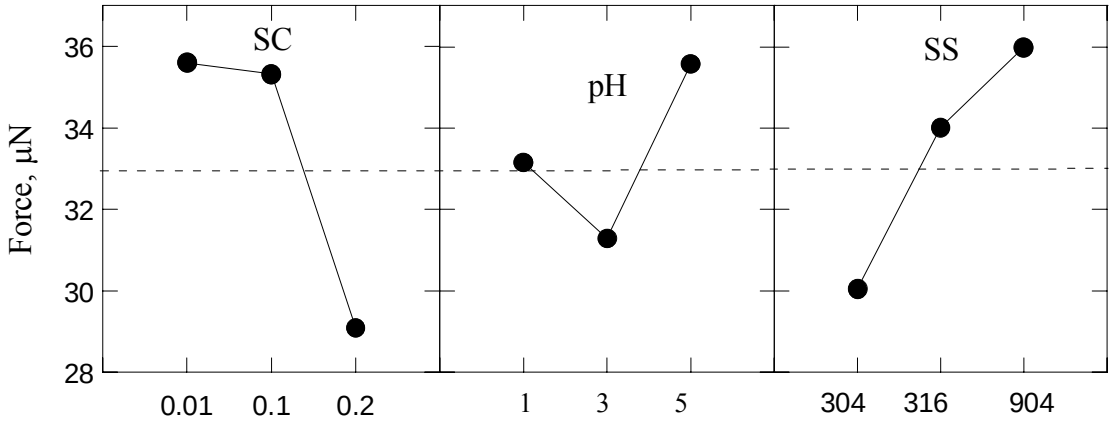

Figure 5-2 The effect of the controlled factors (salt concentration, pH, and stainless alloy composition) on the load at which the passive films fractured

Figure 5-2 is the main effect plot, which represents the summary of how the fracture load is affected by the variables being controlled. It is a plot of the fracture load of the passive film, in µN, on the Y axis versus alloy chemistry (304SS, 316SS, 904L), pH (1, 2, and 3), and salt concentration (0.01, 0.1, and 0.2M) on the X axis. The dashed line illustrates the overall average of the fracture load for all conditions. During these experiments, the passive film fracture load was affected by the substrate on which it was grown. The fracture load increased with changing the substrate on which the films were grown from 304 SS to 316 SS to 904 L. Increasing the chloride concentration, using

NaCl, in the solutions from 0.01 M NaCl to 0.1M NaCl had almost a negligible effect on the load needed to break the films. A further increase in chloride concentration to 0.2M NaCl decreased the average fracture load of the films from 35μN to 29 μN. The effect of the salt concentration on the fracture load of the films formed at a metastable pitting potential might have been due to the increasing the chloride ion adsorption on the film surface. This might affect the repassivation and depassivation processes which influence the stability of the film [55]. Increasing the pH of the solution from 1 to 3 decreased the load needed to break the films. A larger load is needed to break the films when the solution pH is increased from 3 to 5.

Figure 5-3 is the half-normal probability plot shows the importance of the factors in the fracture load of the passive film formed at a metastable pitting potential. Generally, all the factors influence the load at fracture. The linear effects of the salt concentration

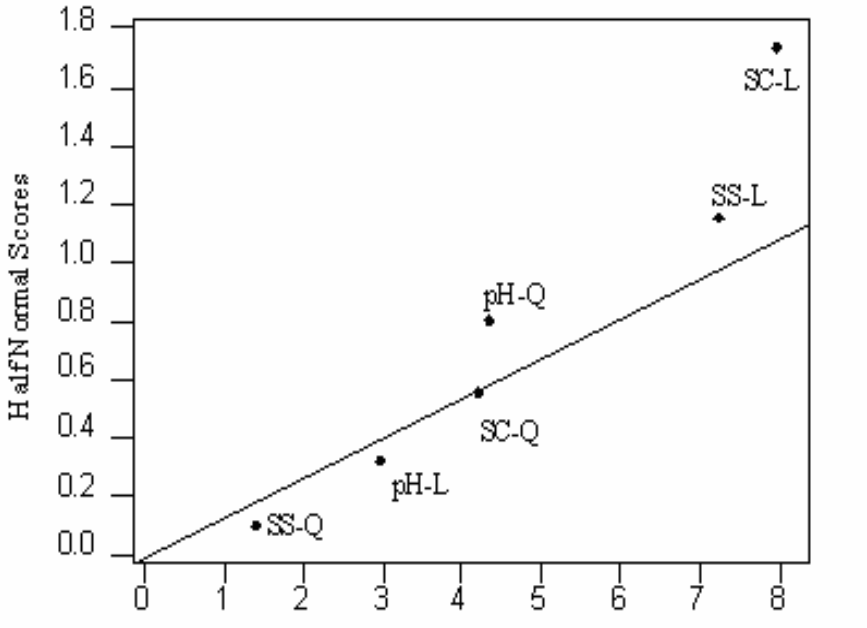

Figure 5-3 half-normal probability plot of the control factor affecting the passive film formed at a metastable pitting potential

and the alloy chemistry were the most important factors affecting the load at fracture of the passive film formed at metastable pitting potential.

The influence of factors that are associated with the operational environment, temperature and time, is shown in Figure 5-4. Prolonged anodic ageing time for the films formed at 15°C had a negligible effect on the fracture load. On the other hand, prolonged anodic ageing time for the films formed at 40°C decreased the load needed to fracture the passive films. Increasing the ageing time from 60 minutes to 120 minutes decreased the average of the loads needed to break the passive film from 34.5 μN to 30.4 μN.

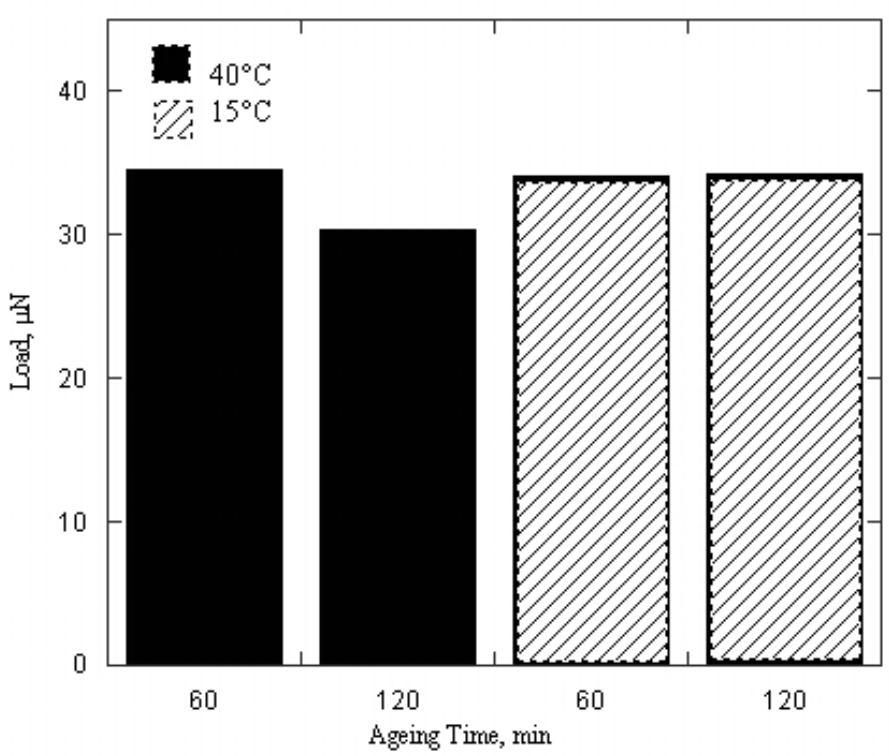

Figure 5-4 The effect of noise factors on the fracture load

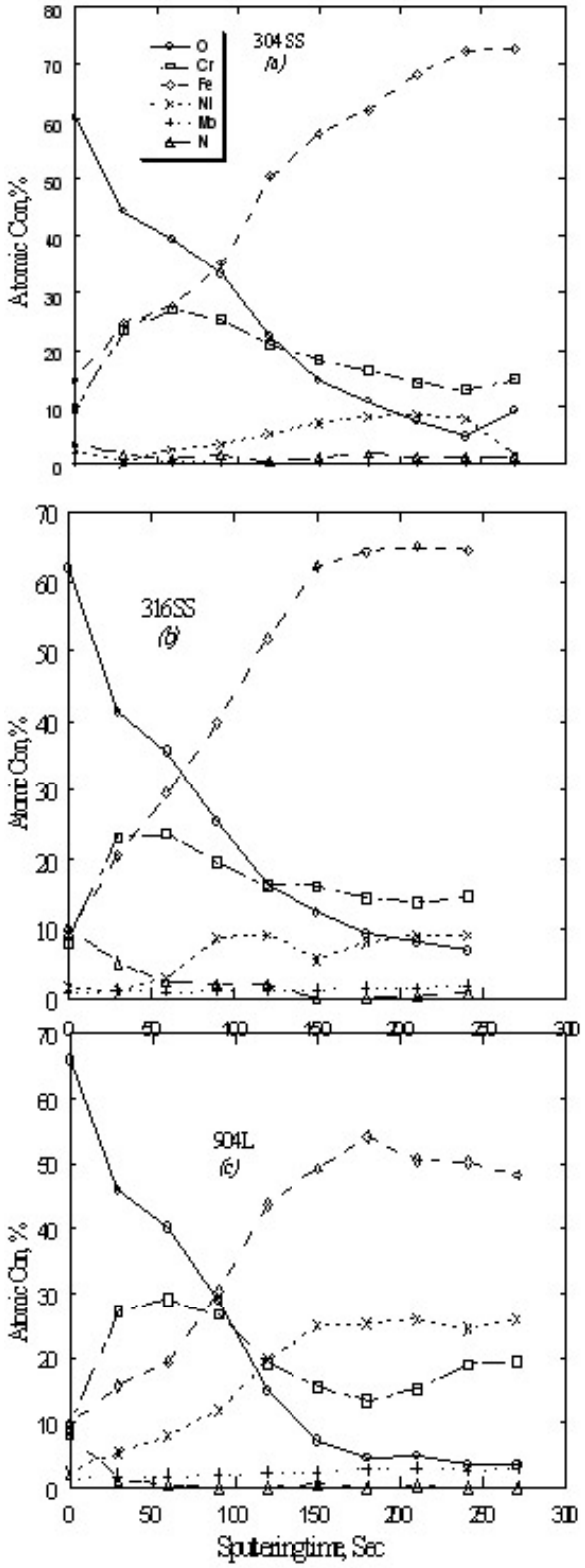

Figure 5-5 XPS- depth profile of passive films formed on (a) 304 SS, (b) 316 SS, and (c) 904L

The influence of ageing time on the fracture load of passive films formed in the metastable pitting potential region at 40°C could have been indicative of increasing the incorporation of chloride ions into the films[48,55,109]. Increasing the passivation time at a metastable pitting potential might have led to the formation of breakthrough pores [40], and consequently the diffusion of chloride ions into the film may be enhanced. The chloride ions, then, may have influenced the strength of the film through inducing an internal stress and/or accelerating local film dissolution.

To study the influence of the different substrates on the strength of passive films, passive films were formed on three different substrates,

304SS, 316SS, and 904L, held for two hours in0.01M NaCl and pH 1 at 0.05V. X-ray photoelectron spectroscopy (XPS) was used to identify the chemical composition of the films under the same growth conditions. Depth profiles are shown in Figure 5-5. A relative thickness of the films formed on different substrates was determined by measuring the sputtering time needed for oxygen to reach 50% of the maximum oxygen concentration [83]. Thus, the thickest films were grown on a 904L SS. The atomic concentration curves for Cr, Ni, Mo, N, and Fe were integrated to obtain the chemistry of the metallic atoms in the film. The areas under each curve were used to calculate the ratio of the metallic atoms among each others. The fracture load appears to follow an inverse relationship with the ratio of iron to the total metallic atoms, as shown in figure 5-6. A similar relationship was observed between the fracture load and the iron concentration in the films formed in the stable passive region.

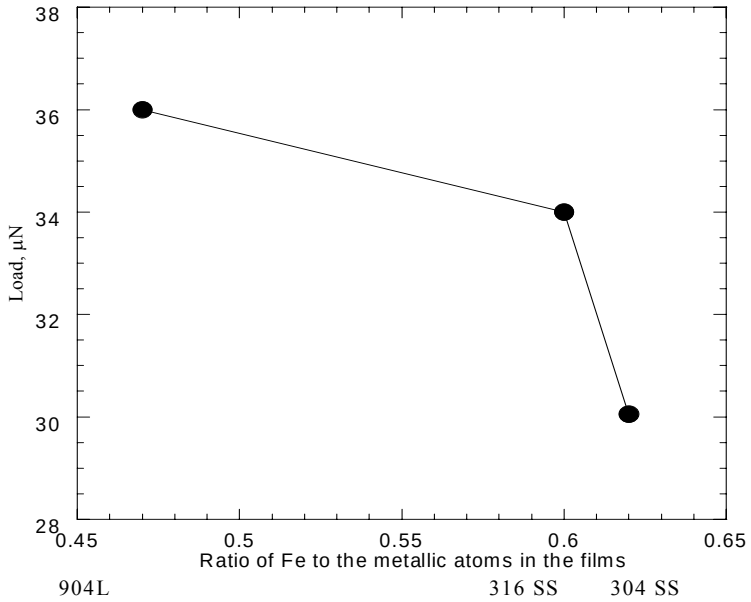

Figure 5-6 The fracture load of passive films as a function of total iron concentration in the films formed at a metastable pitting potential

The effect of the applied potential on the fracture load of the passive films formed in two different potential regions, the metastable pitting potential and the stable passive potential, can be illustrated by comparing the results of this work to those in the previous chapter. The overall average loads needed to break the films formed in the metastable pitting potential and stable passive regions were 33 μN and 52 μN, respectively. The ageing time had a significant effect on the fracture load of the passive films formed at a stable passive potential. Increasing the ageing time in the stable potential regime, from one to two hours, resulted in stronger film. On the other hand, increasing the ageing time of the films formed at a metastable pitting potential at 40°C mechanically weakened the passive films. Decreasing the fracture load with increasing ageing time in the metastable pitting region can be explained by the repeated repassivation-depassivation process. Dawson and Ferreira [110] observed the repassivation-depassivation process as pulses of current in the polarization curves, and ascribed the repassivation-depassivation process to the film breaking down due to mechanical effects of chloride adsorption on the film. In the stable potential regime the chloride would be less likely to adsorb and become incorporated in the film, leading to less sensitivity of film fracture to anodic polarization time.

Hara and Sugimoto [61], Okamoto [43], and Olefjord and Wegrelius [4] pointed out that a consequence of increasing the applied potential in both the passive and transpassive regions was the enrichment of the passive film by Fe^{3+}; on the other hand, the Cr^{3+} content in the film was decreased. Another effect of increasing the applied potential was the instability of the passive film due to the depassivation-repassivation process which was the result of the passive film breakdown. Their work implied that the

composition and, then, the stability of the film was potential-iron-chromium dependent; increasing both the iron content in the film and the applied potential led to electrochemically instable passive film. In this study, the nanoindentation results showed that the overall average of the load at fracture for the passive film formed at a metastable pitting potential was less than that for the passive film formed at a stable passive potential. In addition to the nanoindentation results, XPS results of the passive film formed at stable passive and metastable pitting potentials showed that the film strength was inversely proportional to the iron content in the film. Moreover, the total iron content in the passive films formed at metastable pitting potential on 304SS, 316SS, and 904L was larger than the ones formed at a stable passive potential on the same alloy under the same condition. This observation suggests that the iron content in the film alters the mechanical behavior; the load required to fracture the passive film increased as a function of decreasing the iron content in the passive film formed in the passive region.

Conclusion

The Taguchi method was used to study the influence of multiple variables on the mechanical strength of passive films on austenitic stainless steels formed in the metastable pitting potential region. Nanoindentation tests show that both the steel chemistry and salt concentration have significant effects on the fracture load of passive films formed in the metastable pitting potential region. Passive films formed on a 904L stainless steel fractured at an average load of 36 μN. Increasing the salt concentration in the solution to 0.2M NaCl decreased the load needed to break the films to the lowest values, 29 μN. Similarly, prolonged anodic ageing time at 40°C decreased the mechanical strength of passive films held in the metastable pitting potential region. This

could be due to the incorporation of chloride ions in the passive films. In addition, XPS results have shown that the fracture load of passive films was inversely related to the ratio of iron to the metallic atoms in the passive film; fracture loads decreased with increasing the ratio of iron to the total metallic atoms in the films.

Chapter 6

Correlating structure and mechanical behavior of passive films on austenitic stainless steels

It is well established that passive films formed on austenitic stainless steels play an important role in corrosion and stress corrosion cracking. Breakdown of the passive film on the metal surface results in localized corrosion such as pitting of the metal itself. The passive film on austenitic stainless steel has described as distinct bilayers. The inner layer is enriched in chromium oxide and the outer layer is a mixture of iron oxide and a hydroxide film [3,111].

One widely used chemical treatment to improve the corrosion resistance of stainless steel by stabilizing passive films on alloys is a chromate or dichromate treatment [85]. Chiba, and Seo [86,87] used nanoindentation to study the effects of the dichromate treatment on the mechanical properties of passivated surfaces formed on single crystal iron. The dichromate treatment increased the hardness and the ratio of elastic work to plastic work of these surfaces at a depth > 30 nm. Seo and Chiba investigated the effect of the dichromate treatment on the load-displacement curves for iron (100) and (110) surfaces. A load-discontinuity event was observed in the iron (100) surface but not in the (110) surface.

The aim of this chapter is to investigate the effect of alloy chemistry and microstructure on the mechanical properties of passive films. In chapter 4, it was found that the average loads required to fracture the passive films formed on 904L SS, 304 SS, and 316 SS were 59, 54, and 40 μN, respectively. These fracture loads will be correlated to change in chemistry and structure of the films. The effect of dichromate treatment on

the mechanical behavior and chemical composition of the passive film formed on 316 SS alloy at a stable passive potential will also be explored.

Experimental Procedure

Passive films were grown using an EG&G 173 and 175 potentiostat and controller. The chloride test solution, adjusted to a pH of 1 by adding HCl and a salt concentration of 0.01M NaCl, was aerated in a Green cell with Ag/AgCl and graphite as reference and counter electrodes, respectively [82]. To probe the influence of the substrate and dichromate treatment on the chemistry of the passive film, X-ray photoelectron spectroscopy (XPS) was used to identify the chemical composition of the films formed without and after dichromate treatment under the same sputtering conditions. The specimens were prepared from rods 12 mm long and 6 mm in diameter. The compositions of the alloys studied are given in Table 3-1. Specimens were abraded through 1200 grit SiC paper and then electropolished in a solution of 95% acetic acid 5% perchloric acid at room temperature at a current density of ~ 1mA/mm^2. The exposed area of the test was 28 mm^2. To grow the films, the samples were held cathodically for 30 minutes and then anodically polarized to -0.13V (vs. Ag/AgCl) with a scanning rate of 2mV/s and held for 2 h. The samples were then removed from the electrochemical cell, rinsed with deionized water, and examined by XPS using a Kratos Axis-165 electron spectrometer. Monochromated X-rays at 1486.6 eV (Al Kα) was used as the excitation source. Binding energies (BE) were calibrated against the Au 4f $_{7/2}$ peak located at BE = 84 eV.

Samples for transmission electron microscopy (TEM) analysis were prepared from 5 mm long and 6 mm diameter discs. The samples were thinned to ~150 μm by

mechanical polishing, and cut into 3-mm diameter discs. The samples were electropolished in a solution of 95% acetic acid 5% perchloric acid at room temperature at an applied voltage of 45 V using a double jet polisher. The samples were then anodically polarized using the same procedure described above and examined using a Philips CM200 TEM operated at 200 keV.

Fracture loads for passive films were determined using a Hysitron Triboscope with a Park Autoprobe CP scanning probe microscope (SPM). Nanoindentations were performed using a cube corner tip with loading rates of 50μN/s. To test a sample with dichromate treatments a specimen was then held cathodically in the same solution for 1h to reduce the anodic oxide film, removed from the cell, rinsed with deionized water, and naturally immersed in 0.05M $K_2Cr_2O_7$ solution for about 40 h. The specimen was potentiostatically polarized in a chloride solution, 0.01M NaCl and pH of 1, held for 2 h at -0.13V, and then rinsed with deionized water.

Results

A typical polarization curve for 316 SS in the chloride solution is shown in Figure 6-1. The arrow in this figure indicates the potential at which the films were formed for this study. Figure 6-2 shows typical load-displacement curves for 316 SS with the passive film and then after the dichromate treatment. The curves shown in Figure 6-2 are typical of more than 20 indents on each sample into different grains. Without a dichromate treatment there is clear evidence of a “pop-in” event the film fractures at a depth of ~ 6 nm. The load-displacement curve for passivated 316 SS after the dichromate treatment shows a different behavior. . A “pop-in” event is not observed as shown in

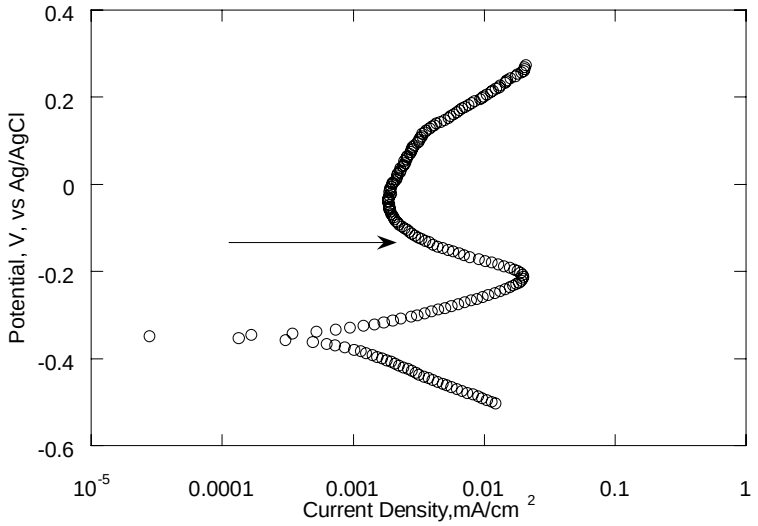

Figure 6-1A typical polarization curve of 316 SS in chloride solution, 0.01M NaCl and pH of 1 adjusted by adding HCl

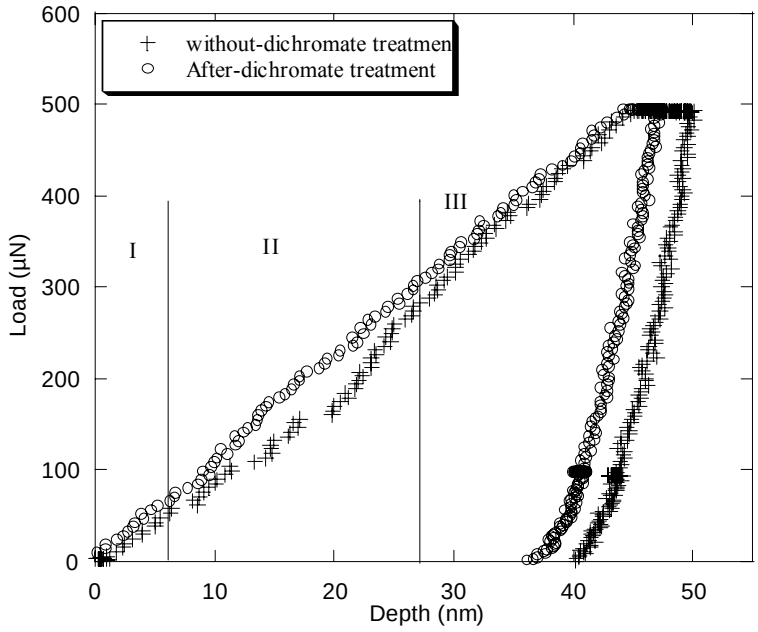

Figure 6-2load displacement curve measured for 316 SS alloy passivated at -0.13V for two hours in chloride solution, pH 1 and 0.01 M NaCl, without and after dichromate treatment

figure 6-2. Also, the surface of 316SS after dichromate treatment had a smaller penetration depth, i.e. the surface is harder after the treatment. The response of the passivated 316 SS before and after the dichromate treatment can be described as follows:

Region I- The behaviors of the two surfaces are almost identical

Region II- The behavior of the passivated 316SS without dichromate treatment showed a "pop-in" event while the behavior of the passivated 316SS after dichromate treatment is represented by a steeper slope without a "pop-in" event.

Region III- The behaviors of the two surfaces are almost identical.

Depth profiles generated by the combination of Ar^+ ion sputtering and XPS acquisitions of Fe 2p, Cr 2p, O 1s, Ni 2p and Mo 3d signals on the passive films formed on 304 SS, 904L SS, and 316 SS before and after the dichromate treatment are shown in Figure 6-3. The areas under the peaks were used to determine the atomic concentration of each element present in the films. The atomic concentration ratio of iron and chromium to other metallic elements are summarized in Table 6-1. Although the chromium content in bulk 904L SS is larger than the one in 304SS, the ratio of chromium to other metallic elements in the film formed on 904L SS is smaller than that formed on 304 SS.

Table 6-1 The ratios of iron and chromium to other metallic elements

Substrate	Fe/(Cr+Mo+Ni+Fe) %	Cr/(Cr+Mo+Ni+Fe) %
304SS	51	39
316SS	65	24
904L SS	42	31
316SS after-dichromate treatment	45	44

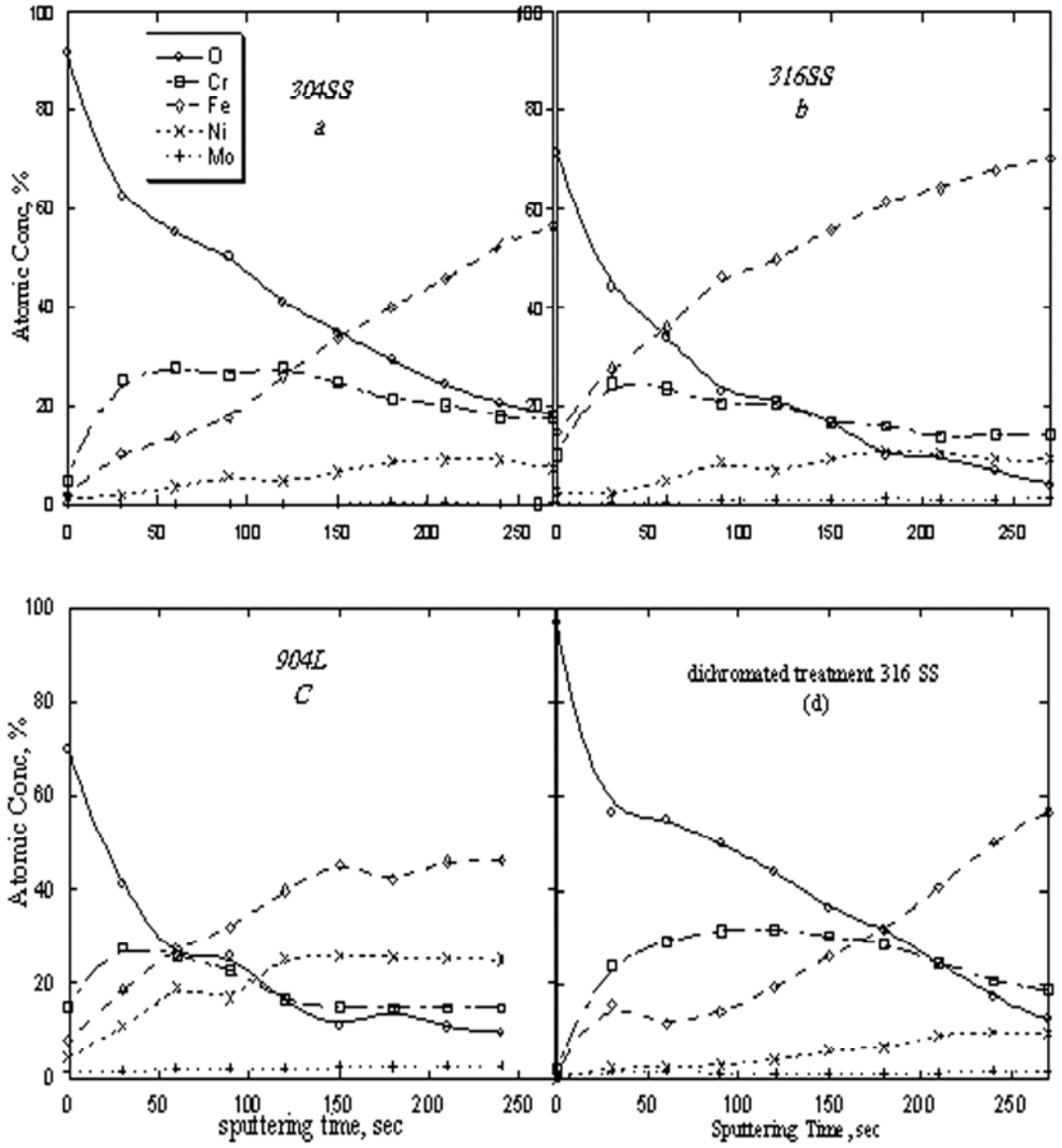

Figure 6-3 Sputter depth profiles for the passive films formed on: a) 304, b) 316, c) 904L, and d) 316 with dichromate treatment

To correlate the mechanical behavior and microstructure, passive films were examined using TEM. Figure 6-4 shows the [011] selected area diffraction pattern (SAD) of 904L SS before the growth of the passive oxide film. The reflections are due to the

substrate. The absence of any other reflections indicates that the surface of the sample is free from any detectable oxide layer.

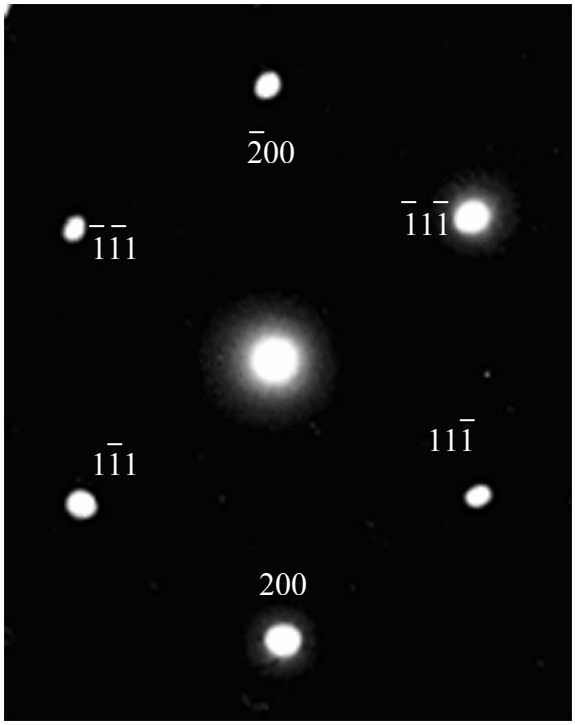

Figure 6-4 diffraction pattern for 904L SS before the growth of the oxide film beam direction [011]

Figure 6-5a shows a bright field image of the passive oxide film formed on 904L SS. Moiré fringes are visible in the image and this appearance is consistent with the extra spots in the diffraction pattern, figure 6-5b. Figure 6-6a shows a bright field image of the passive oxide film formed on 304 SS. The film consists of small islands, which strongly diffracted the electron beam, in an amorphous matrix. Figure 6-6b shows the [011] SAD pattern where the polycrystalline nature of the islands can be clearly seen.

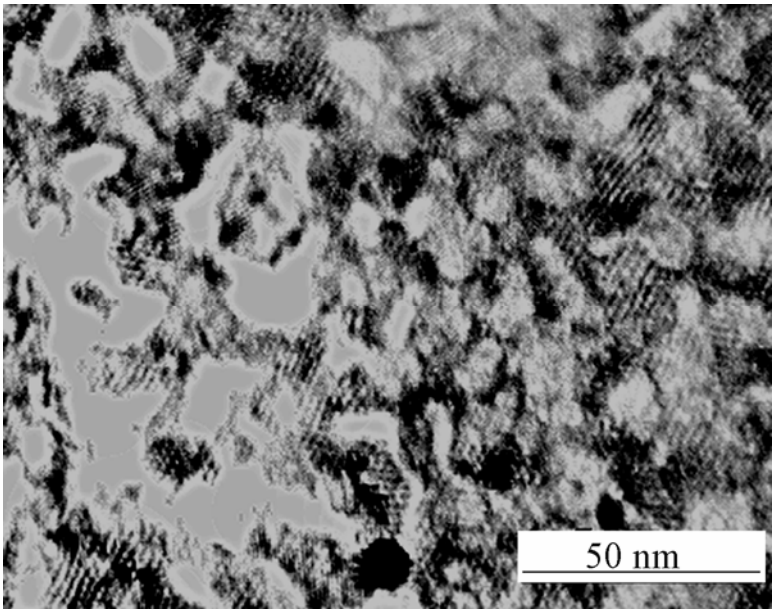

(a)

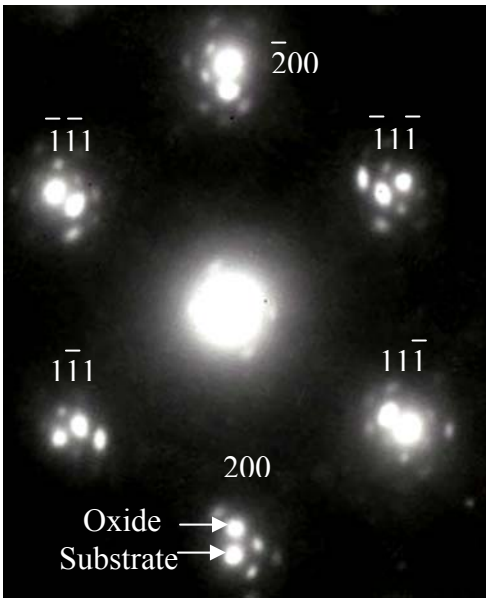

(b)

Figure 6-5 (a) a bright field image and (b) [011] diffraction pattern of the passive film formed on 904L SS

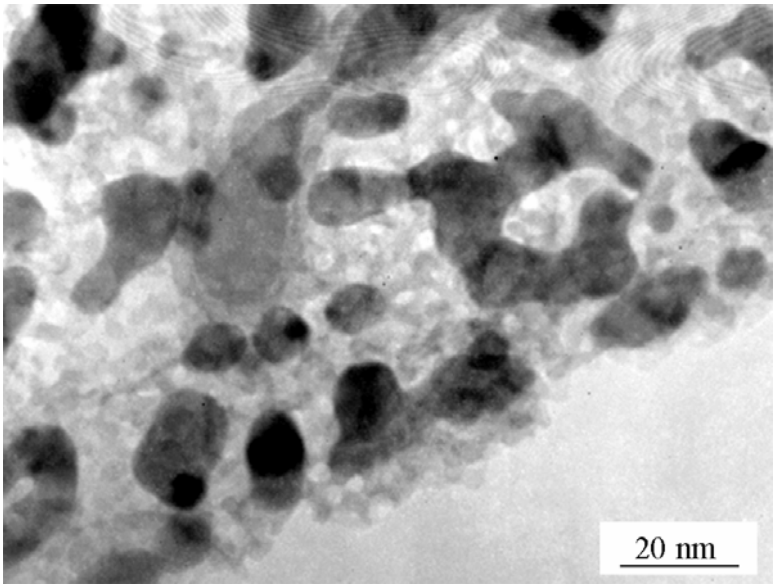

(a)

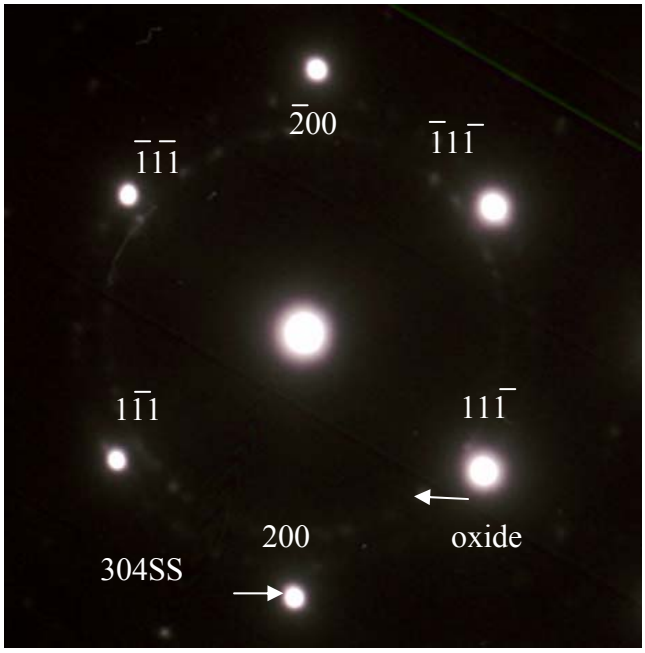

(b)

Figure 6-6 (a) a bright field image and (b) [011] diffraction pattern of thin film formed on 304 SS.

Figure 6-7 shows a bright field image of the passive oxide film formed on 316 SS without the dichromate treatment. The film consists of small islands, which strongly reflect the electron beam, in an amorphous matrix. Figure 6-8 corresponds to the TEM micrographs of the passive oxide film formed on 316 SS after the dichromate treatment. Similar to the 904L SS sample, moiré fringes are seen in the bright field image. Extra reflections are seen in the diffraction pattern shown in figure 6-8, which are the result of double diffraction.

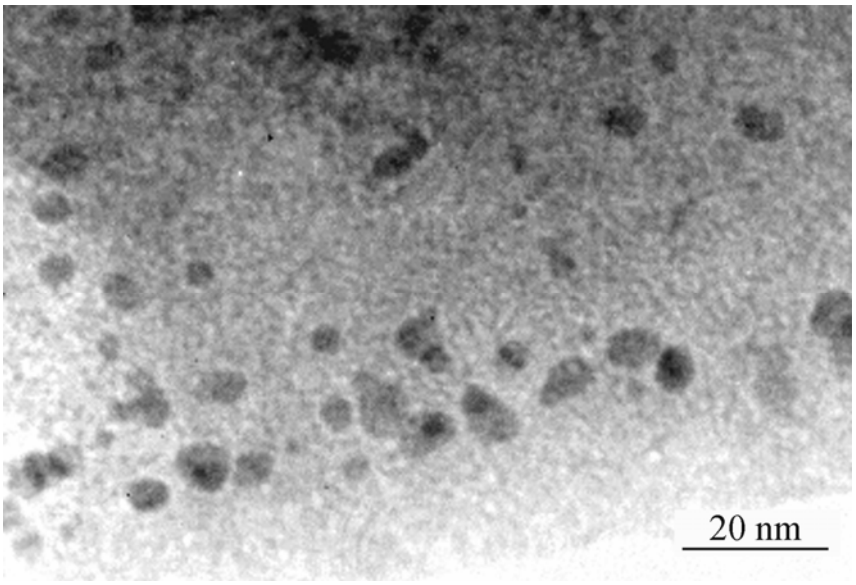

Figure 6-7 A bright field image of the passive film formed on 316 SS.

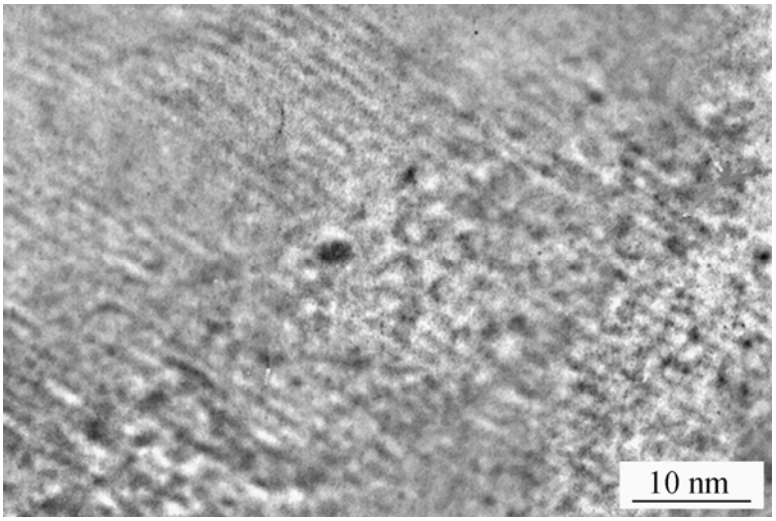

(a)

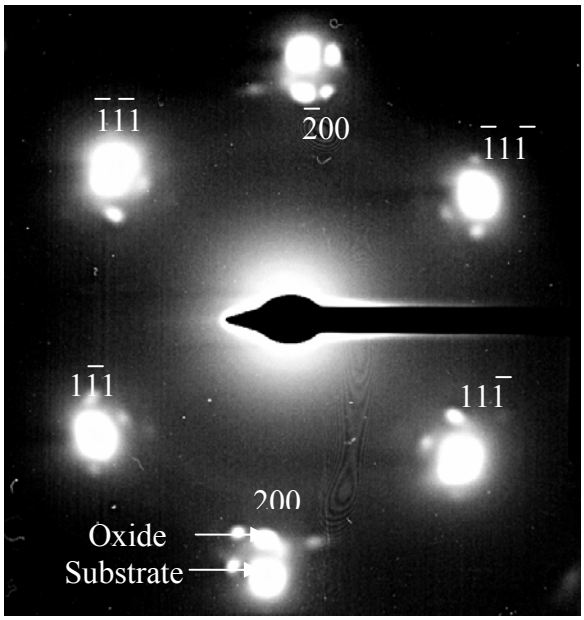

(b)

Figure 6-8 The effect of pre-dichromate treatment on the passive film grown on 316 SS; (a) a bright field image and (b) [011] diffraction pattern of the passive film formed on 316SS after dichromate treatment.

Discussion

It is well known that the passive oxide film formed on stainless steel consists primarily of chromium oxide, Cr_2O_3, [4,21,112]. The bulk form of Cr_2O_3 has a hexagonal crystal structure with lattice parameters *a=0.495*nm and *c=1.366*nm [113]. Recent analysis of Rao *et al* shows that Cr_2O_3 can also form with a cubic crystal structure having an FCC lattice [114]. Analysis of the diffraction pattern in figure 6-5b shows that the crystal lattice of the Cr_2O_3 layer formed on 904L SS is FCC with a lattice parameter *a=0.415* nm. This result is consistent with the value reported by Rao of *a=0.407* nm [114]. It is also evident from the diffraction pattern that the oxide film is epitaxial with the stainless steel substrate. The orientation relationship between the chromium oxide and 904L SS can be obtained from the diffraction patterns and was found to be:

$$(\bar{1}\bar{1}1)_{Cr_2O_3} \parallel (\bar{1}\bar{1}1)_{SS}; [011]_{Cr_2O_3} \parallel [011]_{SS}$$

This orientation relationship is in agreement with the high resolution transmission electron microscopy analyses of the Cr_2O_3 film formed on chromium [114]. This is the first observation to date of this same structure on engineering stainless steel.

While the oxide film grown on 904L SS was an epitaxial, the film formed on 304 SS consisted of small randomly oriented crystalline islands (Fig. 6-6a). The diffraction contrast of the region between the islands remained unchanged when the sample was tilted around the <011> zone axis, which suggests that the region between the islands is amorphous. The analyses of the SAD pattern shown in figure 6-6b indicate that the crystal structure of these islands is FCC. A bright field image of the oxide film formed on 316 SS showed that, similar to the film grown on 304 SS, the film consisted of crystalline islands in an amorphous matrix (Fig. 6-7).

Classical research has shown that the film growth kinetics are logarithmic with respect to time [14,15]. The passive film thickness in an electrolyte reaches a steady-state due to being controlled by diffusion and the reaction of the oxygen ions with cation ions [15,16]. Furthermore, the passive film consists of chromium oxide, Cr_2O_3, and iron oxide, Fe_2O_3, as inner and outer layers, respectively [22,115,116]. Therefore, it is reasonable to assume the oxide layer has a constant volume consisting of chromium and iron oxides. As a result of this assumption, changing the relative concentration of one of the oxides, Fe_2O_3 or Cr_2O_3, might affect the film strength. Regardless of the differences in the load at film fracture the overall average depth at fracture for all the films formed was 7.4 ± 0.6 nm, implying the film fracture was strain controlled. XPS results show that the iron ratio to other metallic elements in the passive films formed on 904L SS, 304SS, and 316SS decreased, respectively. The elastic moduli of Cr_2O_3 and Fe_2O_3 are equal to 325 and 275GPa, respectively [117,76]. Therefore, to achieve the same strain, it is reasonable to assume that the higher loads required to cause fracture could be due to an increase stiffness of the passive film due to chemical and structural variations.

TEM results associated with the change in the iron ratio to other metallic elements in the film indicate that there was a change in the microstructure of the film. When the iron ratio was the lowest, the passive oxide film formed on 904L SS had an epitaxial structure and the load required to fracture the film was the largest. On the other hand, when this ratio increased, the structure of the passive film formed on 316 SS and 304 SS consisted of crystalline islands in an amorphous matrix and the loads required to fracture the passive film was lower than those on 904L SS. Also, the fracture load of the oxide film formed on 316 SS, which had the highest iron ratio, was lower than that of the film

formed on 304 SS. This observation may be explained by the fact that the film on 316SS (Fig. 6-7) has lower density of crystalline islands in comparison to the film on 304SS (Fig. 6-6a). The lower density of crystalline islands in the film formed on 316 SS could be attributed to the lower chromium content in bulk 316SS.

TEM analysis of the oxide film formed on 316 SS after dichromate treatment showed that, similar to the film grown on 904L SS, the film was epitaxial. The orientation relationship was found to be the same orientation of the 904L:

$$(\bar{1}\bar{1}1)_{Cr_2O_3} \parallel (\bar{1}\bar{1}1)_{SS}; [011]_{Cr_2O_3} \parallel [011]_{SS}$$

The change of the microstructure of the film formed on 316 SS due to the dichromate treatment prior the film growth might be attributed to the chromium enrichment in the surface of 316 SS. This enrichment increases the chromium cation concentration with which oxygen ions react during the growth of the film. Therefore, the chromium content in the film increases as can be seen in table 6-1.

TEM investigations indicate that the increase in the Cr content of the film assists in the conversion of the microstructure from crystalline islands to an epitaxial form. This change could explain the absence of a “pop-in” event which is associated with the formation of a large crack during the penetration of the tip. The change of the film structure to an epitaxial layer might lead to the presence of small cracks to relieve stress and, therefore, the “pop-in” cannot be observed. A similar effect of dichromate treatment on the mechanical behavior of the iron (110) surface has also been reported by Chiba *et al* [86]. Also the smaller penetration depth of the tip into 316 SS after the dichromate treatment, as seen in region III of figure 6-2, is related to an increase in the hardness of the film due to increasing the chromium content. This higher concentration of Cr_2O_3

could lead to a higher, as well as stiffer, passive film than an amorphous matrix film with a higher Fe_2O_3 content.

Conclusion

The microstructure and chemistry of the passive films grown on 904L SS, 304 SS, and 316 SS were studied and correlated to the required fracture load. It was determined that the fracture load of the passive films was depended on the degree of crystallinity of the passive film. The passive film on 316 SS with a lower density of crystalline islands than that of the 304 SS had the lowest fracture load. In contrast, when the film was epitaxial, the fracture load was the largest. The dichromate treatment results indicate that the increase in degree of crystallinity of the passive films is associated with the increase in the chromium content of the substrate.

Chapter 7

Comparison between the in-situ and ex-situ results of the passive film strength formed on austenitic stainless steels

The passive film on stainless steel alloys is a dynamic system which continuously reacts with its surrounding environment. This makes structural and properties characterization challenging. Whatever precaution is taken to transfer the sample on which the film is grown from the electrolyte to an ultra high vacuum chamber, the passive film changes during the transformation [3]. In-situ studies of the passive films overcome the change in the passive film due to the exposure to atmosphere and allow investigation of the films in their service conditions. While many surface analysis methods are not compatible with aqueous environments, mechanical properties of the passive films can be compatible with these solutions.

In this chapter, in-situ nanoindentation tests were preformed to simultaneously evaluate the effect of multiple variables, particularly salt concentration, time, pH, temperature, and alloy composition on the load at fracture of passive films formed on austenitic stainless steel alloys at two different potentials, stable passive and metastable pitting potentials, using the Taguchi method. The loads at fracture for the film tested in-situ and ex-situ, chapters 4 and 5, were used to roughly compute and compare the tensile stress applied needed to fracture the passive film using Hertzian contact mechanics.

Experimental procedure

The materials and the procedure used to prepare the specimens is similar to that used in chapters 4 and 5. In summary, an EG&G 173 and 175 potentiostat and controller were used to grow the passive films. Chloride test solutions, adjusted to the required pH

and salt concentration by HCl and NaCl, were used to fill a small glass electrochemical cell especially designed for in-situ nanoindentation as shown in figure 7-1, with Ag/AgCl and platinum as reference and counter electrodes, respectively.

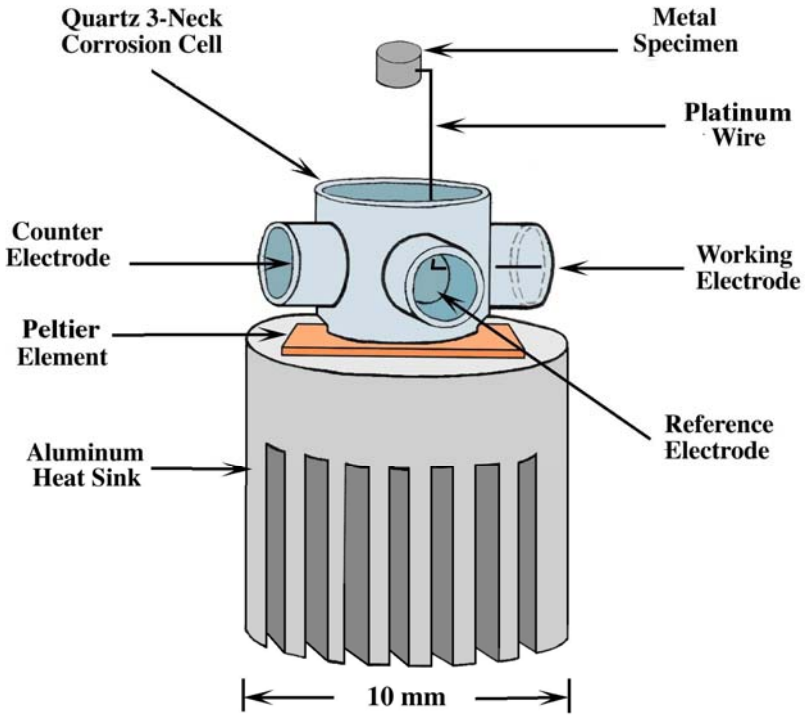

Figure 7-1Structure of electrochemical cell for in situ nanoindentation

A Peltier element was used to achieve the desired temperature of the electrolyte. The required solution temperatures were measured prior to experimentation by using thermocouple and were determined by varying the applied DC voltage to the Peltier element until the desired temperature was reached. To protect the scanner of the scanning probe microscope, an aluminum heat sink was used to minimize temperature gradient between the cell and scanner. Nanoindentation fracture load measurements of anodically passive films formed were performed using a Hysitron Triboscope with a Park Autoprobe

CP Scanning Probe Microscope (SPM). A maximum force of 500 μN was used for the nanoindentation tests. The in-situ indentation tests were made using a Berkovich tip with a tip radius of curvature of approximately 730nm and a loading rate of 50 μN s^{-1}. Solutions of 0.01, 0.05, and 0.1 M NaCl salt concentrations at pH's of 1, 3, and 5 were used in this study. To measure the fracture load of the passive film formed in an electrolyte, the potential was held cathodically for approximately 40 minutes. Then the sample was anodically polarized at constant rate of 2mV/s to and then held for two hours to grow the passive film; indentations were performed while the sample was under the electrochemical control using the potentiostat. The spring constant calibration for the nanoindentation loading system was performed within a couple micrometers of the sample surface to minimize the effect of contact angle between the electrolyte surface and the extension of the tip. Other researchers have found that this angle influences the loading capabilities due to surface tension [77].

Results

Figure 7-2 shows the anodic polarization behavior of 304 SS in an aqueous solution of pH of 1 adjusted by adding HCl and salt concentration of 0.01 M NaCl, respectively; the arrows indicated to the stable passive and metastable pitting potentials at which the films were grown. Figure 7-3 illustrates the load-depth curves of ex-situ and in-situ nanoindentations for the passive film formed on 904L SS using the rounded Berkovich indenter tip.

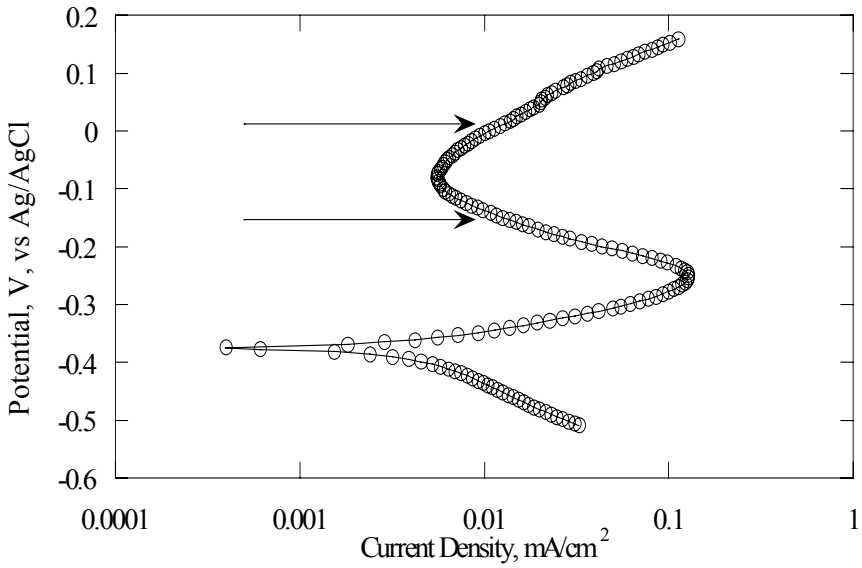

Figure 7-2 typical polarization curve for 304 SS in chloride solution, the arrows indicate to the potentials used to grow the films

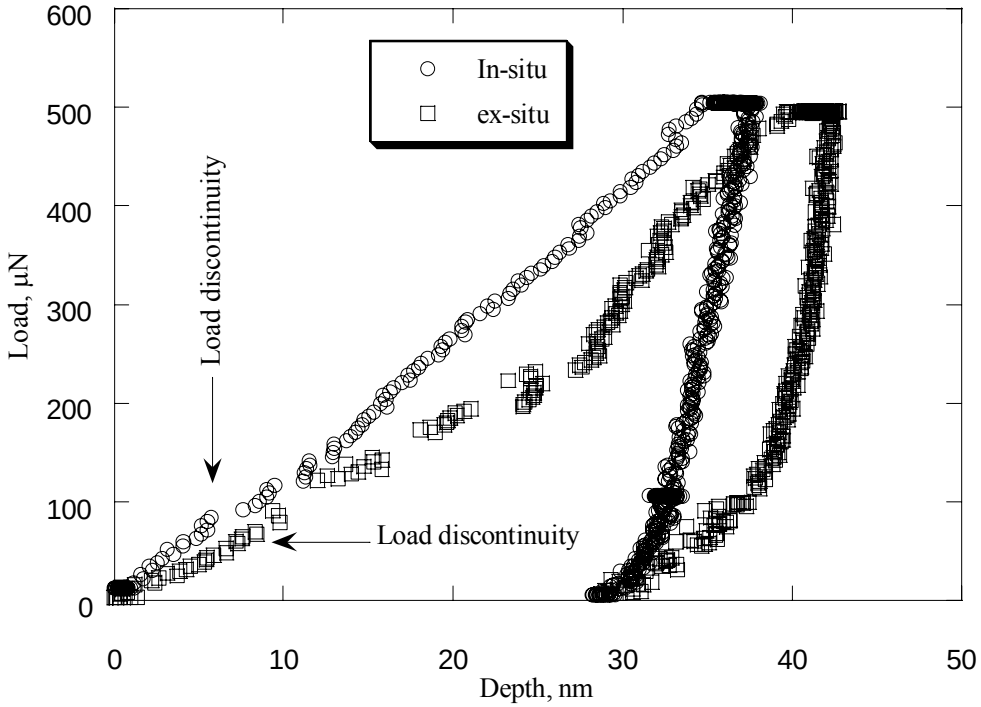

Figure 7-3 Ex-situ and in-situ nanoindentation curves of the passive film formed on 904L in chloride solution

Tables 7-1and 7-2 show the design, conditions, the averages and the standard deviations of the loads at fracture for the passive films formed at the stable passive and metastable pitting potentials, respectively. Each cell in the two tables represents the average load at fracture of at least six indents in two different grains.

Table 7-1 The design, conditions, and average fracture load of passive films formed in the stable passive potential region

Time (min)			60	120	60	120
Temperature (°C)			40	40	15	15
SS	pH	S.C	Fracture Load, μN			
304	1	0.01	80 ±9	86 ±9	74 ±15	87 ±8
304	3	0.05	83 ±11	87 ±11	81 ±10	90 ±5
304	5	0.1	89 ±18	86 ±17	82 ±12	94 ±13
316	1	0.1	69 ±8	91 ±13	76 ±16	74 ±16
316	3	0.01	73 ±8	87 ±6	82 ±10	82 ±11
316	5	0.05	74 ±7	80 ±13	89 ±3	86 ±4
904	1	0.05	103 ±11	100 ±9	93 ±6	96 ±5
904	3	0.1	92 ±9	92 ±11	95 ±12	96 ±9
904	5	0.01	98 ±16	96 ±9	99 ±14	105 ±14

Table 7-2 The design, conditions, and average fracture load of passive films formed in the metastable pitting potential region

Time (min)			60	120	60	120
Temperature(°C)			40	40	15	15
SS	pH	SC	Fracture Load, μN			
304	1	0.01	41 ±8	45 ±11	38±9	42 ±9
304	3	0.05	44 ±9	40 ±8	48 ±7	39±3
304	5	0.1	36 ±6	41 ±6	30 ±6	39 ±3
316	1	0.1	40 ±11	35 ±5	43 ±11	42 ±4
316	3	0.01	49 ±6	53 ±11	43 ±6	54 ±6
316	5	0.05	45 ±7	42 ±5	42 ±5	49 ±7
904	1	0.05	49 ±8	53 ±4	46 ±4	56 ±4
904	3	0.1	43 ±5	43 ±5	43 ±5	44 ±6
904	5	0.01	51 ±5	59 ±3	54 ±3	60 ±8

Forcing an indenter into a hard film, the passive oxide film, on a relatively soft substrate, the stainless steel, causes the substrate to deform easier than the film. To accommodate the deformation of the substrate a large tensile stress is developed in the film leading to film fracture. The shape of the tip influences the load required to fracture the passive film. Two different tips were used in this study. A cube corner tip was utilized to indent the passive film in ambient air. In situ nanoindentation measurements were preformed using a Berkovich tip. Rather than solely compare loads for fracture, one possible method to approximate the applied tensile stress is to use a first order estimation

by assuming the initial loading is similar to the elastic loading of surface by a sphere. The maximum radial tensile stress at the contact surface for elastic contacts can estimated by using Hertzian contact mechanics of spherical bodies which is given by [118]

$$\sigma = \frac{1-2\upsilon}{3}\left[\frac{6PE^{*2}}{\pi^3 R^2}\right]^{\frac{1}{3}} \qquad (7\text{-}1)$$

where P is the load at fracture, E^* is the reduced modulus, R is the effective radius of curvature which is defined as [74]

$$\frac{1}{E^*} = \frac{(1-\upsilon_i^2)}{E_i} + \frac{(1-\upsilon_f^2)}{E_f} \qquad (7\text{-}2)$$

where E and ν are the elastic modulus and Poisson's ratio of the indenter and the film, respectively. The in-situ nanoindentation measurements for the loads at fracture were used to roughly estimate the radial stress by using equations (7-1) and (7-2). The elastic modulus and Poisson ratio of the passive film and the tip were assumed to be 325GPa and 0.25 and 1140 GPa and 0.07, respectively [117, 74]. The values of stress were statistically analyzed using Minitab®, a commercial software program, as shown in appendix 1-4.

The significant level was set at 0.05. Therefore, any test resulting in a p value under 0.05 would be significant. In-situ nanoindentation measurements of the passive film formed at the stable passive potential showed that the alloy chemistry had the most significant effect on the load at fracture with P values equal to 0.032 and 0.028 for the linear and quadratic effects respectively. On the other hand, the linear influences of both the alloy chemistry and the salt concentration had the significant influences on the load at

fracture for the passive film formed at a metastable pitting potential; the *P* values were equal to 0.042 and 0.049, respectively.

Figures 7-4 and 7-5 show the main effect plots based on in situ measurements for the tensile stress required to fracture the passive film formed at the stable passive and metastable pitting potential, respectively. The Y axis represents the applied tensile stress. On the X axis, the levels of the control factors, alloy chemistry, pH, and salt concentration, are represented. The dashed line illustrates the overall average of the applied tensile stress at fracture for all testing conditions.

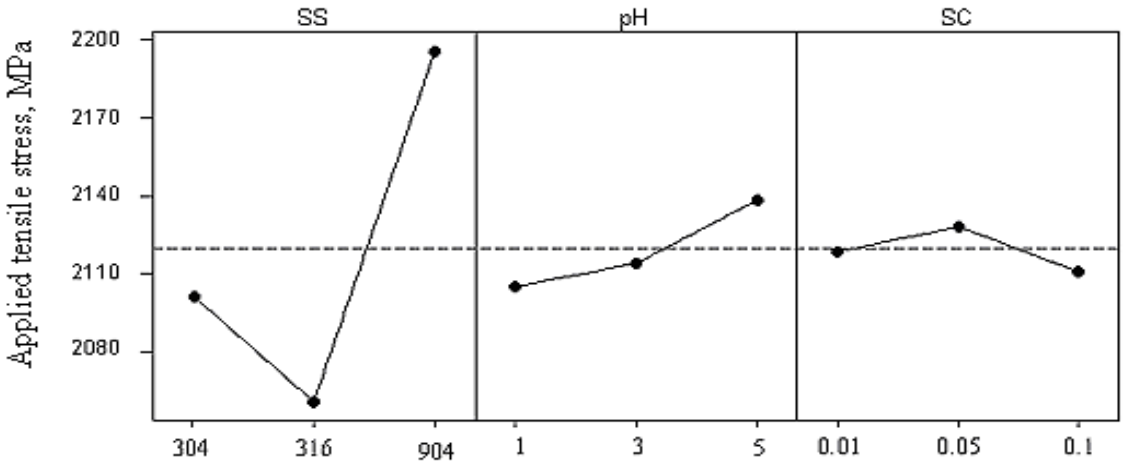

Figure 7-4The effect of the controlled factors (salt concentration, pH, and stainless alloy composition) on the tensile stress applied to the passive films formed at a stable passive potential

For the passive films formed at the stable passive potential, figure 7-4 shows that the substrate on which the passive film is formed was the most important factor affecting the tensile stress required to fracture the film; changing the substrate from 316SS to 304SS to 904L SS increased the strength of the passive film correspondingly. The influences of pH and the salt concentration are almost negligible. Similar results were obtained for the films indented in air in chapter 4.

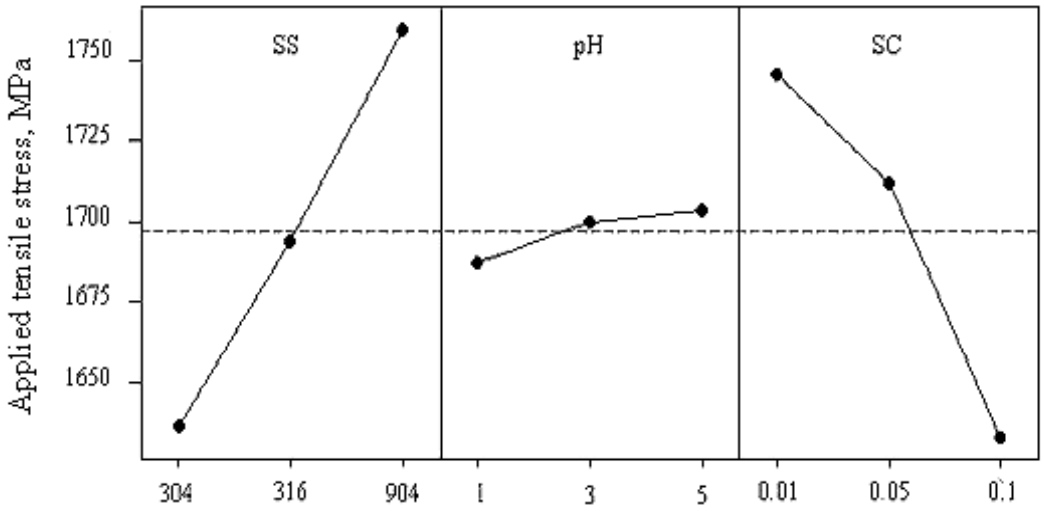

Figure 7-5 The effect of the controlled factors (salt concentration, pH, and stainless alloy composition) on the tensile stress applied to the passive films formed at metastable pitting potential

For the passive film formed at the metastable pitting potential, on the other hand, figure 7-5 shows that the tensile stress required to fracture the film is significantly influenced by both the salt concentration in the electrolyte and the substrate on which the film was formed. Increasing the salt concentration in the electrolyte from 0.01 to 0.05 to 0.1 M NaCl decreased the applied tensile stresses needed to fracture the film from (1.74 ± 0.09 to 1.70 ± 0.06 to 1.63 ± 0.05) GPa, respectively. The applied tensile stresses needed to fracture the film reduced from (1.76 ± 0.08 to 1.70 ± 0.06 to 1.63 ± 0.04) GPa when the substrate on which the film was formed was changed from 904L SS to 316SS to 304SS.

Figures 7-6 and 7-7 illustrate the influence of the applied potential on ex situ and in situ measurements, respectively, for the applied tensile stresses caused the fracture of the passive film formed at the different conditions. The X axis illustrates the growth

conditions corresponding to the rows in tables 7-1 and 7-2. The bars show the standard deviation while the circles and squares illustrate the average applied tensile stress that caused passive film fracture for each condition.

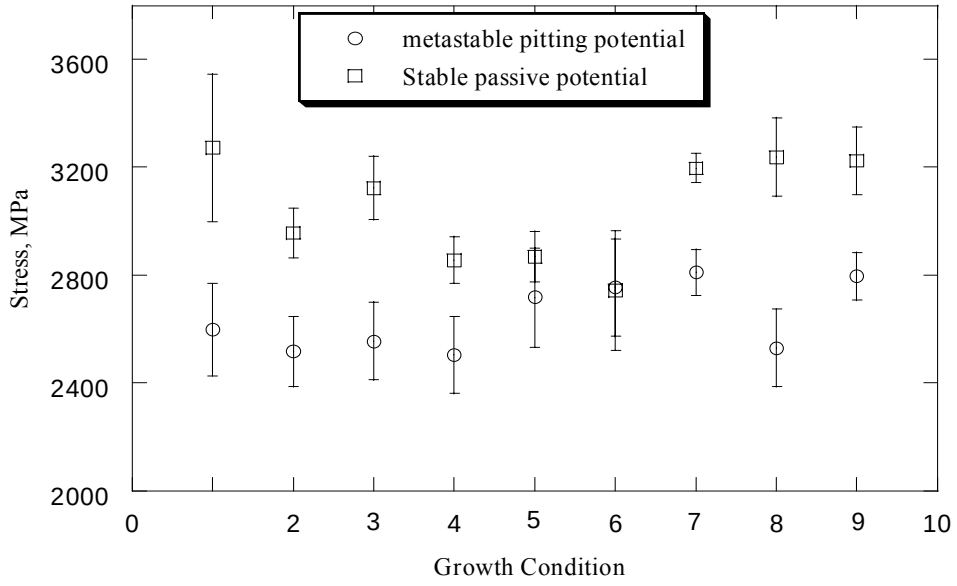

Figure 7-6 Ex-situ results of the tensile stress required to fracture the passive film

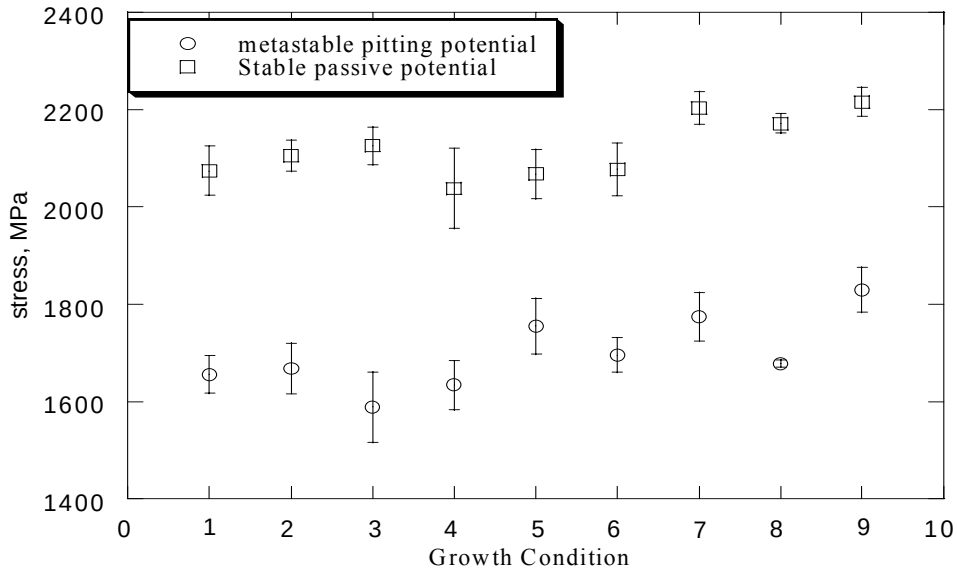

Figure 7-7 In-situ results of the tensile stress required to fracture the passive film

Figures 7-6 and 7-7 shows that the passive films formed at the stable passive potential were stronger than those formed at a metastable pitting potential. The overall average tensile stress required to fracture the passive film formed at the stable passive potential was decreased from 3.05GPa to 2.10GPa when the test environment was changed from ex situ to in situ. For the passive film formed at the metastable pitting potential changing the test environment from ex situ to in situ reduces the tensile stress required to break the film from 2.60GPa to 1.7GPa as shown in figure 7-8.

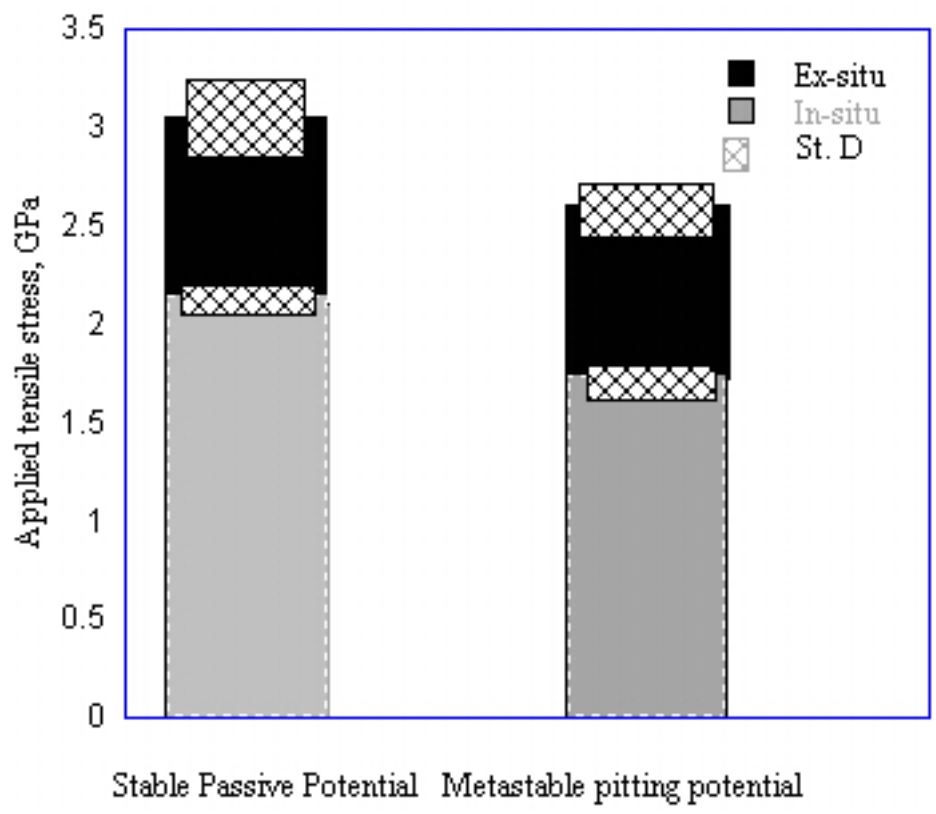

Figure 7-8 The overall averages of the applied tensile stress required to fracture the passive films formed at stable passive and metastable pitting potentials and indented in ambient air and in situ

The general contribution of each control factor in the overall average strength of the film formed and indented at different conditions is represented by figure 7-9.

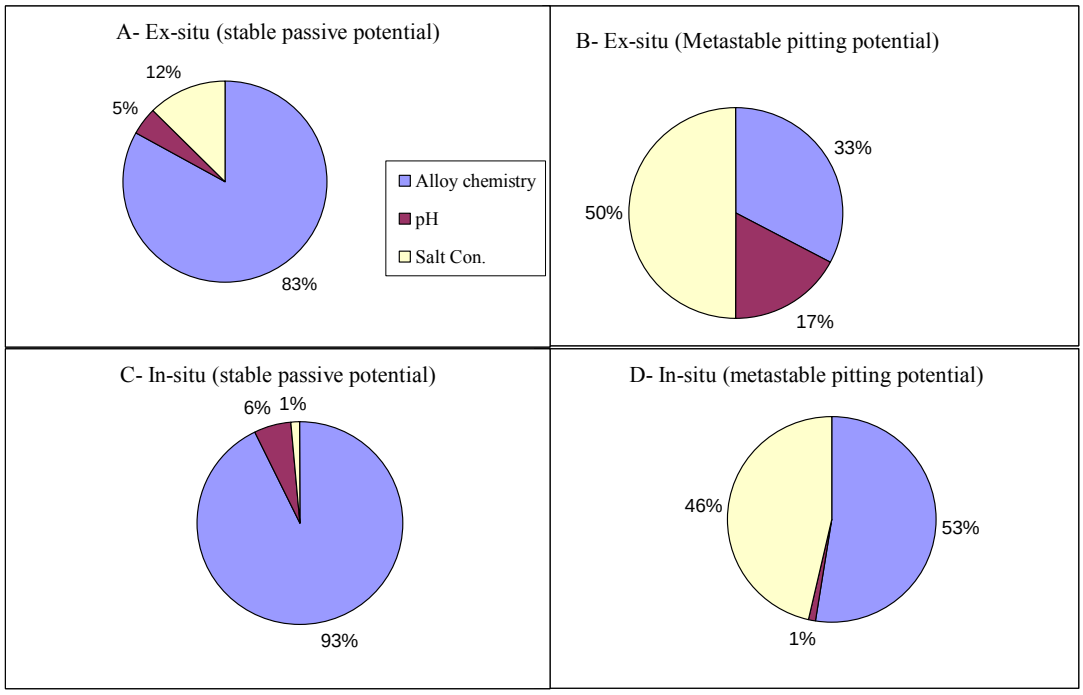

Figure 7-9 The general contribution of each control factor in the strength of the passive films formed at stable passive and metastable pitting potentials, respectively, and ex-situ indented (A and B) and the strength of the passive film formed at stable passive

For the passive film formed at the stable passive potential and ex-situ indented, 83% of the film strength was contributed by alloy chemistry. This contribution increased to 93% when the film was in-situ indented. On the other hand, for the film formed at the metastable pitting potential, the film strength was salt concentration and alloy chemistry dependent.

Discussion

The influence of the alloy chemistry on the tensile stress required to fracture the passive film formed at the stable passive potential could be due to the change of the film structure. It was found that the film formed on 904L SS was an epitaxial layer while for the films formed on 304SS and 316SS consisted of small crystalline islands.

Generally, both ex-situ and in situ measurements indicate that the films formed at the stable passive potential were stronger than that formed at the metastable pitting potential. The influence of the applied potential on the tensile stress needed to fracture the films might be explained by the two possible mechanisms: The first could be the repeated repassivation-depassivation process which takes place at the metastable pitting potential Dawson and Ferreira [110] observed the repassivation-depassivation process as pulses of current in the polarization curves, and described the repassivation-depassivation process to the film breaking down due to mechanical effects of chloride adsorption on the film. In the stable potential regime the chloride would be less likely to adsorb and become incorporated in the film. The second reason for the decrease in the film strength at increased potential is that an increase of the applied potential increases the iron content in the film [4,43]. This increase could mechanically weaken the passive film formed on austenitic stainless steels due to subsequent changes in film structure.

The passive film tested in air was slightly stronger than films indented in-situ. This might be due to the reaction of the film with the ambient environment during the transfer from the electrolyte to the nanoindenter which might have increased the film stability [119,120].Moreover, the difference in the tensile stress values of the ex situ and in situ film could be attributed to the capillary effect of the thin water layer between the nanoindenter tip and the surface while measuring in situ passive films, which other authors have found to impact the surface mechanical behavior [46,121]

Conclusion

For the passive films formed at stable passive potentials on austenitic stainless steels, the alloy chemistry was the most important factor affecting the strength of the

passive film. The salt concentration and the alloy chemistry were the two important factors that affected the mechanical strength passive film formed at a metastable pitting potential. The strength of passive films measured in situ during electrochemical film growth is less than when the same films are testing in ambient conditions after removed from solutions. However, the similarity between trends in film strength with alloy chemistry and salt concentration implies the in-situ and ex-situ tests are indeed measuring similar mechanical properties of these anodically grown passive films.

Chapter 8

Summary

In this study, the influence of alloy chemistry as well as the solution chemistry on the electrochemical and mechanical behaviors of the anodic passive film was investigated. Three different types of stainless steels, 304 SS, 316 SS, and 904L SS, were used as substrates on which passive films were anodically grown. The factors affected the solution chemistry were pH and a salt concentration of an electrolyte. The Taguchi method was utilized to design the experiments and analyze the data. For the electrochemical behavior, the pH of an electrolyte was found to be the most important factor affecting the corrosion rate. An increase of the pH led to a lower corrosion rate. The mechanical behavior of passive films on austenitic stainless steels was studied at stable passive and metastable pitting potentials. The alloy chemistry had the most significant effect on the load required to fracture the passive film formed at a stable passive potential. The average loads needed to break the passive films formed on 904L SS, 304SS, and 316SS were 59, 54, and 40μN, respectively. XPS results showed that the loads required to fracture the films increased as a function of decreasing iron concentration at a stable passive potential.

The increase in degree of crystallinity of the passive films was associated with the increase in the chromium content of the substrate. TEM results showed that the passive film formed on 304SS and 316 SS appeared as small crystalline islands in an amorphous matrix, whereas the film formed on 904L SS was an epitaxial layer. A dichromate treatment of 316 SS increased both the hardness and ratio of chromium content to the metallic elements in the film while decreasing the iron content of the film. The

dichromate treatment significantly changed the chromium oxide to an epitaxial film on the 316SS.

For the passive films formed at a metastable pitting potential, the salt concentration in an electrolyte and alloy chemistry mostly influenced the mechanical behavior. The load required to fracture the passive films increased by changing the substrate on which the films were grown from 304SS to 316SS to 904L SS, respectively. An increase of the salt concentration of an electrolyte mechanically weakened the passive films. The load required to break the film formed at stable passive potential was proportional to the aging time. On the other hand, the load at fracture of the passive films formed at a metastable pitting potential was inversely proportional to the aging time.

Nanoindentation performed in-situ during anodic polarization led to similar behavior and results. For the films formed at a stable passive potential, the alloy chemistry factor played the most significant effect on the fracture load; the average fracture load using a tip with a 750 nm radius of curvature was 87 μN. Again, the passive films on 904L were stronger than the films on the 300 series alloys. Both the salt concentration and the alloy chemistry controlled the load at fracture for the passive films formed at a metastable pitting potential; the average fracture load was 52% of the load applied to fracture the film a stable passive potential. The measured strength of films measured in ambient conditions after removed from the electrolyte was greater than when the films were measured in situ. However, the trends in film strength as a function of environment are the same between in situ and ex situ testing, suggesting the two tests are both feasible methods of analyzing environment effects of film strength.

Appendix

Appendix 1-1

Electrochemical behavior of the films formed at a stable passive potential.

```
MTB > name c1'SS'
MTB > set c1
DATA> -1 -1 -1 0 0 0 1 1 1
DATA> end
MTB > name c2'pH'
MTB > set c2
DATA> -1 0 1 -1 0 1 -1 0 1
DATA> end
MTB > name c3'S.C'
MTB > set c3
DATA> -1 0 1 0 1 -1 1 -1 0
DATA> end
MTB > name c4'IP-1-ob'
MTB > set c4
DATA> 0.00158 0.0005 0.00016 0.0019 0.0006 0.0001 0.001 0.0003 0.0002
DATA> end
MTB > name c5'IP-2-ob'
MTB > set c5
DATA> 0.00188 0.0011 0.00015 0.0016 0.0006 0.00008 0.00074 0.00047 0.0001
DATA> end
MTB > name c6'IP-3-ob'
MTB > set c6
DATA> 0.0018 0.0006 0.0002 0.0016 0.00065 0.00014 0.001 0.00027 0.0001
DATA> end
MTB > name c7'Average'
MTB > rmean c4-c6 c7
MTB > name c8'CC-1-ob'
MTB > set c8
DATA> 0.03456 0.00067 0.0001 0.019 0.0007 0.000095 0.0018 0.0004 0.00014
DATA> end
MTB > name c9'CC-2-ob'
MTB > set c9
DATA> 0.038 0.001 0.0001 0.015 0.0008 0.000058 0.0037 0.00058 0.00009
DATA> end
MTB > name c10'CC-3-ob'
MTB > set c10
DATA> 0.045 0.0005 0.00014 0.016 0.00078 0.00014 0.0035 0.0003 0.000097
DATA> end
MTB > name c11'CC-average'
MTB > name c7'IP-average'
MTB > rmean c8-c10 c11
MTB > name c12'SS-L'
MTB > set c12
DATA> -1 -1 -1 0 0 0 1 1 1
DATA> end
MTB > name c13'SS-Q'
MTB > set c13
DATA> -1 -1 -1 2 2 2 -1 -1 -1
DATA> end
MTB > name c14'pH-L'
MTB > set c14
DATA> -1 0 1 -1 0 1 -1 0 1
DATA> end
MTB > name c14'pH-L'
MTB > name c15'pH-Q'
```

```
MTB > set c15
DATA> -1 2 -1 -1 2 -1 -1 2 -1
DATA> end
MTB > name c16'SC-L'
MTB > set c16
DATA> -1 0 1 0 1 -1 1 -1 0
DATA> end
MTB > name c17'SS-Q'

* ERROR * Duplicate name not permitted.


MTB > name c17'SC-Q'
MTB > set c17
DATA> -1 2 -1 2 -1 -1 -1 -1 2
DATA> end
MTB > table c1;
SUBC> means c7.
```

Tabulated Statistics: SS

```
 Rows: SS

    IP-avera
        Mean

 -1 0.000886
 0  0.000808
 1  0.000464
 All0.000719

MTB > table c2;
SUBC> means c7.
```

Tabulated Statistics: pH

```
 Rows: pH

    IP-avera
        Mean

 -1 0.001456
 0  0.000566
 1  0.000137
 All0.000719

MTB > table c3;
SUBC> means c7.
```

Tabulated Statistics: S.C

```
 Rows: S.C

    IP-avera
        Mean

 -1 0.000736
 0  0.000856
 1  0.000567
 All0.000719

MTB > regr c7 6 c12-c17;
SUBC> coef c18.
```

Regression Analysis: IP-average versus SS-L, SS-Q, ...

```
The regression equation is
IP-average =0.000719 -0.000211 SS-L +0.000044 SS-Q -0.000659 pH-L
           -0.000077 pH-Q -0.000084 SC-L +0.000068 SC-Q

Predictor        Coef     SE Coef          T        P
Constant   0.00071926  0.00007283       9.88    0.010
SS-L      -0.00021056  0.00008920      -2.36    0.142
SS-Q       0.00004426  0.00005150       0.86    0.481
pH-L      -0.00065944  0.00008920      -7.39    0.018
pH-Q      -0.00007685  0.00005150      -1.49    0.274
SC-L      -0.00008444  0.00008920      -0.95    0.444
SC-Q       0.00006815  0.00005150       1.32    0.317

S = 0.0002185   R-Sq = 97.1%     R-Sq(adj) = 88.2%

Analysis of Variance

Source            DF          SS          MS         F        P
Regression         6 3.14316E-06 5.23859E-07     10.97    0.086
Residual Error     2 9.54840E-08 4.77420E-08
Total              8 3.23864E-06

Source       DF      Seq SS
SS-L          1 2.66002E-07
SS-Q          1 3.52599E-08
pH-L          1 2.60920E-06
pH-Q          1 1.06312E-07
SC-L          1 4.27852E-08
SC-Q          1 8.35951E-08



MTB > set c19
DATA> 6 18 6 18 6 18
DATA> copy c18 c18;
SUBC> omit 1.
MTB > let c19=sqrt (c19)
MTB > let c20=c19*c18
MTB > let c21=c20**2
MTB > let c22=100*(c21/sum(21))
MTB > prin c18-c22
```

Data Display

```
 Row         C18       C19         C20         C21         C22

   1  -0.0002106   2.44949  -0.0005158   0.0000003   0.0000013
   2   0.0000443   4.24264   0.0001878   0.0000000   0.0000002
   3  -0.0006594   2.44949  -0.0016153   0.0000026   0.0000124
   4  -0.0000769   4.24264  -0.0003261   0.0000001   0.0000005
   5  -0.0000844   2.44949  -0.0002068   0.0000000   0.0000002
   6   0.0000681   4.24264   0.0002891   0.0000001   0.0000004

MTB > let c23=abso (c20)
MTB > dotplot c23
```

Dotplot: C23

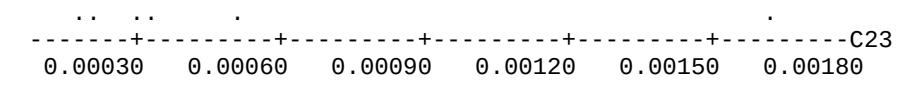


```
MTB > %daniel.mac c23
Executing from file: C:\WINDOWS\Desktop\Minitab\Minitab
13\MTBDEMO\MACROS\daniel.mac
Macro is running ... please wait
```

Daniel plot

```
NOTE: No Effect labels provided.
```

Daniel Plot for C23

```
MTB > %Main 'SS' 'pH' 'S.C';
SUBC>   Response 'IP-average'.
Executing from file: C:\WINDOWS\Desktop\Minitab\Minitab
13\MTBDEMO\MACROS\Main.MAC

Macro is running ... please wait
```

Main Effects Plot for IP-average

```
MTB > table c1;
SUBC> means c11.
```

Tabulated Statistics: SS

```
 Rows: SS

    CC-avera
        Mean

 -1 0.013341
 0  0.005841
 1  0.001179
 All0.006787

MTB > table c2;
```

```
SUBC> means c11.
```

Tabulated Statistics: pH

```
 Rows: pH

    CC-avera
        Mean

 -1 0.019618
 0  0.000637
 1  0.000107
 All0.006787

MTB > table c3;
SUBC> means c11.
```

Tabulated Statistics: S.C

```
 Rows: S.C

    CC-avera
        Mean

 -1 0.013237
 0  0.005833
 1  0.001291
 All0.006787

MTB > regr c11 6 c12-c17;
SUBC> coef c24.
```

Regression Analysis: CC-average versus SS-L, SS-Q, ...

```
The regression equation is
CC-average = 0.00679 - 0.00608 SS-L - 0.00047 SS-Q - 0.00976 pH-L
           - 0.00308 pH-Q - 0.00597 SC-L - 0.00048 SC-Q

Predictor        Coef     SE Coef          T        P
Constant     0.006787    0.003526       1.92    0.194
SS-L        -0.006081    0.004319      -1.41    0.294
SS-Q        -0.000473    0.002493      -0.19    0.867
pH-L        -0.009756    0.004319      -2.26    0.152
pH-Q        -0.003075    0.002493      -1.23    0.343
SC-L        -0.005973    0.004319      -1.38    0.301
SC-Q        -0.000477    0.002493      -0.19    0.866

S = 0.01058     R-Sq = 84.1%     R-Sq(adj) = 36.5%

Analysis of Variance

Source            DF          SS          MS         F        P
```

```
Regression         6   0.0011853   0.0001976      1.77    0.405
Residual Error     2   0.0002238   0.0001119
Total              8   0.0014091

Source       DF      Seq SS
SS-L          1   0.0002219
SS-Q          1   0.0000040
pH-L          1   0.0005710
pH-Q          1   0.0001702
SC-L          1   0.0002141
SC-Q          1   0.0000041



MTB > set c25
DATA> 6 18 6 18 6 18
DATA> let c25=sqrt (c25)
MTB > let c26=c25*c24
MTB > let c27=c26**2
MTB > let c28=100*(c27/sum(c27))
MTB > prin c24-c28
```

Data Display

Row	C24	C25	C26	C27	C28
1	-0.0060813	2.44949	-0.0148960	0.0002219	18.7201
2	-0.0004728	4.24264	-0.0020059	0.0000040	0.3395
3	-0.0097556	2.44949	-0.0238961	0.0005710	48.1750
4	-0.0030752	4.24264	-0.0130469	0.0001702	14.3609
5	-0.0059729	2.44949	-0.0146307	0.0002141	18.0590
6	-0.0004770	4.24264	-0.0020238	0.0000041	0.3455

```
MTB > let c29=abso (c26)
MTB > dotplot c29
```

Dotplot: C29

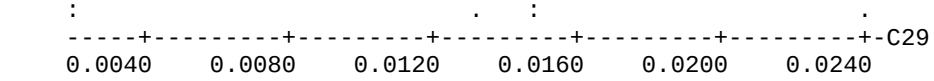


```
MTB > %daniel.mac c29
Executing from file: C:\WINDOWS\Desktop\Minitab\Minitab
13\MTBDEMO\MACROS\daniel.mac
Macro is running ... please wait
```

Daniel plot

```
NOTE: No Effect labels provided.
```

Daniel Plot for C29

```
MTB > %Main 'SS' 'pH' 'S.C';
SUBC>   Response  'CC-average'.
Executing from file: C:\WINDOWS\Desktop\Minitab\Minitab
13\MTBDEMO\MACROS\Main.MAC
```

```
Macro is running ... please wait

MTB > Stop.
```

Appendix 1-2

Fracture load of the films formed at a stable passive potential.

```
MTB > name c1'SS'
MTB > set c1
DATA> -1 -1 -1 0 0 0 1 1 1
DATA> end
MTB > name c2'pH'
MTB > set c2
DATA> -1 0 1 -1 0 1 -1 0 1
DATA> end
MTB > name c3'SC'
MTB > set c3
DATA> -1 0 1 1 -1 0 0 1 -1
DATA> end
MTB > name c4'1-ob'
MTB > set c4
DATA> 42.11 49.78 46.66 46.39 41.489 26.49 55.18 65.67 51.48
DATA> end
MTB > name c5'2-ob'
MTB > set c5
DATA> 68.15 50.06 57.91 40.086 48.03 40.52 60.83 68.45 62.59
DATA> end
MTB > name c6'3-ob'
MTB > set c6
DATA> 74.89 43.20 53.27 37.52 38.01 35.32 56.65 50.48 58.24
DATA> end
MTB > name c7 '4-ob'
MTB > set c7
DATA> 69.00 41.89 60.48 42.75 41.58 47.21 60.93 58.93 67.84
DATA> end
MTB > rmean c4-c7 c8
MTB > name c9'SS-L'
MTB > set c9
DATA> -1 -1 -1 0 0 0 1 1 1
DATA> end
MTB > name c10'SS-Q'
MTB > set c10
DATA> -1 -1 -1 2 2 2 -1 -1 -1
DATA> end
MTB > name c11'pH-L'
MTB > set c11
DATA> -1 0 1 -1 0 1 -1 0 1
DATA> end
MTB > name c12'pH-Q'
MTB > set c12
DATA> -1 2 -1 -1 2 -1 -1 2 -1
DATA> end
MTB > name c13'SC-L'
MTB > set c13
DATA> -1 0 1 1 -1 0 0 1 -1
DATA> end
MTB > name c14'SC-Q'
MTB > set c14
DATA> -1 2 -1 -1 -1 2 2 -1 -1
DATA> end
MTB > table c1;
SUBC> means c8.
```

Tabulated Statistics

```
 Rows: SS

          C8
        Mean

 -1   54.783
 0    40.450
 1    59.773
 All  51.668

MTB > name c8'Average'
MTB > table c2;
SUBC> means c8.
```

Tabulated Statistics

```
 Rows: pH

     Average
        Mean

 -1   54.541
 0    49.797
 1    50.668
 All  51.668

MTB > table c3;
SUBC> means c8.
```

Tabulated Statistics

```
 Rows: SC

     Average
        Mean

 -1   55.284
 0    47.338
 1    52.383
 All  51.668

MTB > regr c8 6 c9-c15;
SUBC> coef c15.
```

Regression Analysis

```
The regression equation is
Average = 51.7 + 2.49 SS-L - 5.61 SS-Q - 1.94 pH-L - 0.936 pH-Q - 1.45 SC-L
           - 2.17 SC-Q

Predictor        Coef       StDev          T        P
Constant       51.668       1.333      38.75    0.001
```

```
SS-L            2.495       1.633       1.53    0.266
SS-Q          -5.6094      0.9427      -5.95    0.027
pH-L           -1.937       1.633      -1.19    0.357
pH-Q          -0.9355      0.9427      -0.99    0.426
SC-L           -1.451       1.633      -0.89    0.468
SC-Q          -2.1651      0.9427      -2.30    0.148

S = 4.000       R-Sq = 95.9%     R-Sq(adj) = 83.4%

Analysis of Variance

Source            DF          SS          MS         F        P
Regression         6      738.98      123.16      7.70    0.119
Residual Error     2       31.99       16.00
Total              8      770.97

Source       DF      Seq SS
SS-L          1       37.34
SS-Q          1      566.39
pH-L          1       22.50
pH-Q          1       15.75
SC-L          1       12.62
SC-Q          1       84.38



MTB > set c16
DATA> 6 18 6 18 6 18
DATA> copy c15 c15;
SUBC> omit 1.
MTB > let c16=sqrt (c16)
MTB > let c17=c16*c15
MTB > let c18=c17**2
MTB > let c19=100*(c18/sum (c18))
MTB > print c15-c19
```

Data Display

```
 Row       C15       C16       C17       C18       C19

   1    2.4946   2.44949    6.1105    37.338    5.0526
   2   -5.6094   4.24264  -23.7989   566.386   76.6445
   3   -1.9365   2.44949   -4.7434    22.500    3.0448
   4   -0.9355   4.24264   -3.9691    15.754    2.1318
   5   -1.4505   2.44949   -3.5531    12.624    1.7084
   6   -2.1651   4.24264   -9.1856    84.375   11.4179

MTB > let c20= abso (c17)
MTB > dotplot c20
```

Dotplot

```
            .. .  .       .                                .
          ---+---------+---------+---------+---------+---------+---C20
           4.0       8.0      12.0      16.0      20.0      24.0

MTB > %daniel.mac c17
Executing from file: C:\Program Files\MTBWINST\MACROS\daniel.mac
```

```
Macro is running ... please wait
```

Daniel plot

```
NOTE: No Effect labels provided.
MTB > %Main 'SS' 'pH' 'SC';
SUBC>   Response 'Average'.
Executing from file: C:\Program Files\MTBWINST\MACROS\Main.MAC

Macro is running ... please wait
MTB > Save  "G:\force_s_p_cl.MPJ";
SUBC>    Project;
SUBC>    Replace.
Saving file as: G:\force_s_p_cl.MPJ
```

Appendix 1-3.

Fracture load of the films formed at a metastable pitting potential.

```
MTB > name c1'SS'
MTB > set c1
DATA> -1 -1 -1 0 0 0 1 1 1
DATA> end
MTB > name c2'pH'
MTB > set c2
DATA> -1 0 1 -1 0 1 -1 0 1
DATA> end
MTB > name c3'SC'
MTB > set c3
DATA>  -1 0 1 1 -1 0 0 1 -1
DATA> end
MTB > name c4'1-ob'
MTB > set c4
DATA> 32.33 26.20 25.59 32.14 35.13 45.06 42.83 27.08 44.64
DATA> end
MTB > name c5'2-ob'
MTB > set c5
DATA> 30.30 25.09 28.74 27.32 26.83 37.93 36.67 23.28 37.39
DATA> end
MTB > name c6'3-ob'
MTB > set c6
DATA> 24.31 27.74 27.96 31.34 43.17 39.58 42.87 34.10 36.35
DATA> end
MTB > name c7'4-ob'
MTB > set c7
DATA> 39.36 35.36 37.68 21.97 39.56 28.03 36.53 31.94 38.04
DATA> end
MTB > name c8'Average'
MTB > rmean c4-c7 c8
MTB > name c9'SS-L'
MTB > set c9
DATA> -1 -1 -1 0 0 0 1 1 1
DATA> end
MTB > name c10'SS-Q'
MTB > set c10
DATA> -1 -1 -1 2 2 2 -1 -1 -1
DATA> end
MTB > name c11'pH-L'
MTB > set c11
DATA>  -1 0 1 -1 0 1 -1 0 1
DATA> end
MTB > name c12'pH-Q'
MTB > set c12
DATA>  -1 2 -1 -1 2 -1 -1 2 -1
DATA> end
MTB > name c13'SC-L'
MTB > set c13
DATA>  -1 0 1 1 -1 0 0 1 -1
DATA> end
MTB > name c14'SC-Q'
MTB > set c14
DATA>  -1 2 -1 -1 -1 2 2 -1 -1
DATA> end
MTB > table c1;
SUBC> means c8.
```

Tabulated Statistics: SS

```
 Rows: SS

     Average
        Mean

 -1   30.055
 0    34.005
 1    35.977
 All  33.346

MTB > table c2;
SUBC> means c8.
```

Tabulated Statistics: pH

```
 Rows: pH

     Average
        Mean

 -1   33.164
 0    31.290
 1    35.583
 All  33.346

MTB > table c3;
SUBC> means c8.
```

Tabulated Statistics: SC

```
 Rows: SC

     Average
        Mean

 -1   35.618
 0    35.324
 1    29.095
 All  33.346

MTB > regr c8 6 c9-c14;
SUBC> coef c15.
```

Regression Analysis: Average versus SS-L, SS-Q, pH-L, pH-Q, SC-L, SC-Q

```
The regression equation is
Average = 33.3 + 2.96 SS-L + 0.330 SS-Q + 1.21 pH-L - 1.03 pH-Q - 3.26 SC-L
          + 0.989 SC-Q
```

```
Predictor        Coef     SE Coef          T        P
Constant       33.346       1.003      33.24    0.001
SS-L            2.961       1.229       2.41    0.138
SS-Q           0.3297      0.7094       0.46    0.688
pH-L            1.209       1.229       0.98    0.429
pH-Q          -1.0278      0.7094      -1.45    0.284
SC-L           -3.261       1.229      -2.65    0.117
SC-Q           0.9893      0.7094       1.39    0.298

S = 3.010       R-Sq = 90.0%     R-Sq(adj) = 60.2%

Analysis of Variance

Source            DF          SS          MS         F        P
Regression         6     163.774      27.296      3.01    0.270
Residual Error     2      18.115       9.057
Total              8     181.889

Source       DF      Seq SS
SS-L          1      52.599
SS-Q          1       1.957
pH-L          1       8.773
pH-Q          1      19.014
SC-L          1      63.815
SC-Q          1      17.617



MTB > set c16
DATA> 6 18 6 18 6 18
DATA> copy c15 c15;
SUBC> omit 1.
MTB > let c16=sqrt (c16)
MTB > let c17=c16*c15
MTB > let c18=c17**2
MTB > let c19=100*(c18/sum (c18))
MTB > prin c15-c19
```

Data Display

```
 Row       C15       C16       C17       C18       C19

   1    2.9608   2.44949   7.25253   52.5992   32.1169
   2    0.3297   4.24264   1.39889    1.9569    1.1949
   3    1.2092   2.44949   2.96184    8.7725    5.3565
   4   -1.0278   4.24264  -4.36049   19.0139   11.6098
   5   -3.2612   2.44949  -7.98840   63.8145   38.9650
   6    0.9893   4.24264   4.19727   17.6171   10.7569

MTB > let c20=abso (c17)
MTB > dotplot c20
```

Dotplot: C20

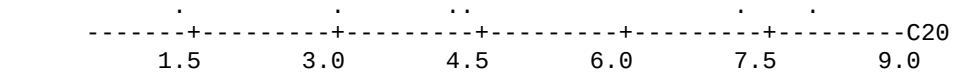

```
MTB > %daniel.mac c20
Executing from file: C:\WINDOWS\Desktop\Minitab\Minitab
13\MTBDEMO\MACROS\daniel.mac
Macro is running ... please wait
```

Daniel plot

```
NOTE: No Effect labels provided.
```

Daniel Plot for C20

```
MTB > %Main 'SS' 'pH' 'SC';
SUBC>   Response 'Average'.
Executing from file: C:\WINDOWS\Desktop\Minitab\Minitab
13\MTBDEMO\MACROS\Main.MAC

Macro is running ... please wait
```

Main Effects Plot for Average

```
MTB > Save  "D:\force-pp-cl.MPJ";
SUBC>    Project;
SUBC>    Replace.
Saving file as: D:\force-pp-cl.MPJ
```

Appendix 1-4

Ex-situ Results

1- Applied tensile stress fracturing the passive films formed at a stable passive potential

```
MTB > name c1'SS'
MTB > set c1
DATA> -1 -1 -1 0 0 0 1 1 1
DATA> end
MTB > name c2'pH'
MTB > set c2
DATA> -1 0 1 -1 0 1 -1 0 1
DATA> end
MTB > name c3'SC'
MTB > set c3
DATA> -1 0 1 1 -1 0 0 1 -1
DATA> end
MTB > name c4'stress1'
MTB > set c4
DATA> 2868 3033 2968 2962 2854 2458 3139 3326 3067
DATA> end
MTB > name c5'stress2'
MTB > set c5
DATA> 3367 3038 3189 2822 2997 2832 3242 3372 3273
DATA>  end
MTB > name c6'stress3'
MTB > set c6
DATA> 3475 2893 3102 2760 2772 2705 3166 3047 3195
DATA> end
MTB > name c7'stress4'
MTB > set c7
DATA> 3381 2863 3236 2883 2856 2980 3244 3208 3362
DATA> end
MTB > name c8'Mean'
MTB > rmean c4-c7 c8
MTB > name c9'SS-L'
MTB > set c9
DATA> -1 -1 -1 0 0 0 1 1 1
DATA> end
MTB > name c10'SS-Q'
MTB > set c10
DATA> -1 -1 -1 2 2 2 -1 -1 -1
DATA> end
MTB >  name c11'pH-L'
MTB > set c11
DATA> -1 0 1 -1 0 1 -1 0 1
DATA> end
MTB > name c12'pH-Q'
MTB > set c12
DATA> -1 2 -1 -1 2 -1 -1 2 -1
DATA> end
MTB >  name c13'SC-L'
MTB > set c13
DATA> -1 0 1 1 -1 0 0 1 -1
DATA> end
```

```
MTB > name c14'SC-Q'
MTB > set c14
DATA> -1 2 -1 -1 -1 2 2 -1 -1
DATA> end
MTB > table c1;
SUBC> means c8.
```

Tabulated Statistics: SS

```
 Rows: SS

        Mean
        Mean

 -1    3117.8
 0     2823.4
 1     3220.1
 All   3053.8

MTB > table c2;
SUBC> means c8.
```

Tabulated Statistics: pH

```
 Rows: pH

        Mean
        Mean

 -1    3109.1
 0     3021.6
 1     3030.6
 All   3053.8

MTB > table c3;
SUBC> means c8.
```

Tabulated Statistics: SC

```
 Rows: SC

        Mean
        Mean

 -1    3122.3
 0     2966.1
 1     3072.9
 All   3053.8
```

```
MTB > regr c8 6 c9-c14;
SUBC>  coef c15.
```

Regression Analysis: Mean versus SS-L, SS-Q, pH-L, pH-Q, SC-L, SC-Q

```
The regression equation is
Mean = 3054 + 51.2 SS-L - 115 SS-Q - 39.2 pH-L - 16.1 pH-Q - 24.7 SC-L
           - 43.8 SC-Q

Predictor        Coef     SE Coef          T        P
Constant      3053.75       21.47     142.23    0.000
SS-L            51.17       26.30       1.95    0.191
SS-Q          -115.17       15.18      -7.59    0.017
pH-L           -39.25       26.30      -1.49    0.274
pH-Q           -16.08       15.18      -1.06    0.400
SC-L           -24.67       26.30      -0.94    0.447
SC-Q           -43.83       15.18      -2.89    0.102

S = 64.41       R-Sq = 97.4%     R-Sq(adj) = 89.5%

Analysis of Variance

Source            DF          SS          MS         F        P
Regression         6      306583       51097     12.32    0.077
Residual Error     2        8298        4149
Total              8      314881

Source       DF      Seq SS
SS-L          1       15708
SS-Q          1      238740
pH-L          1        9243
pH-Q          1        4656
SC-L          1        3651
SC-Q          1       34585
```

```
MTB >  set c16
DATA>  6 18 6 18 6 18
DATA> copy c15 c15;
SUBC> omit 1.
MTB > let c16=sqrt (c16)
MTB >  let c17=c16*c15
MTB > let c18=c17**2
MTB > let c19=100*(c18/sum (c18))
MTB > print c15-c19
```

Data Display

```
 Row       C15       C16       C17       C18       C19

   1     51.17   2.44949   125.332     15708    5.1236
   2   -115.17   4.24264  -488.611    238740   77.8713
   3    -39.25   2.44949   -96.142      9243    3.0150
   4    -16.08   4.24264   -68.236      4656    1.5187
   5    -24.67   2.44949   -60.421      3651    1.1908
   6    -43.83   4.24264  -185.969     34585   11.2806
```

```
MTB > let c20= abso (c17)
```

```
MTB > dotplot c20
```

Dotplot: C20

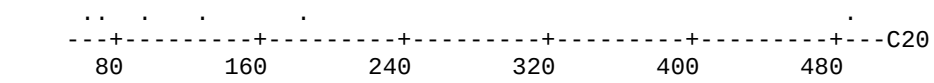


```
MTB > %daniel.mac c17
Executing from file: C:\WINDOWS\Desktop\Minitab\Minitab
13\MTBDEMO\MACROS\daniel.mac
Macro is running ... please wait
```

Daniel plot

```
NOTE: No Effect labels provided.
```

Daniel Plot for C17

```
MTB > %Main 'SS' 'pH' 'SC';
SUBC>   Response 'Mean'.
Executing from file: C:\WINDOWS\Desktop\Minitab\Minitab
13\MTBDEMO\MACROS\Main.MAC

Macro is running ... please wait
```

Main Effects Plot for Mean

```
MTB > Save  "C:\Documents and Settings\Administrator\My
Documents\Thesis\stresses\elastic-ex-sp-stress.MPJ";
SUBC>    Project;
SUBC>    Replace.
```

2- Applied tensile stress fracturing the passive films formed at a metastable pitting potential

```
MTB > name c1'SS'
MTB > set c1
DATA> -1 -1 -1 0 0 0 1 1 1
DATA> end
MTB > name c2'pH'
MTB > set c2
DATA> -1 0 1 -1 0 1 -1 0 1
DATA> end
MTB > name c3'SC'
MTB > set c3
DATA> -1 0 1 1 -1 0 0 1 -1
DATA> end
MTB > name c4'stress-1'
MTB > set c4
DATA> 2627 2449 2430 2622 2700 2934 2885 2476 2925
DATA> end
MTB > name c5'stress-2'
MTB > set c5
DATA> 2571 2414 2526 2483 2469 2770 2739 2355 2757
DATA> end
MTB > name c6'stress-3'
MTB > set c6
DATA> 2389 2496 2503 2600 2892 2810 2885 2674 2731
DATA> end
MTB > name c7'stress-4'
MTB > set c7
DATA> 2805 2706 2764 2310 2809 2505 2736 2616 2773
DATA> end
MTB > name c8'Mean'
MTB > rmean c4-c7 c8
MTB > name c9'SS-L'
MTB > set c9
DATA> -1 -1 -1 0 0 0 1 1 1
DATA> end
MTB >  name c10'SS-Q'
MTB > set c10
DATA>  -1 -1 -1 2 2 2 -1 -1 -1
DATA> end
MTB > name c11'pH-L'
MTB > set c11
DATA>  -1 0 1 -1 0 1 -1 0 1
DATA> end
MTB >  name c12'pH-Q'
MTB > set c12
DATA> -1 2 -1 -1 2 -1 -1 2 -1
DATA> end
MTB > name c13'SC-L'
MTB > set c13
DATA> -1 0 1 1 -1 0 0 1 -1
DATA> end
MTB >  name c14'SC-Q'
MTB > set c14
DATA> -1 2 -1 -1 -1 2 2 -1 -1
DATA> end
MTB > table c1;
SUBC> means c8.
```

Tabulated Statistics: SS

```
 Rows: SS

        Mean
        Mean

 -1   2556.7
 0    2658.7
 1    2712.7
 All  2642.7

MTB > table c2;
SUBC> means c8.
```

Tabulated Statistics: pH

```
 Rows: pH

        Mean
        Mean

 -1   2637.7
 0    2588.0
 1    2702.3
 All  2642.7

MTB > table c3;
SUBC> means c8.
```

Tabulated Statistics: SC

```
 Rows: SC

        Mean
        Mean

 -1   2704.0
 0    2694.1
 1    2529.9
 All  2642.7

MTB > regr c8 6 c9-c14;
SUBC> coef c15.
```

Regression Analysis: Mean versus SS-L, SS-Q, pH-L, pH-Q, SC-L, SC-Q

```
The regression equation is
Mean = 2643 + 78.0 SS-L + 8.0 SS-Q + 32.3 pH-L - 27.3 pH-Q - 87.0 SC-L
           + 25.7 SC-Q

Predictor        Coef     SE Coef          T        P
Constant      2642.67       26.86      98.40    0.000
SS-L            78.00       32.89       2.37    0.141
SS-Q             8.00       18.99       0.42    0.715
pH-L            32.33       32.89       0.98    0.429
pH-Q           -27.33       18.99      -1.44    0.287
SC-L           -87.04       32.89      -2.65    0.118
```

```
SC-Q            25.71       18.99       1.35    0.309

S = 80.57       R-Sq = 89.8%     R-Sq(adj) = 59.3%

Analysis of Variance

Source            DF          SS          MS         F        P
Regression         6      114731       19122      2.95    0.275
Residual Error     2       12983        6492
Total              8      127714

Source       DF      Seq SS
SS-L          1       36504
SS-Q          1        1152
pH-L          1        6273
pH-Q          1       13448
SC-L          1       45458
SC-Q          1       11897



MTB > set c16
DATA> 6 18 6 18 6 18
DATA> copy c15 c15;
SUBC> omit 1.
MTB > let c16=sqrt (c16)
MTB > let c17=c16*c15
MTB > let c18=c17**2
MTB > let c19=100*(c18/sum (c18))
MTB > print c15-c19
```

Data Display

```
 Row       C15       C16       C17       C18       C19

   1     78.00   2.44949   191.060   36504.0   31.8171
   2      8.00   4.24264    33.941    1152.0    1.0041
   3     32.33   2.44949    79.200    6272.7    5.4673
   4    -27.33   4.24264  -115.966   13448.0   11.7214
   5    -87.04   2.44949  -213.208   45457.5   39.6210
   6     25.71   4.24264   109.071   11896.5   10.3691

MTB > let c20= abso (c17)
MTB > dotplot c20

dotplot c20
```

Dotplot: C20

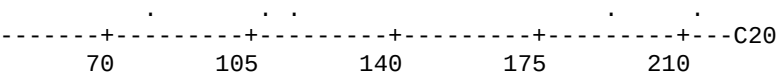


```
MTB > %daniel.mac c17
Executing from file: C:\WINDOWS\Desktop\Minitab\Minitab
13\MTBDEMO\MACROS\daniel.mac
Macro is running ... please wait
```

Daniel plot

```
NOTE: No Effect labels provided.
```

Daniel Plot for C17

```
MTB > %Main 'SS' 'pH' 'SC';
SUBC>   Response 'Mean'.
Executing from file: C:\WINDOWS\Desktop\Minitab\Minitab
13\MTBDEMO\MACROS\Main.MAC

Macro is running ... please wait
```

Main Effects Plot for Mean

```
MTB > Save  "C:\Documents and Settings\Administrator\My
Documents\Thesis\stresses\elastic-ex-pp-stress.MPJ";
SUBC>    Project;
SUBC>    Replace.
```

In-situ results

1- Applied tensile stress fracturing the passive films formed at a stable passive potential

```
MTB > name c1'SS'
MTB > set c1
DATA> -1 -1 -1 0 0 0 1 1 1
DATA> end
MTB > name c2'pH'
MTB > set c2
DATA> -1 0 1 -1 0 1 -1 0 1
DATA> end
MTB > name c3'SC'
MTB > set c3
DATA> -1 0 1 1 -1 0 0 1 -1
DATA> end
MTB > name c4'stress-1'
MTB > set c4
DATA> 2063 2086 2134 1961 1997 2011 2240 2162 2203
DATA> end
MTB > name c5'stress-2'
MTB > set c5
DATA> 2107 2116 2112 2153 2116 2058 2219 2156 2190
DATA> end
MTB > name c6'stress-3'
MTB > set c6
DATA> 2008 2073 2081 2029 2080 2131 2164 2180 2211
DATA> end
MTB > name c7'stress-4'
MTB > set c7
DATA> 2118 2144 2173 2009 2077 2107 2190 2186 2258
DATA> end
MTB > name c8'Mean'
MTB > rmean c4-c7 c8
MTB > name c9'SS-L'
MTB > set c9
DATA> -1 -1 -1 0 0 0 1 1 1
DATA> end
MTB > name c10'SS-Q'
MTB > set c10
DATA> -1 -1 -1 2 2 2 -1 -1 -1
DATA> end
MTB > name c11'pH-L'
MTB > set c11
DATA> -1 0 1 -1 0 1 -1 0 1
DATA> end
MTB >  name c12'pH-Q'
MTB > set c12
DATA> -1 2 -1 -1 2 -1 -1 2 -1
DATA> end
MTB > name c13'SC-L'
MTB > set c13
DATA> -1 0 1 1 -1 0 0 1 -1
DATA> end
MTB > name c14'SC-Q'
MTB > set c14
DATA> -1 2 -1 -1 -1 2 2 -1 -1
DATA> end
MTB > table c1;
SUBC> means c8.
```

Tabulated Statistics: SS

```
 Rows: SS

        Mean
        Mean

 -1   2101.3
 0    2060.8
 1    2196.6
 All  2119.5

MTB > table c2;
SUBC> means c8.
```

Tabulated Statistics: pH

```
 Rows: pH

        Mean
        Mean

 -1   2105.1
 0    2114.4
 1    2139.1
 All  2119.5

MTB > table c3;
SUBC> means c8.
```

Tabulated Statistics: SC

```
 Rows: SC

        Mean
        Mean

 -1   2119.0
 0    2128.3
 1    2111.3
 All  2119.5

MTB > regr c8 6 c9-c14;
SUBC> coef c15.
```

Regression Analysis: Mean versus SS-L, SS-Q, pH-L, pH-Q, SC-L, SC-Q

```
The regression equation is
Mean = 2120 + 47.7 SS-L - 29.4 SS-Q + 17.0 pH-L - 2.56 pH-Q - 3.83 SC-L
           + 4.36 SC-Q

Predictor        Coef     SE Coef          T        P
Constant      2119.53        7.12     297.65    0.000
SS-L           47.667       8.721       5.47    0.032
SS-Q          -29.389       5.035      -5.84    0.028
pH-L           17.000       8.721       1.95    0.191
pH-Q           -2.556       5.035      -0.51    0.662
SC-L           -3.833       8.721      -0.44    0.703
SC-Q            4.361       5.035       0.87    0.478

S = 21.36       R-Sq = 97.2%     R-Sq(adj) = 88.7%

Analysis of Variance

Source            DF          SS          MS         F        P
Regression         6     31461.5      5243.6     11.49    0.082
Residual Error     2       912.7       456.4
Total              8     32374.2

Source       DF      Seq SS
SS-L          1     13632.7
SS-Q          1     15546.7
pH-L          1      1734.0
pH-Q          1       117.6
SC-L          1        88.2
SC-Q          1       342.3



MTB > set c16
DATA> 6 18 6 18 6 18
DATA> copy c15 c15;
SUBC> omit 1.
MTB > let c16=sqrt (c16)
MTB > let c17=c16*c15
MTB > let c18=c17**2
MTB > let c19=100*(c18/sum (c18))
MTB > print c15-c19
```

Data Display

```
 Row       C15       C16       C17       C18       C19

   1     47.67   2.44949   116.759   13632.7   43.3313
   2    -29.39   4.24264  -124.686   15546.7   49.4151
   3     17.00   2.44949    41.641    1734.0    5.5115
   4     -2.56   4.24264   -10.842     117.6    0.3736
   5     -3.83   2.44949    -9.390      88.2    0.2802
   6      4.36   4.24264    18.503     342.3    1.0881

MTB > let c20= abso (c17)
MTB > dotplot c20
```

Dotplot: C20

```
          :  .         .                              .  .
         +---------+---------+---------+---------+---------+-------C20
         0        25        50        75       100       125
```

```
MTB >  %daniel.mac c17
Executing from file: C:\WINDOWS\Desktop\Minitab\Minitab
13\MTBDEMO\MACROS\daniel.mac
Macro is running ... please wait
```

Daniel plot

```
NOTE: No Effect labels provided.
```

Daniel Plot for C17

```
MTB > %Main 'SS' 'pH' 'SC';
SUBC>   Response 'Mean'.
Executing from file: C:\WINDOWS\Desktop\Minitab\Minitab
13\MTBDEMO\MACROS\Main.MAC

Macro is running ... please wait
```

Main Effects Plot for Mean

```
MTB > Save  "C:\Documents and Settings\Administrator\My
Documents\Thesis\stresses\elastic-instiu-sp-stress.MPJ";
SUBC>    Project;
SUBC>    Replace.
```

2-Applied tensile stress fracturing the passive films formed at a metastable pitting potential

```
MTB > name c1'SS'
MTB > set c1
DATA> -1 -1 -1 0 0 0 1 1 1
DATA> end
MTB > name c2'pH'
MTB > set c2
DATA> -1 0 1 -1 0 1 -1 0 1
DATA> end
MTB > name c3'SC'
MTB > set c3
DATA> -1 0 1 1 -1 0 0 1 -1
DATA> end
MTB > name c4'stress-1'
MTB > set c4
DATA> 1654 1686 1581 1631 1747 1700 1750 1673 1777
DATA> end
MTB > name c5'stress-2'
MTB > set c5
DATA> 1701 1632 1656 1563 1791 1669 1801 1680 1862
DATA> end
MTB > name c6'stress-3'
MTB > set c6
DATA> 1608 1732 1490 1673 1676 1667 1717 1672 1805
DATA> end
MTB > name c7'stress-4'
MTB > set c7
DATA> 1658 1620 1625 1666 1803 1744 1827 1687 1873
DATA> end
MTB > name c8'Mean'
MTB >  rmean c4-c7 c8
MTB > name c9'SS-L'
MTB > set c9
DATA> -1 -1 -1 0 0 0 1 1 1
DATA> end
MTB > name c10'SS-Q'
MTB > set c10
DATA> -1 -1 -1 2 2 2 -1 -1 -1
DATA> end
MTB > name c11'pH-L'
MTB > set c11
DATA> -1 0 1 -1 0 1 -1 0 1
DATA> end
MTB > name c12'pH-Q'
MTB > set c12
DATA> -1 2 -1 -1 2 -1 -1 2 -1
DATA> end
MTB > name c13'SC-L'
MTB > set c13
DATA> -1 0 1 1 -1 0 0 1 -1
DATA> end
MTB > name c14'SC-Q'
MTB > set c14
DATA>  -1 2 -1 -1 -1 2 2 -1 -1
DATA> end
MTB > table c1;
SUBC> means c8.

means c8.
```

Tabulated Statistics: SS

```
 Rows: SS

        Mean
        Mean

 -1   1636.9
 0    1694.2
 1    1760.3
 All  1697.1

MTB > table c2;
SUBC> means c8.

means c8.
```

Tabulated Statistics: pH

```
 Rows: pH

        Mean
        Mean

 -1   1687.4
 0    1699.9
 1    1704.1
 All  1697.1

MTB > table c3;
SUBC> means c8.

means c8.
```

Tabulated Statistics: SC

```
 Rows: SC

        Mean
        Mean

 -1   1746.3
 0    1712.1
 1    1633.1
 All  1697.1

MTB > regr c8 6 c9-c14;
SUBC> coef c15.
```

Regression Analysis: Mean versus SS-L, SS-Q, pH-L, pH-Q, SC-L, SC-Q

```
The regression equation is
Mean = 1697 + 61.7 SS-L - 1.49 SS-Q + 8.3 pH-L + 1.39 pH-Q - 56.6 SC-L
           + 7.47 SC-Q

Predictor        Coef     SE Coef          T        P
Constant      1697.14       10.61     159.90    0.000
SS-L            61.71       13.00       4.75    0.042
SS-Q           -1.486       7.505      -0.20    0.861
pH-L            8.33        13.00       0.64    0.587
pH-Q            1.389       7.505       0.19    0.870
SC-L           -56.58       13.00      -4.35    0.049
SC-Q            7.472       7.505       1.00    0.424

S = 31.84       R-Sq = 95.6%     R-Sq(adj) = 82.2%

Analysis of Variance

Source            DF          SS          MS         F        P
Regression         6       43554        7259      7.16    0.128
Residual Error     2        2028        1014
Total              8       45581

Source       DF      Seq SS
SS-L          1       22848
SS-Q          1          40
pH-L          1         417
pH-Q          1          35
SC-L          1       19210
SC-Q          1        1005



MTB > set c16
DATA> 6 18 6 18 6 18
DATA> copy c15 c15;
SUBC> omit 1.
MTB > let c16=sqrt (c16)
MTB > let c17=c16*c15
MTB > let c18=c17**2
MTB >  let c19=100*(c18/sum (c18))
MTB > print c15-c19
```

Data Display

```
 Row       C15       C16       C17       C18       C19

   1     61.71   2.44949   151.154   22847.5   52.4582
   2     -1.49   4.24264    -6.305      39.8    0.0913
   3      8.33   2.44949    20.412     416.7    0.9567
   4      1.39   4.24264     5.893      34.7    0.0797
   5    -56.58   2.44949  -138.600   19210.0   44.1066
   6      7.47   4.24264    31.702    1005.0    2.3075

MTB > let c20= abso (c17)
MTB > dotplot c20
```

Dotplot: C20

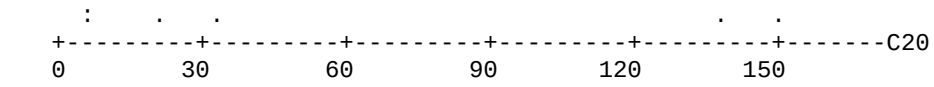


```
MTB > %daniel.mac c17
Executing from file: C:\WINDOWS\Desktop\Minitab\Minitab
13\MTBDEMO\MACROS\daniel.mac
Macro is running ... please wait
```

Daniel plot

```
NOTE: No Effect labels provided.
```

Daniel Plot for C17

```
MTB > %Main 'SS' 'pH' 'SC';
SUBC>   Response 'Mean'.
Executing from file: C:\WINDOWS\Desktop\Minitab\Minitab
13\MTBDEMO\MACROS\Main.MAC

Macro is running ... please wait
```

Main Effects Plot for Mean

```
MTB > Save  "C:\Documents and Settings\Administrator\My
Documents\Thesis\stresses\elastic-insitu-pp-stress.MPJ";
SUBC>    Project;
SUBC>    Replace.
```

References:

1 M. Fontana. Corrosion engineering. McGraw-Hill. New York. (1986)

2 D. Jones. Principles and prevention of corrosion. 2nd edition. Prentice-Hall, Inc. London. UK. (1996)

3 C. O.A. Olsson, and D. Landolt. Passive films on stainless steels- chemistry, structure and growth. *Electrochimica Acta.* **48** (2003) 1093-1104

4 I. Olefjord and L. Wegrelius. Surface analysis of passive state. *Corrosion Science.* **31** (1990) 89-98

5 S. Mischler. A. Vogel. H. Mathieu, and D. Landolt. The chemical composition of the passive film on Fe-24Cr and Fe-24Cr-11Mo studied by AES, XPS, and SIMS. *Corrosion sci.* **32** (1991) 925-944

6 M. F. Montemor, M. G. S. Ferreira, N. E. Hakiki, and M. Da Cunha Belo. Chemical composition and electronic structure of the oxide films formed on 316L stainless steel and nickel based alloys in high temperature aqueous environments. *Corrosion Sci.* **42** (2000) 1635-1650

7 S. J. Doh, J. Je, J. Kim, K Kim, H. Kim, Y. Lee, J. Lee, and Y. Hwu. Influence of Cr and Mo on the passivation of stainless steel 430 (18Cr) and 444 (18Cr-2Mo): In situ XANES study. *Nucl. Instr.and Meth. In phys. Res.* **B 199** (2003)211-215

8 E. William, O. Grady. Mossbauer study of the passive oxide film on iron. *J. electrochem. Soc* **vol 127.** (1980) 555-563

9 H. C. Brookes, J. W. Bayles , and F. J. Graham. Nucleation and growth of anodic films on stainless steel alloys. I. Influence of minor alloying elements and applied potential on passive film growth. Journal of applied electrochemistry. **20** (1990) 223-230

10 H. H. Uhlig. Passivity in metals and alloys. *Corrosion science.* **19** (1979) 777-791

11 L. Tronstad and C. Borgmann. Some optical observations on the passivity of iron and steel in nitric and chromic acids. *Trans. Faraday Soc*. **56** (1934) 349-361

12 N. Sato, and M. Cohen. The kinetics of anodic oxidation of ironin neutral solution. I. Steady Growth Region. *J. electrochem. Soc.***111** (1964) 512-519

13 N. Sato, and M. Cohen. The kinetics of anodic oxidation of ironin neutral solution. II. Initial stages. *J. electrochem. Soc.***111** (1964) 519-522

14 N. Cabrera, and N. Mott. Theory of the oxidation of metals. *Rep. Prog. Phys* **12** (1948-1949) 163-184

15 C. Chao, L. Lin, and D. Macdonald. A point defect model for anodic passive films: I. Film Growth Kinetics. *J. Electrochem. Soc.* **Vol 128** (1981) 1187-1194

16 D. Macdonald. Passivity-the key to our metals-based civilization. *Pure Appl. Chem.* **vol 71** (1999) 951-978

17 H. H. Uhlig, and H Bohni. Environmental factors affecting the critical pitting potential of aluminum. *J. electorchem. Soc.* **vol 116** (1967) 906-910

18 T. P. Hoar, and W. Jacob. The solid state: breakdown of passivity of stainless steel by halide ions.*Nature*, **216** (1967) 1299- 1301

19 N. Sato. A theory for breakdown of anodic oxide films on metals. *Eletcrochimica acta.* **Vol 16.** (1971) 1683-1692

20 L. Lin, C. Chao, and D. Macdonald. A point defect model for anodic passive films: II. Chemical breakdown and pit initiation. *J. Electrochem. Soc.* **Vol 128** (1981) 1194-1198

21 R. Kirchheim, B. Heine, S. Hofmann, and H. Hofsass. Compositional changes of passive films due to differential transport rates and preferential dissolution. *Corrosion Science.* **Vol. 31** (1990) 573-578

22 S. Haupt, and H. Strehblow. A combined surface analytical and electrochemical study of the formation of passive layers on Fe/Cr alloys in 0.5M H_2SO_4. *Corrosion Science.* **Vol. 37**. (1995) 43-54

23 J. M. Bastidas, M. Lopez, A. Gutierrez, and C. Torres. Chemical analysis of passive films on type AISI 304 stainless steel using soft X-ray absorption spectroscopy. *Corrosion Science*. **40** (1998) 431-438

24 M. P. Ryan, S. Fujimoto, G. Thompson, and R. Newman. Disorder and structural relation in passive films on Fe-Cr alloys. *Materials Science Forum.* **185-188** (1995) 233-240

25 D. Costa, W. Yang, and P. Marcus. XPS analysis of passive films formed on chromium in acidic solution without and with chloride ions. *Materials Science Forum.* **185-188** (1995) 325-336

26 D. Hamm, C. Olsson, and D. Landolt. Effect of chromium content and sweep rate on passive film growth on iron-chromium alloys studied by EQCM and XPS. *Corrosion Science.* **44** (2002) 1009-1025.

27 D. Wallinder, J. Pan, C. Leygraf, and A. Delblance-Bauer. EIS and XPS study of surface modification of 316LVM stainless steel after passivation. *Corrosion Science.* **41** (1999) 275-289

28 A. R. Brooks, C.R. Clayton. K. Doss, and Y. Lu. On the role of Cr in the passivity of stainless steel. *J. Electrochem Soc.* **133** (1986) 2459-2464

29 S. Doh, J. Je, J. Kim, K. Kim, H. Kim, Y. Lee, J. Lee, and Y. Hwu. Influence of Cr and Mo on the passivation of stainless steel 430 (18Cr) and 444 (18Cr-2Mo): in situ XANES study. Nucl. Instrum. Meth. **B 199** (2003) 211-215

30 M. Ameer. A. Fakry, and F. Heakal. Electrochemical behavior of passive films on molybdenum-containing austenitic stainless steels in aqueous solutions. *Electrochimica Acta* **50** (2004) 43-49

31 C.R. Calyton, and Y.C. Lu. A bipolar model of passivity of stainless steel: The role of Mo addition. *J. Electrochem. Soc.* **Vol 133.** (1986) 2465-2472

32 C. Clayton, and Y. Lu. A bipolar model of the passivity of stainless steel: the role of Mo addition. *J.Electrochem. Soc***. 133** (1986) 2465-2472

33 . F. Montemor, M. G. S. Ferreira, N. E. Hakiki, and M. Da Cunha Belo. Effects of Mo on the composition and electronic properties of the passive films formed on stainless steel at 350°C. *Materials Science Forum.* **289-292** (1998) 1139-1150

34 L. Wegrlius , F. Falkenberg, and I. Olefjord. Passivation of Stainless steel in hydrochloric acid. *J. Electrochem. Soc.* **146** (1999) 1397-1406

35 A. Lloyd, J. Noel, S. McIntyre, and D. Shoesmith. Cr, Mo, and W alloying additions in Ni and their effect on passivity. *Electrochimica Acta.* **49** (2004) 3015-3027

36 R. Jargelus-Pettersson, and B. Pound. Examination of the role of molybdenum in passivation of stainless steels using AC impedance spectroscopy. **145** (1998) 1462-1469

37 H. Ogawa, H. Omata, I. Itoh, and H. Okada. Auger electron spectroscopic and electrochemical analysis of the effect of alloying elements on the passivation behavior of stainless steel. *Corrosion-NACE.* **34** (1978) 52-59

38 R. Willenbruch, C. Clayton, M. Oversluizen, D. Kim, and Y. Lu. An XPS electrochemical study of the influence of molybdenum and nitrogen on the passivity of austenitic stainless steel. *Corrosion science*. **31** (1990) 179-190

39 V. Maurice, W. Yang, P. Marcus. X-ray photoelectron spectroscopy and scanning tunneling microscopy study of passive films formed on (100) Fe-18Cr-13Ni single-crystal surfaces. *J. Electrochem Soc.* **145** (1998) 909-919

40 N. Sato. Anodic Breakdown of Passive Films on Metals. *J. Electrochem. Soc.* (1982) 255-260

41 H. Hoppe, S. Haupt, and H. Strehblow. Combined surface analytical and electrochemical study of the formation of passive layers on Fe/Cr alloys in1M NaOH. *Surface and interface analysis.* **21** (1994) 514-525

42 C- O. Olsson, D. Hamm, and D. Landolt. Electrochemical Quartz crystal microbalance studies of the passive behavior of Cr in a sulfuric acid solution. *J. electrochem. Soc*. **147** (2000) 2563-2571

43 G. Okamoto. Passive film of 18-8 stainless steel structure and its function. *Corrosion Science.* **13** (1973) 471-489

44 J. A. Bardwell, G. I. Sproule, B. R. Macdougall, M. J. Graham, A. J. Daveport, and H. S. Isaac. In situ XANES detection of Cr(VI) in the passive film on Fe-26Cr. *J. electrochem. Soc.* **139** (1992) 371-374

45 P. Schmutz, and D. Landolt. In-situ microgravimetric studies of passive alloys: potential sweep and potential step experiments with Fe-25Cr and Fe-17Cr-33Mo in acid and alkaline solution. *Corrosion Science*. **41** (1999) 2143-2163

46 U. Kamachi Mudali, and Y. Katada. Electrochemical atomic force microscopic studies on passive films of nitrogen-bearing austenitic stainless steels. *Electrochimia Acta* **46** (2002) 3735-3742

47 Y. S. Zhang, X. M. Zhu, M. Liu, and R. X. Che. Effects of anodic passivation on the constitution, stability, and resistance of corrosion of passive film formed on an Fe-24Mn-4Al-5Cr alloy. *Applied Surface Science*. **222**. (2004) 89-101

48 P. C. Pistorius, and G. T. Burstein. Metastable pitting corrosion of stainless steel and the transition to stability. *Philosophical Transaction: Phys. Sci. Eng.* **341** (1992) 531-559

49 M. Pagitsas, A. Diamantopoulou, and D. Sazou. General and pitting corrosion deduced from current oscillations in the passive-active transition state of the $Fe|H_2SO_4$ electrochemical system. Electrochimica Acta. **47** (2002) 4163-4179

50 E. abd El al. Breakdown of passive film on nickel in borate solutions containing halide anions. *Corrosion Science.* **45** (2003) 759-775

51 Z. Szklarska-Smialowska. Mechanism of pit nucleation by electrical breakdown of passive film. *Corrosion Science.* **44** (2002) 1143-1149

52 V. Mitrovic-Scepanovic, B. MacDougall, and M. Graham. The effect of Cl^- ions on the passivation of Fe-26Cr alloy. *Corrosion Science*. **27** (1987) 239-247

53 T. P. Hoar, the production and breakdown of the passivity of metals. *Corrosion Science.* **7** (1967) 341-355

54 N. Sato. An overview on the passivity of metals. *Corrosion science.* **31** (1990) 1-19

55 P. Ernst, and R. C. Newman. Pit growth studies in stainless steel foils. II. Effects of temperature, chloride concentration and sulphate addition. *Corrosion science* **44** (2002) 943-954

56 M. Pourbaix: "Atlas of Electrochemical Equilibria in Aqueous Solutions", Pergamon, New York, 1966

57 B. Elsener and A. Rossi. Effect of pH on elelctrochemical behavior and passive film composition of stainless steel. *Material science Forum.* **192-194** (1995) 225-236

58 W. M. Carrol and T. G. Walsh. The influence of pH, Temperature and surface pretreatment on the stability of passive films formed on sanicro 28 and 5R60 stainless steels in aqueous chloride solutions. *Corrosion Science.* **29** (1989) 1205-1214.

59 A. U. Malik, P. C. Mayan Kutty, N. Siddiqi, I. N. Andijani, and S. Ahmed. The influence of pH and chloride concentration on the corrosion behavior of AISI 316L steel in aqueous solutions. *Corrosion Science* **33** (1992) 1809-1827

60 D. Buttry and M. Ward. Measurement of interfacial processes at electrode surfaces with electrochemical quartz crystal microbalance. *Chem. Rev* **92** (1992) 1355-1379

61 N. Hara and K. Sugimoto. In situ analysis of passive films on Fe-Cr-Ni alloy by potential modulated UV-visible reflection spectroscopy. *J. Electrochem. Soc.* **138** (1991)1594-1599

62 C. Pallotta, N. Cristofano, R. Salvarezza, and A. Arvia. The influence of temperature and the role of chromium in the passive layer in relation to pitting corrosion of 316 stainless steel in NaCl solution. *Electrochimica Acta.* **31** (1986) 1265-1270

63 W. M. Carroll and M. B. Howley. The influence of temperature, applied potential, buffer and inhibitor addition on the passivation behaviour of a commercial grade 316L steel in aqueous halide solutions. *Corrosion Science* **30** (1990) 643-655

64 S. Jin and A. Atrens. ESCA-studies of the structure and composition of the passive film formed on stainless steel by various immersion temperatures in 0.1M NaCl solution. *Appl. Phys.* **A 45** (1988) 83-91

65 P. D. Bastek, R. C. Newman, R. G. Kelly. Measurement of Passive Film Effects on Scratched Electrode Behavior. *J. electorchem. Soc.* **140** (1993) 1884-1890

66 D. G. Kolman, M.A. Gaudett, and R. J Scully. Modeling of anodic current transients resulting from oxide rupture of plastically strained β+α titanium. *J. electrochem. Soc.* **145** (1998) 1829-1839

67 G. T. Burstein and P.I. Marshall. Growth of passivating films on scratched 304L stainless steel in alkaline solution. *Corrosion Science.*. **23** (1983) 125-137

68 X. Y. Wang & D. Y. Li. Mechanical and electrochemical behavior of nanocrystalline surface of 304 stainless steel. *Electrochimica Acta* **47** (2002) 3939-3947

69 M. Chiba and M. Seo. Potential dependence of frictional coefficient evaluated by in-situ nano-scratching for passive iron surface. Conference of Corrosion science (2003)

70 D. Bahr, J. Nelson, N. Tymiak, and W. Gerberich. The mechanical behavior of a passivating surface under potentiostatic control. *J. Mater. Res*. **12** (1997) 3345-3353

71 M. Seo, F. Nukaya, and K. Azumi. Nanoindentation of the titanium surfaces covered with anodic oxide films. *Electrochemical Society Proceeding.* **99-42** 945-951

72 M. Pang, and D. Bahr. Thin-film fracture during nanoindentation of a titanium oxide film-titanium system. *J. Mater. Res.* **16** (2001) 2634-2643

73 D. F. Bahr, C. L. Woodcock, M. Pang, K.D. Weaver, and N.R. Moody. Indentation induced film fracture in hard film-soft substrate systems. *International Journal of Fracture* **119/120** (2003) 339-349

74 W. Oliver, and G. Pharr. An improved technique for determining hardness and elastic modulus using load and displacement sensing indentation experiments. *J. Mater. Res.* **7** (1992) 1564-1583

75 D. E. Kramer, K. B. Yoder, and W.W. Gerberich. Surface constrained plasticity: oxide rupture and the yield point process. *Philosophical Magazine A* **81** (2001) 2033-2058

76 S. Venkataraman, D. Kohlstedt, and W. Gerberich. Continuous microindentation of passivating surfaces. *J. Mater. Res.* **8** (1993) 685-688

77 A.B. Mann and J.B.Pethica. nanoindentation studies in a liquid environment. *Langmuir*. **12** (1996) 4583-4586

78 W.W. Gerberich, S. Venkataraman, H. Huang, S. Harvey, and D. Kohlstedt. The injection of plasticity by millinewton contacts. *Acta. Metall. Mater.* **43** (1995) 1569-1576

79 D.F. Bahr, D.E. Kramer, and W. W. Gerberich. Nonlinear deformation mechanism during nanoindentation. *Acta. Mater***. 46** (1998) 3605-3617

80 D.F. Bahr, N.I. Tymiak, and W.W. Gerberich, J. Mater Res

81 Y. Yao, X. Cao, L. Qiao, and W. Chu. Yield point phenomena during nanoindentation. *Tribology transactions.* **47** (2004) 239-247

82 D. Rodriguez-Marek, M. Pang, and D.F. Bahr. Mechanical measurements of passive films fracture on an austenitic stainless steel. *Metal. Mater. Trans.* **34A** (2003) 1291-1296

83 M. Pang, D.E. Eakins, M.G. Norton, and D.F.Bahr. structural and mechanical characteristics of anodic oxide films on titanium. *Corrosion.* **57** (2001) 523-531

84 U.Kamachi Mudali, and Y. Katada. Electrochemical atomic force microscopic studies on passive films of nitrogen-bearing austenitic stainless steels. *Electrochimica Acta.* **Vol. 46** (2001) 3735-3742

85 Stoychev, P. Stefanov, D. Nickolova, I. Valov, and Ts. Marinova. Chemical composition and corrosion resistance of passive chromate films formed on stainless steel 316L and 1.4301. *Material chemistry and physics.* **73** (2002) 252-258

86 M. Chiba and M. Seo. Effects of dichromate treatment on mechanical properties of passivated single crystal iron (100) and (110) surfaces. *Corrosion science.* **44** (2002) 2379-2391

87 M. Seo and M. Chiba. Nano-mechano-electrochemistry of passive film surfaces. *Electrochimica Acta* **47** (2001) 319-325

88 W. Fowlkes, and C. Creveling. *Engineering Methods for robust product design*. Reading, Massachusetts: Addison-Wesley. (1995)

89 W. Eureka, and N. Ryan. *Quality up, cost down: a manager's guide to Taguchi methods and QFD.* NewYork: American supplier institute (1995)

90 J. Antony. Design of experiments for engineering and scientists. Boston: Butterworth-Heinemann. (2003)

91 M. Phadke. Quality engineering using robust design. Englewood Cliffs, NJ: Prentice Hall (1989)

92 R. Devor, T. Chang, and J. Sutherland. Statistical quality design and control. New York: Macmillan Publishing company (1992)

93 D. Montgomery. Experimental Design for Product and Process Design and Development. The Statistician, **Vol. 48** (1999) 159-177.

94 N. Logothetis. Box-Cox Transformations and the Taguchi Method. *Applied Statistics.* **39** (1990) 31-48

95 A. Bendell, J. Disney, and W.A. Pridmore. Taguchi methods applications in world industry. New York: Berlin. Heidelberg (1989)

96 J. Devore. Probability and statistics. Pacific Grove, CA: Duxbury (1999)

97 Michael Jacroux. ' personal communication'. Department of Statistics, Washington State University.

98 X. Hou and C. F. J. Wu. On the determination of robust settings in parameter design experiments. *Statistics & Probability Letters.* **54**, (2001) 137-145

99 S. Phadnis, A. Satpati, K. Muthe, J. Vyas, and R. Sundaresan. Comparison of rolled and heat treated SS304 in chloride solution using electrochemical and XPS techniques. *Corrosion Science.* **45** (2003) 2467-2483

100 M Graham. The application of surface techniques in understanding corrosion phenomena and mechanisms. *Corrosion Science.* **37** (1995) 1377-1397

101 C. Brundle, C. Evans, and S. Wilson. Encyclopedia of materials characterization. Boston: Butterworth-Heinemann (1992)

102 D. Williams and C. Carter. Transmission electron microscopy: Basic I. New York: Plenum Press (1996)

103 D. Williams and C. Carter. Transmission electron microscopy: Diffraction II. New York: Plenum Press (1996)

104 B. Lucas, W. Oliver, and J. Swindeman. The dynamics of frequency-specific, Depth Sensing Indentation testing. *Mat.Res. Soc. Symp. Proc.* **522** (1998) 3-14

105 F. R. Brotzen. Mechanical testing of thin film. *International Materials Reviews.* **39** (1994) 24-42

106 Y. Zuo, H. Wang, J. Zhao, and J. Xiong. The effects of some anions on metastable pitting of 316L stainless steel. *Corrosion Science.* **44** (2002) 13-24

107 H.P. Leckie and H.H. Uhlig. Environmental factors affecting the critical potential for pitting in 18-8 stainless steel. *J. Electrochem. Soc*., **113** (1966) 1262

108 S. Bera, S. Rangarajan, and S. V. Narasimhan. Electrochemical Passivation of iron alloys and the film characterization by XPS. *Corrosion Science* **42** 1709-1724. (2000)

109 N. Stolica . pitting corrosion on Fe-Cr and Fe-Cr-Ni alloys. *Corrosion Science.* **9** (1969) 455-470

110 J.L. Dawson, and M. Ferreira. Electrochemical studies of the pitting of austenitic stainless steel. *Corrosion Science.* **Vol 26** (1986) 1009-1026

111 J.C Colson and J.P. Larpin. High-Temperature Oxidation of Stainless Steels. *MRS Bull.* **10** (1994) 23-26

112 L. Wegrilius, F. Falkenberg, and I. Olefjord. Passivation of stainless steels in hydrochloric acid. *J. electrochem. Soc.* **146** (1999) 1397-1406

113 J.D. Hanawalt, W. H. Rinn, and K.L. Frevel. Chemical analysis by X-ray diffraction. Classification and use of x-ray diffraction patterns. *Anal. Chem.* **10** (1938) 475-512

114 J. C. Rao, X. X. Zhang, B. Qin, and K. K. Fung. High-resolution transmission electron microscopy study of epitaxial passive films on nanocubes of chromium. *Philos Mag litt.* **83** (2003) 395-401

115 M. da Cunha Belo, M. Walls, N. E. Hakiki, J. Corset, E. Picquenard, G. Sagon and D. Noël. Composition, structure and properties of the oxide films formed on the stainless steel 316L in a primary type PWR environment**.** *Corrosion science.* **40** (1998) 447-463

116 M. da Cunha Belo, M. Walls, N. E. Hakiki, J. Corset, E. Picquenard, G. Sagon and D. Noël. Composition, structure and properties of the oxide films formed on the stainless steel 316L in a primary type PWR environment**.** *Corrosion science.* **40** (1998) 447-463

117 P. Hones and F. Lovy. Influence of deposition parameters on mechanical properties of sputter-deposited Cr_2O_3 thin films. *J. Mater. Res.* **14** (1999) 3623-3629

118 K.L. Johnson: Contact Mechanics, (Cambridge University Press, Cambridge, U.K., (1985)

119 S. Haupt, C. Calinski, U. Collisi, H.W. Hoppe, H.D. Speckmann, and H.H. Strehblow. XPS and ISS examinations of electrode surfaces and passive layers with a specimen transfer in a closed system. *Surf. Interface Anal.* **9** (1986) 357-365

120 J.A.Bardwell, G.I.Sproule, and M.J. Graham. Ex situ surface analysis of passive films on iron-chromium alloys. When is it valid? *J. Electrochem. Soc* **140** (1993) 50-53

121 S.A. Syed Asif, K.J. Wahl, and R.J. Colton. The influence of oxide and adsorbates on the nanomechanical response of silicon surfaces. *J. Mater .Res.* **15** (2000) 546-553